Studies on the Reversible Photo-regulation of Strand Displacement with Azobenzene-tethered DNA

(アゾベンゼン導入 DNA による鎖交換反応の可逆的な光制御に関する研究)

Bohao Cheng

2019

Contents

Abstract

Recent decades of years, DNA has drawn much attention for its possibility as an outstanding engineering molecule in nanotechnology. By programming sequence of DNA, precise control of DNA binding behavior is accessible. Considering employing light, a green and constant resource in nature, as tools to manipulate DNA conveniently, Asanuma group has established a facile protocol that achieves reversible photo-regulation of DNA binding behavior by incorporating photo-responsive azobenzene moieties into DNA strands. There have been several photo-controllable DNA nanodevices developed based on this protocol, such as a photo-responsive DNA tweezer or a photo-regulated DNAzyme.

In this study, the first part describes the development of the first photo-driven DNA strand displacement reaction, based on azobenzene-tethered oligonucleotides as modulators and poly(L-lysine)-*graft*-dextran (PLL-*g*-Dex) as an accelerator. By thoroughly investigating mechanisms of all processes in this reaction, a reversible strand displacement behavior was achieved without decline of the efficiency.

In the second part, photo-driven DNA strand displacement reaction is applied to an amplification assay that is regulatable by alternating irradiation with UV and visible light. It is demonstrated that the photo-regulatable amplification assay achieved linear yield and showed predominant discriminability of mismatches in the target template. It is promisingly contributing to developing clinical diagnostic tools for genetic disease detection.

Chapter 1. An Introduction to DNA and DNA nanotechnology

1.1. Deoxyribonucleic acids (DNA)

Though deoxyribonucleic acid, DNA, was first reported in 1870s, it has started attracting attentions in 1950s when James Watson and Francis Crick discovered its famous double helical structure.[1] Since then, DNA as one of the most important biomacromolecules have been being widely researched in medicine, biology and chemistry.

Nowadays, scientists have known that DNA double helix contains two chains hybridized with each other, both of which are polymerized in a specific order by four types nucleotides. Each nucleotide composes of a sugar scaffold D-deoxyribose, a phosphate group and one of the four nucleobases, adenine (**A**), thymine (**T**), cytosine (**C**) or guanine (**G**). The specific order of nucleotides, which is called sequence, stores genetic information of organisms. Two DNA strands who are sequentially complementary binds to each other according to Watson-

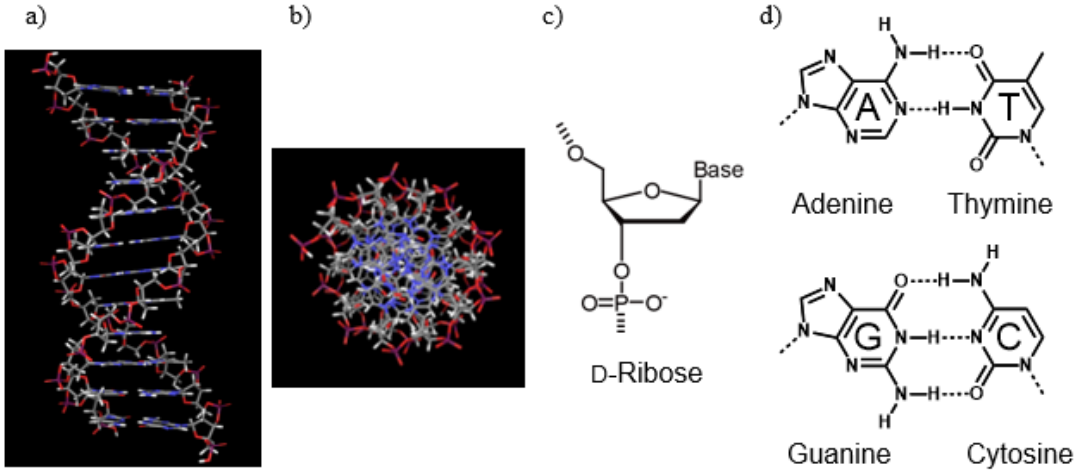

Figure 1.1. The structure of a) side view and b) top view of B-DNA. Chemical structures of c) D-deoxyribose backbone and d) nucleobases with complementary hydrogen bonds.

Crick base pairing rule, **A** combines with **T** via three hydrogen bonds while **C** combines with **G** via two bonds. This correlation ensures the stable storage of genetic code for expression and heredity through replication, transcription and translation. All these structure-endowed properties make DNA one of the most research objects and also research tools.

1.2. DNA as engineering molecule in nanotechnology

Despite DNA's fundamental rolls in biological research field, it has also been researched as an excellent engineering molecule in nanotechnology for recent decades of years.

As described in section 1.1, binding behavior of DNA strands strictly follows Watson-Crick base pairing rule, which provides opportunities for scientists to control its binding behavior by programming sequence of DNA strands. Especially in recent decade, solid-phase synthesis of DNA has becoming cheaper and reaching a higher yield, which further promotes plenty of exciting researches emerging in DNA nanotechnology field.

To control the hybridizing manner of DNA strands, sequence of each strands are designed and synthesized as proposed to give complementary regions and incomplementary regions. For example, two DNA strands designed in the sequence that only part of region is complementary, then only this complementary part will hybridize to form duplex and other incomplementary parts remain single-stranded, as shown in Scheme 1.1.

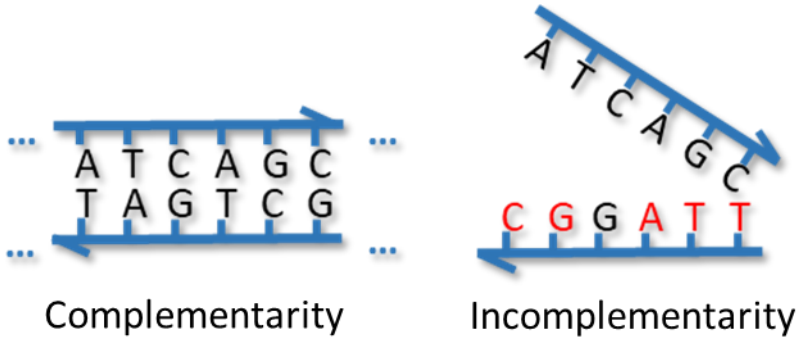

Scheme 1.1. DNA binding behavior controlled by programing sequences

Based on this concept, many structure can be achieved by control the hybridization of DNA strands, such as sticky end, three-way junction[2] or hairpin, as shown in Scheme 1.2.

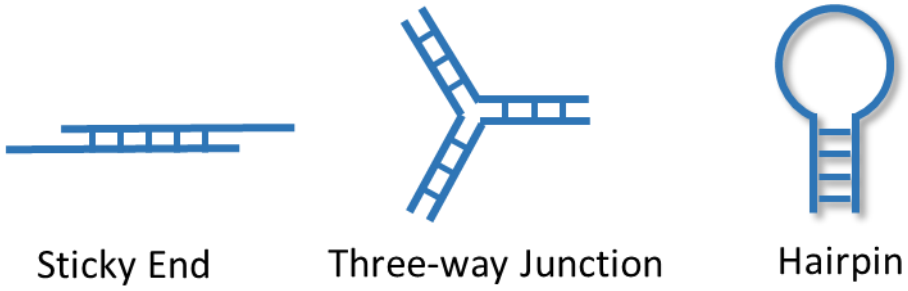

Scheme 1.2. Several basic nano-structures achieved by programming DNA sequences

Utilizing this building blocks of nano-structure, more complex structures or dynamics are able to be designed. The most famous example should be DNA Origami,[3] which is a DNA complex that holds two- or three-dimensional shapes in nano-scale. It is realized by forming of multiple programmed staple strands onto a long single viral DNA, forcing the folding of viral DNA into customized two- or three-dimensional structures, as shown in Fig. 1.2.

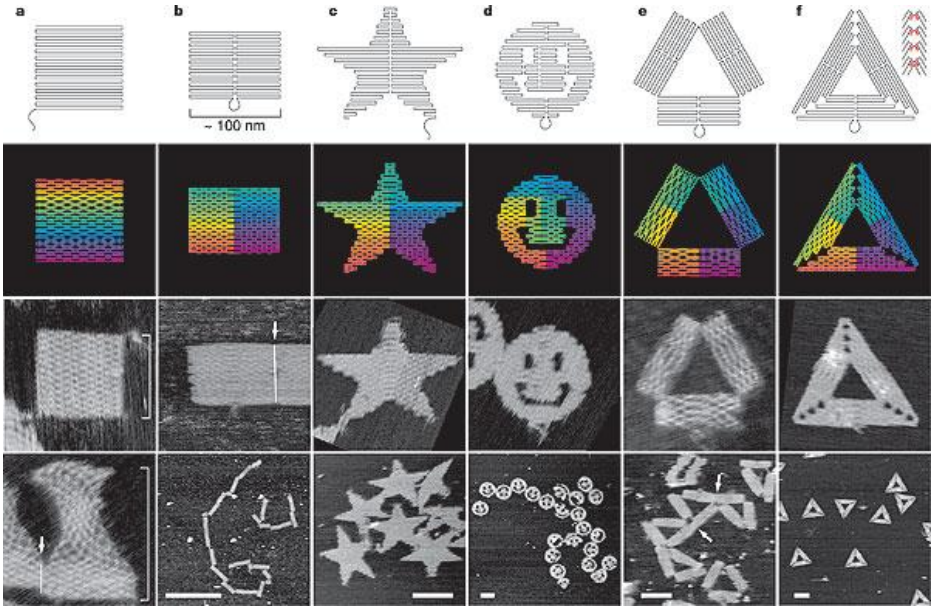

Figure 1.2. DNA Origami observed under atomic force microscopy

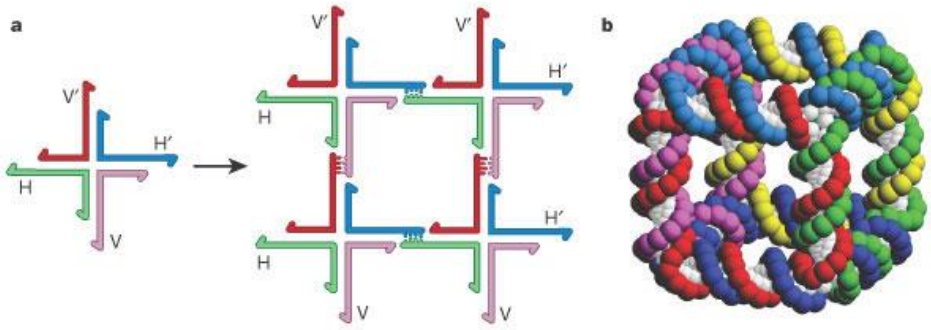

Figure 1.3. The schematic illustration of DNA lattice. a) four-way junction DNA building blocks and b) structure of a DNA cube

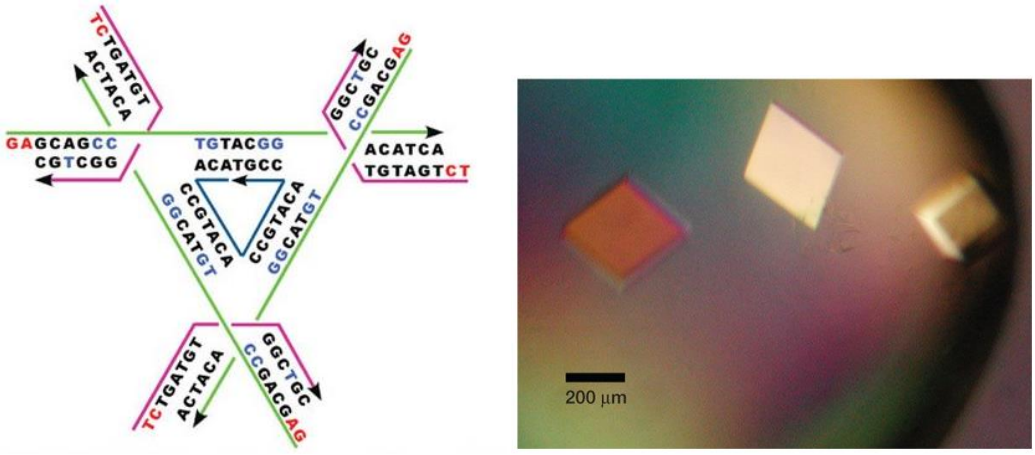

Figure 1.4. DNA crystal under microscopy

There are some other static structures like DNA lattices[4] (Fig. 1.3) and self-assembled 3D DNA crystal[5] (Fig. 1.4) as well. All of these examples suggest promising perspective to employ DNA as engineering molecules to achieve precisely designable nano-structures.

Besides static nano-structures, DNA are also applied to develop spontaneous or stimulus-responsive nano-devices/robots, such as a proton-fueled *i*-motif[6] (Scheme 1.5a), a reversible DNA tweezer[7] (Scheme 1.5b) and a DNA walker based on toehold strand displacement[8] (Scheme 1.5c). These successful DNA dynamics enable the control of mechanical motions

in nano-scale. Some of the nano-devices based on DNA are even applied to extra- or intra-cellular environment[9-12] for mRNA imaging or drug delivery proposes.

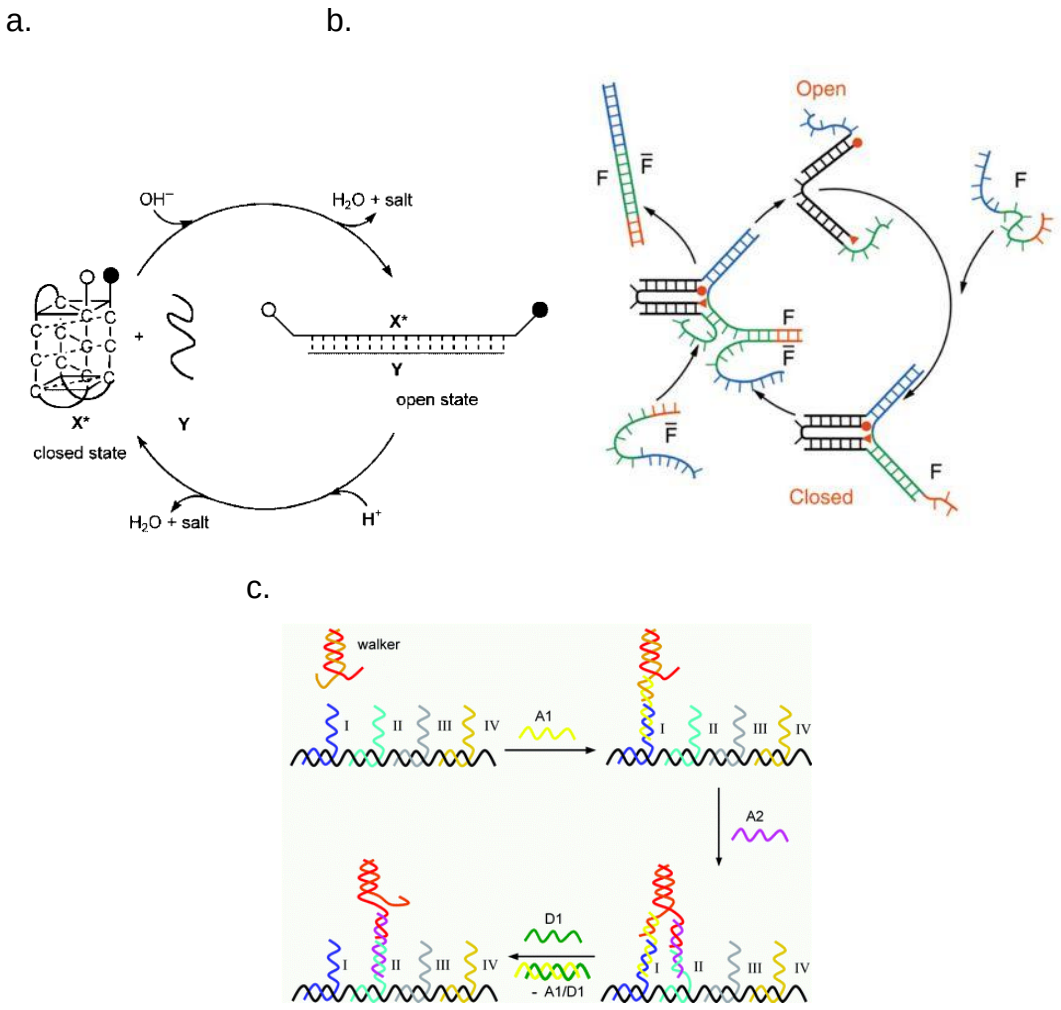

Figure 1.5. DNA nano-dynamic application: a) proton-fueled *i*-motif, b) a DNA tweezer fueled by toehold strands and c) a DNA walker fueled by toehold strands

As one of the cleanest resources in nature, there have been many attempts to employ light as energy to drive mechanical motions in nanoscale through inducing photon-fueled structural changes, always by photoisomerization of molecules. Accessible small molecules that response to light irradiation includes spiropyran,[13-14] diarylethene,[15-17] stilbene[18-20] and azobenzene[21] as well as their derivatives.

Out of all these molecules, azobenzene derivatives are most widely used in various applications due to its simple synthetic pathway and chemical stability.

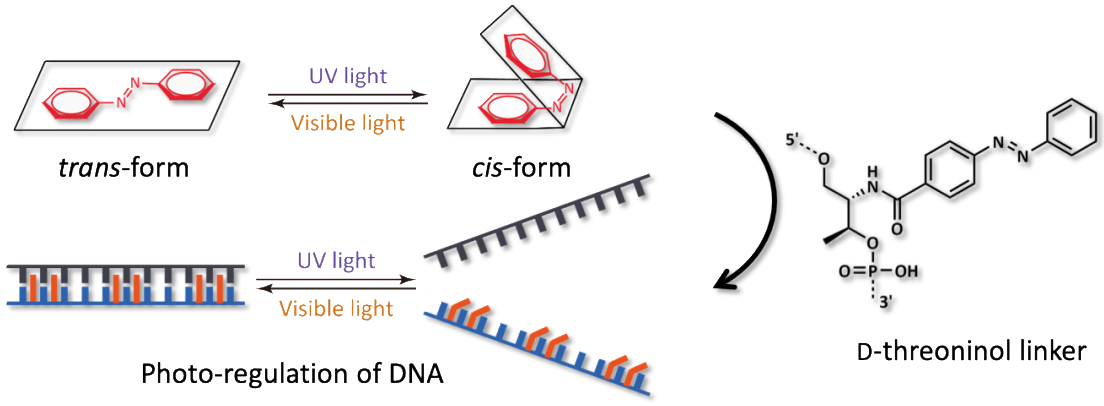

Scheme 1.3. Schematic illustration of photo-regulation of DNA binding behavior

Azobenzene undergoes *trans*-to-*cis* isomerization upon ultraviolet (UV) radiation around 350 nm, and reversed *cis*-to-*trans* isomerization upon visible light in longer wavelength than 400 nm. Because of its planar configuration in *trans*-form and nonplanar configuration in *cis*-form, light irradiation achieves reversibly control of mechanical motions through exciting structural change of azobenzene.

Asanuma *et al*. designed an acyclic tetrose linker as a scaffold to tether azobenzene into DNA, called D-threoninol[22-26] (Scheme 1.3). Utilize of D-threoninol instead of normal deoxyribose avoids synthetic complexity[27] and keeps right-handed double helical structure of DNA. NMR research[28] demonstrated a stabilization of azobenzene-incorporated DNA duplex due to azobenzene's stacking with the adjacent base pair in *trans*-form; and a destabilization of duplex as nonplanar *cis*-azobenzene induces large steric hindrance. Therefore, repetitive regulation of stabilization and destabilization of DNA duplex tethering azobenzene derivatives, always resulting in hybridization and dissociation of duplex respectively, can be approached by conveniently irradiating sample with visible and UV light.

Several photo-controllable nanomachines have been developed with the participation of azobenzene-tethered DNA strand. A photon-fueled DNA tweezer[29] was designed and controlled by employing a photoresponsive strand as an engine, as shown in Fig. 1.6. With

visible light irradiation, azobenzene moieties in *trans*-form allow the hybridization of photo-engine onto tweezer handles thus "close" the molecular tweezer. Once UV irradiation was applied, dissociation of photo-engine strand "open" the molecular tweezer due to the *cis*-to-*trans* isomerization of azobenzene that highly destabilize the DNA duplex. In this way, alternating irradiation with visible and UV irradiation reversibly control the "open" and "close" of DNA tweezer without losing efficiency. Another DNA nanomachine called "DNA seesaw" was developed by combining non-modified azobenzene and 2,6-dimethyl-4-(methylthio)-azobenzene, an azobenzene derivatives that undergoes *trans*-to-*cis* isomerization responding to visible light. This machine composes of a template strand that hybridizes two strands tethering two different azobenzene derivatives respectively. This machine could be controlled by light in three wavelengths to achieve changes among four states (Fig. 1.7).

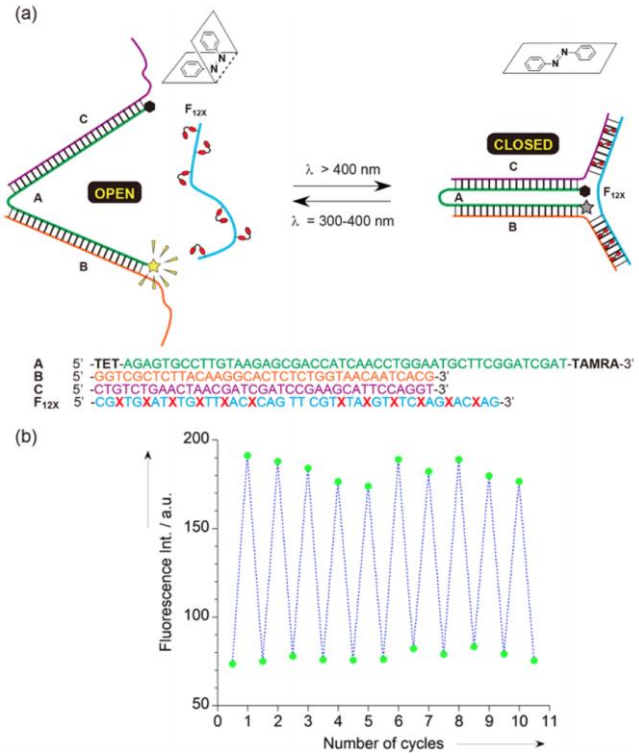

Figure 1.6. A photon-fueled DNA tweezer that is reversibly regulated by alternating irradiation with UV and visible light.

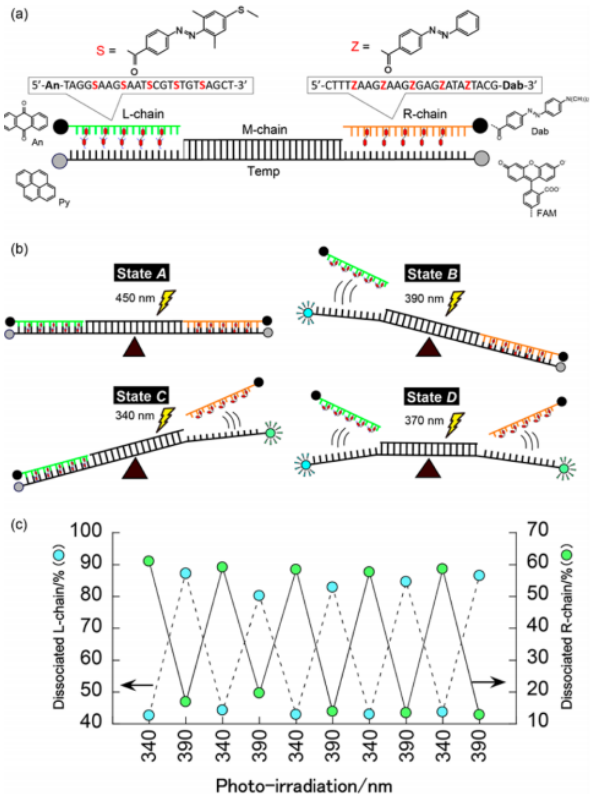

Figure. 1.7. DNA "seesaw" motivated by two kinds of light engines.

1.3. Purpose of this study

So far, photo-responsive oligonucleotides are applied to mainly linear binding behavior such as duplex hybridization, duplex dissociation, triplex formation and so on. A dynamic photo-driven process involving more than two DNA strands has been ignored.

In this study, a photo-driven strand displacement reaction is developed and systemically investigated in Chapter 2. This technique is further applied to establish the first photo-regulatable DNA strand displacement reaction in Chapter 3.

1.4. Reference

[1] J. D. Watson, F. H. C. Crick, *Nature,* **1953**, *171*, 737-738.

[2] D. R. Duckett, D. M. J. Lilley, *EMBO J.,* **1990**, *9*, 1659-1664.

[3] P. W. K. Rothemund, *Nature,* **2006**, *440*, 297-302.

[4] J. H. Chen, N. C. Seeman, *Nature,* **1991**, *350*, 631-633.

[5] J. P. Zheng, J. J. Birktoft, Y. Chen, T. Wang, R. J. Sha, P. E. Constantinou, S. L. Ginell, C. D. Mao, N. C. Seeman, *Nature,* **2009**, *461*, 74-77.

[6] D. S. Liu, S. Balasubramanian, *Angew. Chem. Int. Ed.,* **2003**, *42*, 5734-5736.

[7] B. Yurke, A. J. Turberfield, A. P. Mills, F. C. Simmel, J. L. Neumann, *Nature,* **2000**, *406*, 605-608.

[8] J. S. Shin, N. A. Pierce, *J. Am. Chem. Soc.,* **2004**, *126*, 10834-10835.

[9] H. M. T. Choi, V. A. Beck, N. A. Pierce, *Acs Nano,* **2014**, *8*, 4284-4294.

[10] M. J. Levesque, P. Ginart, Y. C. Wei, A. Raj, *Nat. Methods,* **2013**, *10*, 865-+.

[11] M. Rudchenko, S. Taylor, P. Pallavi, A. Dechkovskaia, S. Khan, V. P. Butler, S. Rudchenko, M. N. Stojanovic, *Nat. Nanotechnol.,* **2013**, *8*, 580-586.

[12] S. M. Douglas, I. Bachelet, G. M. Church, *Science,* **2012**, *335*, 831-834.

[13] C. Beyer, H. A. Wagenknecht, *Synlett,* **2010**, 1371-1376.

[14] C. Brieke, A. Heckel, *Chem-Eur J,* **2013**, *19*, 15726-15734.

[15] M. Singer, A. Jaschke, *J. Am. Chem. Soc.,* **2010**, *132*, 8372-8377.

[16] S. Barrois, C. Beyer, H. A. Wagenknecht, *Synlett,* **2012**, 711-716.

[17] S. Barrois, H. A. Wagenknecht, *Beilstein J Org Chem,* **2012**, *8*, 905-914.

[18] F. D. Lewis, X. Y. Liu, *J. Am. Chem. Soc.,* **1999**, *121*, 11928-11929.

[19] H. Kashida, T. Doi, T. Sakakibara, T. Hayashi, H. Asanuma, *J. Am. Chem. Soc.,* **2013**, *135*, 7960-7966.

[20] S. Ogasawara, M. Maeda, *Angew. Chem. Int. Ed.,* **2008**, *47*, 8839-8842.

[21] K. Yamana, A. Yoshikawa, H. Nakano, *Tetrahedron Lett.,* **1996**, *37*, 637-640.

[22] H. Kashida, X. G. Liang, H. Asanuma, *Curr. Org. Chem.,* **2009**, *13*, 1065-1084.

[23] H. Asanuma, T. Ito, T. Yoshida, X. G. Liang, M. Komiyama, *Angew. Chem. Int. Ed.,* **1999**, *38*, 2393-2395.

[24] H. Asanuma, X. G. Liang, T. Yoshida, M. Komiyama, *Chembiochem,* **2001**, *2*, 39-44.

[25] H. Asanuma, T. Takarada, T. Yoshida, D. Tamaru, X. G. Liang, M. Komiyama, *Angew. Chem. Int. Ed.,* **2001**, *40*, 2671-2673.

[26] H. Asanuma, X. Liang, H. Nishioka, D. Matsunaga, M. Liu, M. Komiyama, *Nat. Protoc.,* **2007**, *2*, 203-212.

[27] W. Szymanski, J. M. Beierle, H. A. V. Kistemaker, W. A. Velema, B. L. Feringa, *Chem. Rev.,* **2013**, *113*, 6114-6178.

[28] X. G. Liang, H. Asanuma, H. Kashida, A. Takasu, T. Sakamoto, G. Kawai, M. Komiyama, *J. Am. Chem. Soc.,* **2003**, *125*, 16408-16415.

[29] X. G. Liang, H. Nishioka, N. Takenaka, H. Asanuma, *Chembiochem,* **2008**, *9*, 702-705.

1.5. Contents of schemes and figures.

Chapter 2. Study on photo-driven DNA strand displacement

2.1. Introduction

2.1.1. Toehold strand displacement reaction

Toehold strand displacement reaction is one of the most conventional and useful mechanisms in DNA nanotechnology.

As shown in Scheme.2.1, a toehold strand displacement reaction is starting from an initially hybridized duplex, which composed of a pair of strands in different length, which are partially complementary to each other. There is a single-stranded overhang portion, named toehold portion, which is able to hybridize with external strand. The toehold strand displacement is triggered by the addition of the input strand fully complementary to toehold-included strand in the initial duplex; therefore, toehold portion firstly hybridizes with input strand followed by a strand migration process to release the pre-hybridized strand partially complementary (output strand) to the toehold-included strand. Finally, the input strand fully binds to the toehold-included strand to give the product duplex, while the output strand is single-stranded. In this toehold strand displacement reaction, input strand is the stimulus to trigger the reaction; after a strand migration process, releasing output strand is the motion occurred in the nano-environment.

By designing toehold and adding input strand, relievable and precise control of DNA behavior has been achieved.[1]

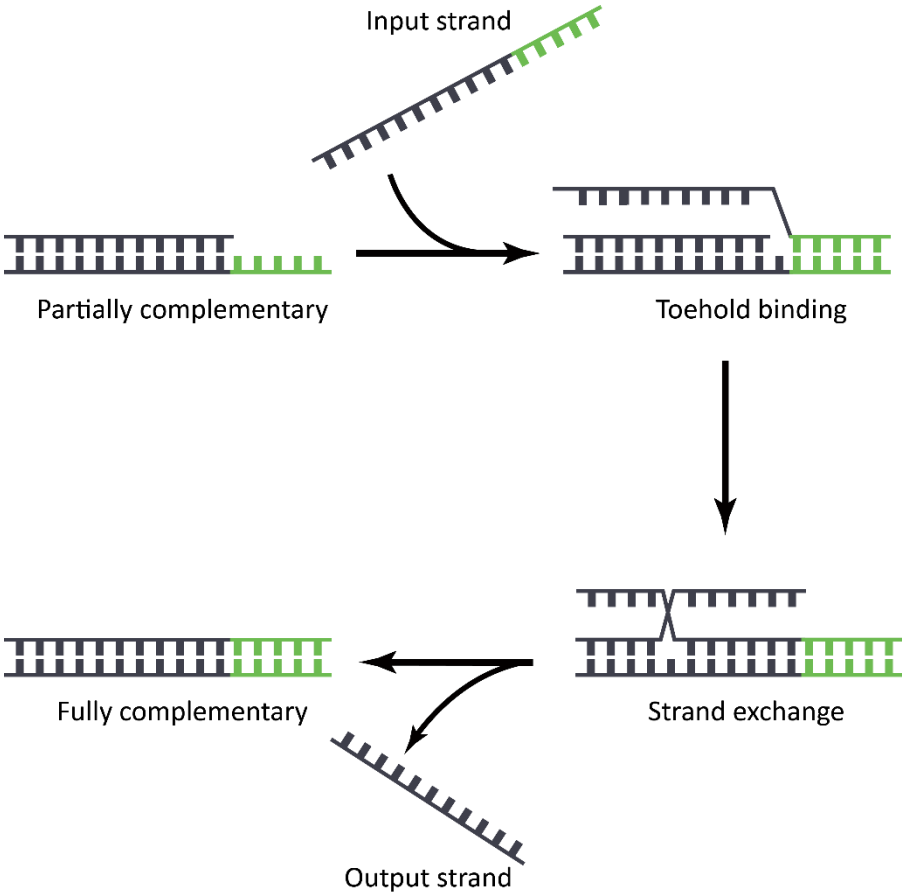

Scheme 2.1. Mechanism of toehold strand displacement. The initial duplex composes of a pair of partially complementary DNA strands to leave an overhang region, called toehold (in green color). When an input strand that is fully complementary to the toehold-included strand in initial duplex is added, the toehold strand displacement is triggered. Firstly, the input strand partially binds to the toehold portion, followed by a continuous strand exchange process that the partially complementary starnd is replaced and released as the output strand. Finally, the duplex that contains longer hybridized portion is formed.

2.1.2. Nano-devices based on toehold strand displacement

There have been various DNA nanodevices developed based on this mechanism.

The first and one of the most renowned DNA nanodevices achieving a controllable behavior was reported by B. Yurke and coworkers in 2000,[2] after which DNA started to draw more attentions not as a genetic information carrier but one kind of engineering

molecule. This nanodevice, or DNA tweezers, consists of three strands, two of which partially binds to another strand and leave toehold portions, as shown in Fig. 2.1. This is the "open" state of the DNA tweezers. When an external strand that can binds to both toehold and leave other two toeholds is added, the hybridization results in forming of a triangle structure, so called "close" of the DNA tweezers. As another external strand is added, its fully complementary binding onto the pre-added strand produces a waste duplex and reverses DNA tweezers to "open" state. In this way, reversible "close" and "open" of DNA tweezers could be regulated through alternatingly adding two strands.

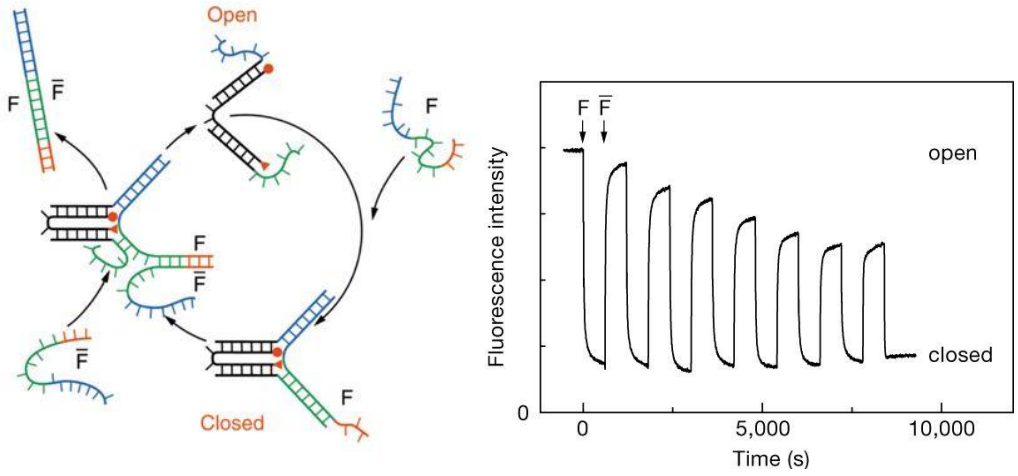

Figure 2.1. DNA tweezer that is reversibly driven by addition of two input strands. However, accumulation of waste in nano-environment resulted in a reducing efficiency after several turn over.

There are some other nano-devices involves toehold strand displacement to achieve regulatability such as a two-state DNA lattice[3] and so on.[4-6]

However, there remains problem that in every cycle of controllable change, for example in DNA tweezers case, there is a waste duplex that composed of two added strand having triggering toehold strand displacement. After several cycles, such waste duplexes accumulate in solution inducing a decreasing efficiency of further toehold strand displacements by influencing the equilibrium during toehold strand displacement.

2.2. Method

In this study, establishment of a strand displacement mechanism that efficiently responses to light irradiation is aimed. This mechanism employing one of the cleanest resources in nature, light, should be able to be applied to future development of DNA-based nanodevices and endow them accessible photo-irradiation-based controllability.

Asanuma and co-workers have demonstrated the introduction of azobenzene moieties into oligonucleotide via acyclic tetrose linkers D-threoninol could achieve efficient photo-regulation of DNA hybridizing behavior.[7-11] This is validated to be a practical solution for creating photon-fueled systems, including a photo-driven DNA strand displacement.

2.2.1. Model of controlling DNA behavior

When the control of processes/movements/devices performed in nano-scale is compared with the control of those performed in macro-scale world, the common model can be used to describe how these controls occur and how they should be designed. As a simplest example, a stimulus triggered a series of changes thereby induces a motion/transformation. In macro-scale, it could be typing the keyboard to input the sentence or turning the steering wheel to round the corner. However, when it comes to nano-scale world, this relation would not be always obvious and touchable. Since indirect and non-mechanical interactions such as static interaction or chemical interaction are main interactions among nano-processes/movements/devices, stimulus that triggers the nano-level motion should differentiate from macro-level motion.

As for DNA nanotechnology, one of the most useful interactions in designing structures or manipulating behaviors of DNA-composed objects is the complementary hybridization, based on Watson-Crick base paring rule: adenine (A) combines with thymine (T) while cytosine (C) combines with guanine (G). These strong hydrogen bonds between A/T and C/G ensure that only the two strands that perfectly match each other in sequence are allowed to hybridize efficient and form stable duplex. By programming the sequences, it is convenient

for scientist to manage the binding behaviors of DNA strands thus various structures and motions have been developed. Especially, when these nano-structures presented specific binding affinity to any input stimulus, e.g. ions, pH, DNA strands, temperature, proteins, they could be considered potential in being utilized as molecular building blocks for a nanodevice. Here, in response to addition of input stimulus, these nano-structures change in entropy- or enthalpy-driven manner to achieve the motions in nano-scale.

2.2.2. Light irradiation as stimulus to trigger the photo-controllable DNA behavior

To find a way controlling such nano-process without contaminating the nano-environment where it took place, light comes up as an alternative stimulus.

Considering employing light as the stimulus that triggers and drives the strand displacement reaction among DNA duplexes, according to the model we have proposed in 2.2.1, the binding energy advantage of result duplex against initial duplex, which is raised by irradiating light should be reasoned.

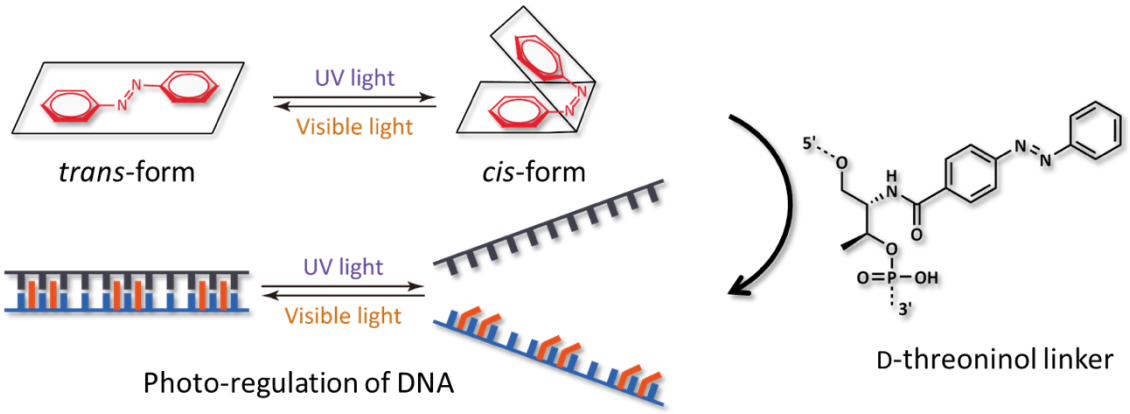

Scheme 2.2. Photo-regulation of dissociation and hybridization of DNA duplex. Photo-responsive molecule azobenzene is able to isomerize reversibly between *trans*-isomer and *cis*-isomer. Azobenzene is incorporated into DNA through a D-threoninol scaffold to endow the DNA duplex with photo-responsivity. DNA duplex tethering azobenzene moieties hybridizes when azobenzene is in *trans*-form and dissociates when azobenzene is in *cis*-form.

Asanuma and co-workers have developed a facile protocol to photo-regulate the hybridizing behavior of DNA double strands, illustrated in Scheme 2.2.[7-11] In this protocol, azobenzene molecules, which sensitively respond to light stimulus and isomerize between *trans*-isomer and *cis*-isomer, are incorporated into DNA as intercalators through D-threoninol linker. When azobenzene moieties are in *trans*-form that is a planar structure, they stack with neighbor bases and stabilize DNA duplex due to their high hydrophobicity; while azobenzene moieties isomerize to *cis*-form that is non-planer, the significantly increased steric hindrance causes the destabilization of duplex thereby dissociation of duplex can be achieved in a appropriate temperature. As isomerization of azobenzene molecule is triggered by visible irradiation (400 nm ~, *cis*-to-*trans*) and ultraviolet (UV) irradiation (~365 nm, *trans*-to-*cis*), hybridization and dissociation of azobenzene-tethered DNA double strands can be conveniently controlled by UV and visible light irradiation. Here, the change of duplex stability induced by configurational change of azobenzene moieties provides the binding energy advantage, which is able to be regulated by light stimulus.

2.2.3. Strategy of achieving photo-driven DNA strand displacement reaction

Utilizing azobenzene-incorporated oligonucleotides, we proposed the first DNA strand displacement that could be sensitively and precisely regulated by light irradiation, without contaminating nano-environment with any external chemicals, which should be able to achieve constant strand displacement performance without any decline of efficiency.

As shown in Scheme 2.3, this strategy employs three DNA strands: a Template strand (**Tem**) tagged with a quencher group at the 3‘-end; a Product strand (**Prod**) that is fully complementary in sequence with **Tem** and is tagged with a fluorophore group at the 5’-end; as well we a Modulator strand (**Mod**) that is also complementary in sequence with the **Tem** and is incorporated with several azobenzene moieties. With these three strands, we designed the photo-driven DNA strand displacement strategy.

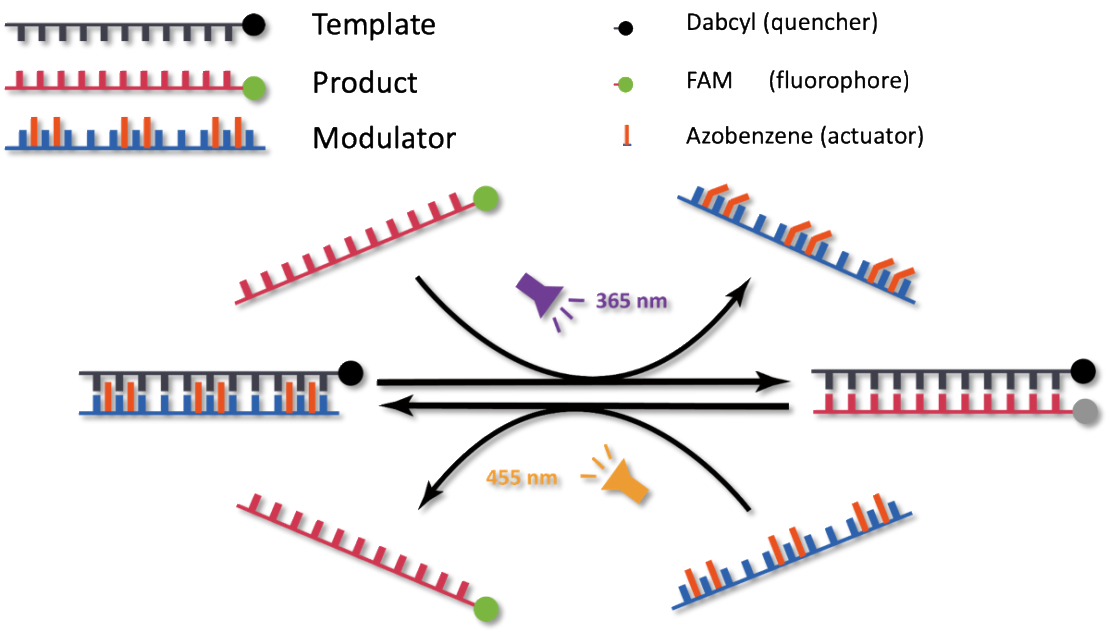

Scheme 2.3. A photo-driven DNA strand displacement without any toehold portion. Alternating irradiation with UV (365 nm) and visible light (455 nm) induced reversible strand displacement process.

In the initial state, **Tem** forms duplex with **Mod**^{trans} when azobenzene moieties are in *trans*-form. The forward strand displacement is triggered when irradiating the system with UV irradiation, inducing a *trans*-to-*cis* isomerization and destabilization of **Tem**/**Mod** duplex, resulting in the forming of **Tem**/**Prod** duplex and the release of **Mod**^{cis}. This forward strand displacement relies on the reverse of stability relation that **Tem**/**Mod**^{trans} is more stable than **Tem**/**Prod** and **Tem**/**Mod**^{cis} is less stable than **Tem**/**Prod**. The difference of duplex stability causes the energy advantage of more stable duplex, ensuring the prediction of processing direction of strand displacement reaction. To drive the reaction back to initial state, visible light is conducted to isomerize azobenzene moieties from *trans*-form to *cis*-form. This starts the backward strand displacement, in which **Mod**^{trans} hybridizes with **Tem** and release **Prod**. In this backward strand displacement process, the same stability relation that **Tem**/**Mod**^{trans} is more stable than **Tem**/**Prod** is followed to predict the formation of **Tem**/**Mod**^{trans} and dissociation of **Tem**/**Prod**.

Therefore, by alternating irradiation with UV and visible light, the reversible DNA strand displacement reaction can be regulated through the photo-induced isomerization of incorporated azobenzene moieties.

Both forward and backward strand displacement is visualized and observed through monitoring the change of fluorescence. When **Tem** binds to **Mod** thus leaves **Prod** single-stranded, fluorescence should be obtained in high level; while **Tem** binds to **Prod**, fluorescence is quenched so that low-level fluorescence should be obtained. By monitoring the change of fluorescence level, the strand displacement reaction can be observed if it works as strategy designed.

2.2.4. Cationic chaperon polymer as accelerator

Maruyama and co-workers have reported a novel polymer, poly(L-lysine)-*graft*-dextran (PLL-*g*-Dex),[12-13] which is a copolymer composed of positive-charged poly(L-lysine) backbone and hydrophilic dextran side chain, as shown in Fig. 2.2. This cationic polymer to present outstanding binding affinity to DNA duplex like and enhance the stability of duplex by alleviating the counterion condensation,[14] which is shown in Scheme 2.4.

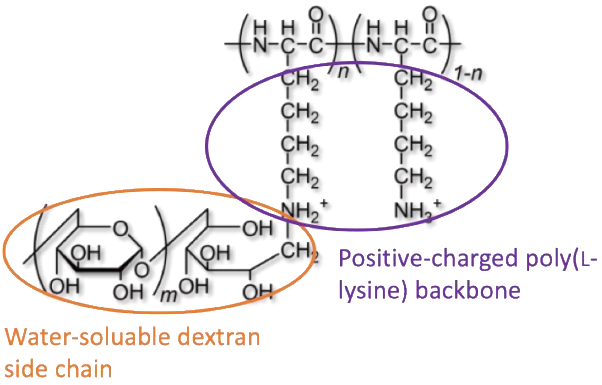

Figure 2.2. Chemical structure of PLL-*g*-Dex. It contains poly(L-lysine) backbone that is positive-charged so that neutralizes the negative charges of DNA backbone by forming complex with DNA. Water-soluble side chain is introduced to increase the solubility of polymer-DNA complex in solution.

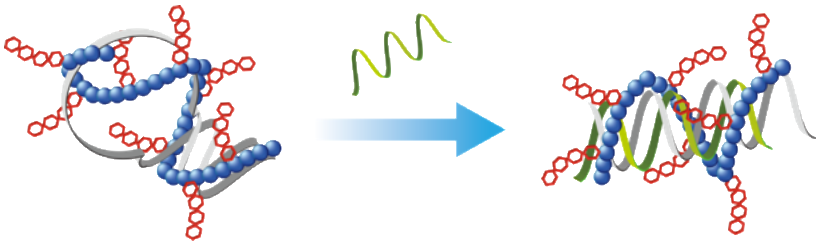

Scheme 2.4. PLL-*g*-Dex forms complex with DNA through static interaction thus negative-charged DNA phosphate backbone is neutralized. This neutralization effectively inhibiting the counterion condensation to encourage approaching of DNA strands with each other.

Accelerating strand displacement by 50000 folds.

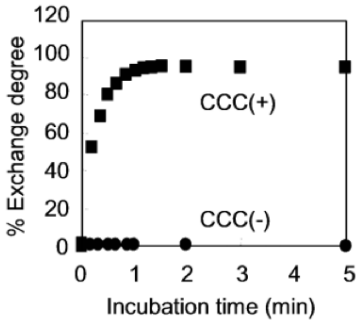

Figure 2.3. Participation of PLL-*g*-Dex significantly improves the speed of DNA strand displacement to a 5 x 10^4 folds. During this process, addition of PLL-*g*-Dex alleviates the counterion condensation to decrease the energy barrier for a toeholdless DNA strand displacement.

What's more, it is reported to highly accelerate the DNA strand displacement by 50000 folds (Fig. 2.3).[14-15]

With employment of PLL-*g*-Dex, kinetic property of the photo-driven DNA strand displacement is expected to be enhanced.

2.3. Thermodynamic and kinetic studies

In this method, azobenzene-tethered oligonucleotides and PLL-*g*-Dex are employed to construct the photo-driven and toehold-less DNA strand displacement. The thermodynamic and kinetic studies are conducted to firstly research the feasibility of both forward strand displacement and backward strand displacement.

For this research, 22-mer **Tem** was synthesized and a 4-([4-(Dimethylamino)phenyl]azo)benzoic (Dabcyl) group was labeled onto its 3'-end as quenchers. 22-mer complementary **Prod** was synthesized tagged with carboxyfluorescein (FAM) as fluorophores. As for **Mod**, six unmodified azobenzene moieties (**umAzo**) were introduced into the sequence, so called **Mod-6um**. Sequences are shown in Table 2.1.

Table 2.1. Sequences used in thermodynamic and kinetic studies

	Sequence
Tem	5'-GTT ACG CAT CGG TGC TAG ATC G-3'
Prod	3'-CAA TGC GTA GCC ACG ATC TAG C-5'
Mod-6um	3'-CAA**X**TGC**X**GTA**X**GCCA**X**CGA**X**TCT**X**AGC-5'

X=unmodified azobenzene moiety

2.3.1. Thermodynamic study

The thermodynamics of photo-driven DNA strand displacement is evaluated by melting temperatures (T_ms) measurement.

T_ms of **Tem**/**Mod**^{trans} duplex, **Tem**/**Mod**^{cis} duplex and **Tem**/**Prod** duplex are measured by monitoring a changing UV-vis absorbance against temperature, as shown in Table 2.2.

Table 2.2. Melting temperature (T_m) of **Tem**/**Mod** duplex and **Tem**/**Prod** duplex

	T_m/°C[a]	
	trans-	*cis*-
Tem/Prod	74.3	
Tem/Mod-6um	77.0	N.A.

[a] Conditions: 1 μM each duplex, 100 mM NaCl, 10 mM phosphate buffer (pH 7.0), PLL-*g*-Dex (N/P=2). When *trans*-T_m of **Tem**/**Mod** is measured, solution containing DNA duplex is firstly incubated at 90°C for 10 min to convert as much azobenzene into *trans*-form. When *cis*-T_m of **Tem**/**Mod** is measured, solution containing DNA duplex is irradiated with UV light (365 nm) for 10 min at 60 °C to isomerize as much azobenzene into *cis*-form. Temperature change in annealing process is 1°C / min.

Result of measurement shows a higher T_m of **Tem**/**Mod-6um** duplex in *trans*-form than the T_m of **Tem**/**Prod** duplex (74.3 °C), indicating **Tem**/**Mod-6um**^{trans} duplex is more stable than **Tem**/**Prod** duplex, as expected. Besides,when azobenzene moieties isomerize to *cis*-form, T_m of **Tem**/**Mod-6um** was not observed from the absorbance measurement, suggesting its T_m is much lower than expected. This reveals the much lower stability of **Tem/Mod-6um**^{cis} duplex than it of **Tem**/**Prod** duplex.

Since duplex stability directly reflects the binding energy of two DNA strands during hybridizing behavior, as expected in section 2.2.4, **Tem**/**Prod** duplex has binding energy advantage rather than **Tem**/**Prod** duplex in the forward strand displacement while **Tem**/**Prod** duplex has binding energy advantage rather than **Tem/Mod-6um**^{cis} in the backward strand displacement.

From this result, it can be concluded that both of the strand displacements are thermodynamically beneficial. Light irradiation is able to control the thermodynamic property of a reversible strand displacement reaction.

2.3.2. Kinetic study

Though melting temperature measurement suggests a thermodynamic feasibility of the photo-driven strand displacement reaction, strand displacement speed still decides if this method occurs in an appropriate manner. Therefore, kinetic properties of both forward and backward strand displacements are investigated by a fluorescence monitoring experiment. In this experiment, effect of accelerator PLL-*g*-Dex was examined as well through conducting the same trial on control samples without PLL-*g*-Dex.

Design of kinetic experiments are shown in Scheme 2.5. To research the forward strand displacement, **Mod** that is pre-irradiated with UV light to isomerize as many as azobenzene moieties to *cis*-form is added to a sample containing pre-hybridized **Tem**/**Prod** duplex. There should be no strand displacement, indicated by no fluorescence change, according to the thermodynamic result. To research the backward strand displacement, **Mod** that is pre-incubated at 90 ^{o}C to isomerize as many as azobenzene moieties to *trans*-form is added to a sample containing pre-hybridized **Tem**/**Prod** duplex. According to the previous thermodynamic study, there should be an increase of fluorescence due to the release of **Prod**. The strand displacement can be evaluated by the increasing speed of fluorescence.

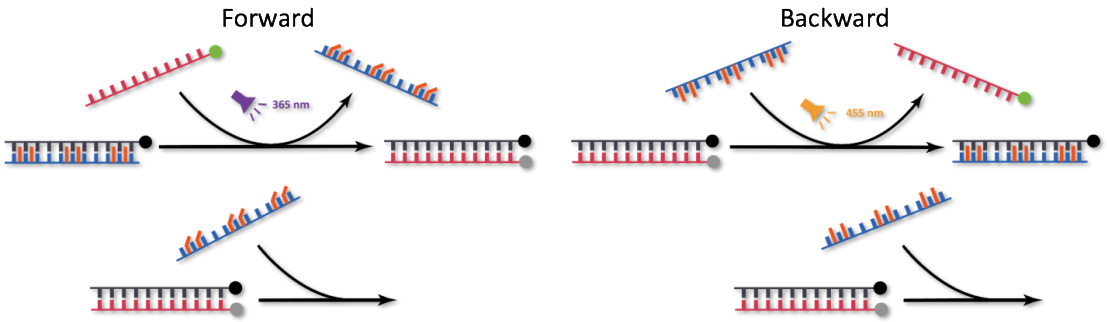

Scheme 2.5. Reversible photo-driven DNA strand displacement reaction is divided into a forward strand displacement process and a backward strand displacement process to be separately studied. Both two processes are photo-driven.

The result is shown in Fig. 2.4. After the addition of **Mod-6um**^{cis} to **Tem**/**Prod**, only slight increase was observed (Fig. 2.4a), suggesting there was almost no strand displacement occurred. This means that forward strand displacement is feasible kinetically. Differently, as

shown in Fig. 2.4b, there was a rapid increase of fluorescence after adding **Mod-6um**^{trans} to **Tem**/**Prod**, indicating an backward strand displacement processed as expected. Especially, the strand displacement reached equilibrium within 3 minutes, demonstrating very efficient initialization and performance of the strand displacement.

a.

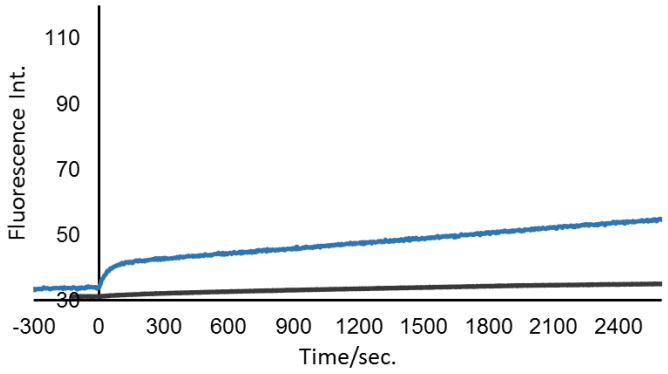

b.

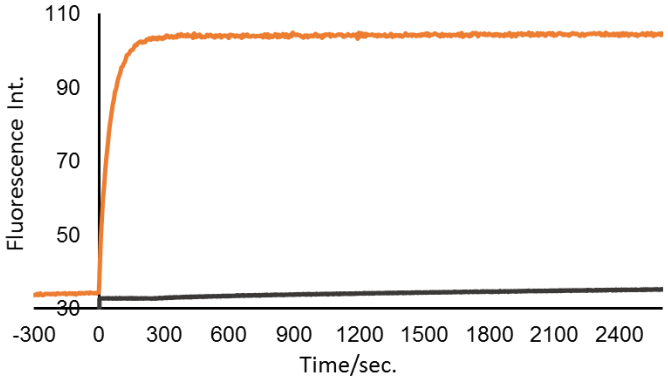

Figure 2.4. Time course of invasion of (a) **Mod-6um**^{cis} and (b) **Mod-6um**^{trans} into the **Tem**/**Prod** duplex. Blue and orange curves indicate the reaction in the presence of PLL-*g*-Dex, while grey curve is in the absence of PLL-*g*-Dex. Conditions: 1 µM **Tem**, 1 µM **Prod**, 1 µM **Mod-6um**, 100 mM NaCl, 10 mM phosphate buffer (pH 7.0), PLL-*g*-Dex (N/P=2), 50 °C.

Moreover, in both forward and backward strand displacements, additions of **Mod** did not induce any fluorescence change in the absence of PLL-*g*-Dex (gray curve). Initial strand displacement reaction constant (k_i) of backward strand displacement in the presence or absence of PLL-*g*-Dex was calculated to compare the strand displacement speed. The calculation is shown in Table 2.3. According to the result, backward strand displacement reaction is initialized in a 750-folds accelerated speed with the assistance of PLL-*g*-Dex, indicating the necessity of adding PLL-*g*-Dex to initialize and accelerate the toehold-less strand displacement.

From above results, it can be concluded that both forward and backward strand displacements are kinetically feasible.

Table 2.3. Initial strand displacement reaction constant (k_i) of backward strand displacement

	Without PLL-*g*-Dex	With PLL-*g*-Dex
Initial rate constant k_i	4.0×10^{-6}	1.5×10^{-3}

2.4. Investigation of Modulator

The alternating irradiation was conducted to examine the reversible DNA photo-driven strand displacement reaction. Standard procedures were followed to evaluate and compare the performance of each photo-driven strand displacement process.

Basically, sample is first set at initial state followed by UV light irradiation and measurement of fluorescence spectra. Then the sample is irradiated with visible light followed by measuring fluorescence spectra again. This is defined as one cycle.

To quantify the extent of strand displacement reactions, the relative amount of dissociated **Prod**, referred to as Dissociated Prod (*DP*), was evaluated based on fluorescence intensity using the following equation:

$$\text{Dissociated Prod } (DT) = (F_x - F_q) / (F_i - F_q)$$

DP here is defined as how many percentages of **Prod** is in single strand out of all **Prod** in the system. F_x is the fluorescent emission intensity measured after each irradiation at 520 nm referring to the emission of FAM group. F_q is the fluorescent emission intensity of sample containing equal equivalent of **Tem** and **Prod** so that only hybridized **Prod** should exist and fluorescence should be quenched. F_i is the fluorescent emission intensity of sample containing only **Prod** in equal equivalent with sample used in measuring F_q, which should be the maximum fluorescence when all **Prod** exists as single strand status.

With the above equation, fluorescence spectra were transformed into bar charts as shown below, Fig. 2.5. For a single alternating irradiation experiment including once UV light irradiation and once visible light irradiation, there are two bars presented in stripped pattern and solid pattern, referring to *DP* obtained after UV light irradiation (DP_{UV}, solid bar, after forward strand displacement) and after visible light irradiation (DP_{vis}, stripped bar, after backward strand displacement). In the theoretical case, DP_{UV} should be 0% while DP_{vis}

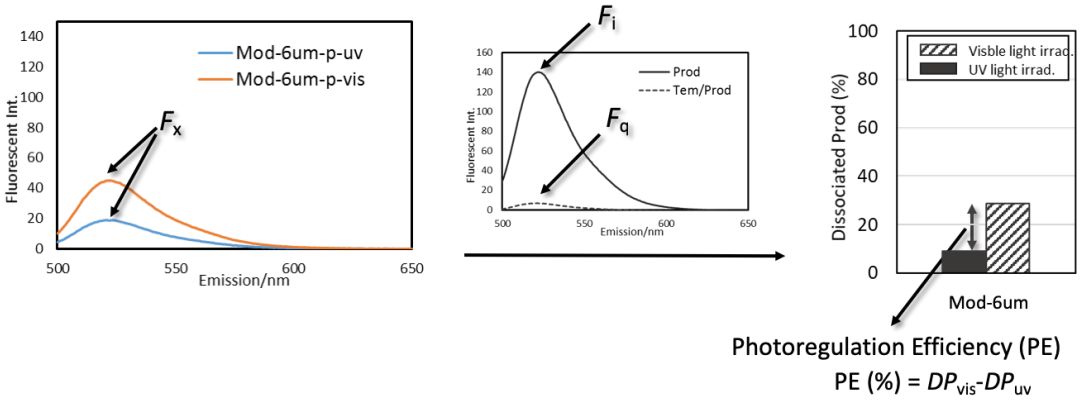

Figure 2.5. Fluorescence spectra of photo-regulation of strand displacement with **Mod-6um**. It shows how to calculate the Dissociated Prod (*DP*) and Photoregulation Efficiency (*PE*) in order to transform fluorescence spectra to bar chart. F_x is the fluorescent emission intensity measured after each irradiation at 520 nm referring to the emission of FAM group. F_q is the fluorescent emission intensity of sample containing equal equivalent of **Tem** and **Prod** so that only hybridized **Prod** should exist and fluorescence should be quenched. F_i is the fluorescent emission intensity of sample containing only **Prod** in equal equivalent with sample used in measuring F_q, which should be the maximum fluorescence when all **Prod** exists as single strand status.

should be 100%, indicating complete of both forward and backward strand displacements.

Through transforming exact fluorescent intensity into *DP* value, the extent of each strand displacement after UV or visible light irradiation can be compared. To evaluate efficiency of the whole reversed strand displacement system, the difference between DP_{vis} and DP_{UV} is defined as Photoregulation Efficiency (*PE*):

$$\text{Photoregulation efficiency } (PE) = DP_{vis} - DP_{UV}$$

PE reflects the ability for a photo-strand displacement reaction to achieve both forward strand displacement and backward strand displacement upon UV/visible light irradiaiton, i.e., an ideal system should show higher DP_{vis} and lower DP_{UV} simultaneously to give higher *PE*.

To improving the efficiency of photo-driven DNA strand displacement or *PE*, enhancement of both forward and backward strand displacement respectively is necessary. This is directly reflected in the increase of DP_{vis} and decrease of DP_{UV}.

If separately looking into the mechanisms of these two processes, researching factors that influence on the mechanisms should give the answer to how generally *PE* can be improved.

As discussed in section 2.2.3, with the incorporation of azobenzene moieties, stability of DNA double helix is enhanced when azobenzenes are in *trans*-form due to the stacking effect by increase of hydrophobicity; while the duplex is destabilized when azobenzenes are in *cis*-form due to the increase of steric hinderance. Since the stability of duplexes in photo-driven DNA strand displacement reaction determines the performance of thermodynamics of each forward and backward strand displacement processes, it can be reasoned that increase of stacking effect in *trans*-form should benefit backward strand displacement while increase of steric hindrance in *cis*-form should benefit forward strand displacement, both of which improve the efficiency of photo-regulation.

There are two factors, chemical modification of azobenzene and incorporating number of azobenzene moiety, considered crucial to properties of azobenzene relating to stacking effect and steric hindrance.

They are individually investigated through experiments in 2.4.1 and 2.4.2.

2.4.1. Chemical modification of azobenzene

According to previous research,[16-17] *ortho*-methylation of benzene ring away from linker strongly change the isomerizing behavior, thermostability, stacking effect and steric hindrance of azobenzene moieties, thereby to influence the efficiency of photo-responsive DNA hybridizing behavior.

This is summarized in the following Fig. 2.6.

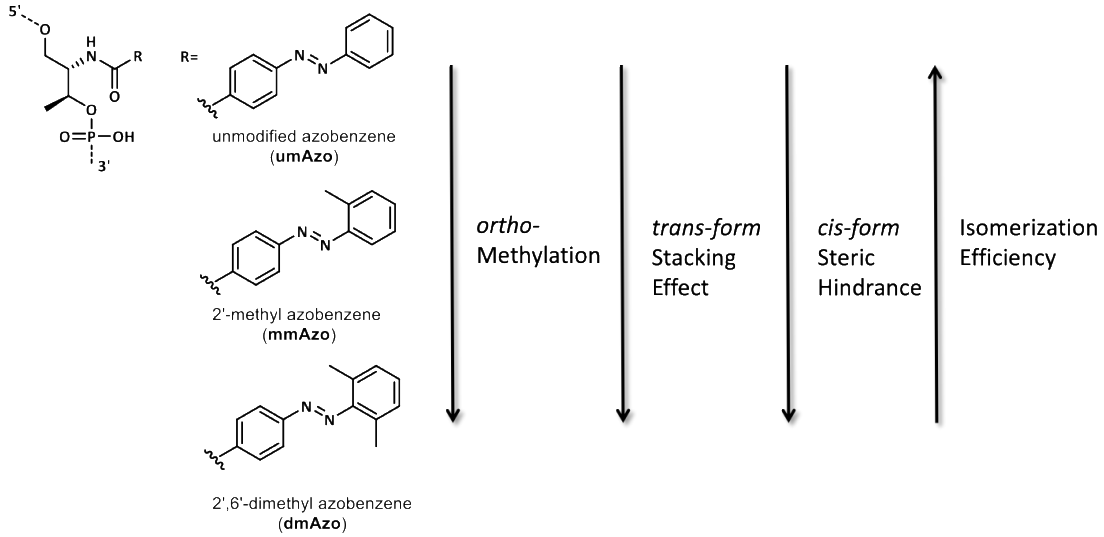

Figure 2.6. Azobenzene with further *ortho*-methylation on its 2'- and 6'-position shows an enhanced stacking effect in *trans*-form and steric hindrance in *cis*-form, whereas the isomerization efficiency is lowered. This change of property influences the photo-regulation of azobenzene-tethered DNA duplex.

With the further methylation of azobenzene (2'-methylation and 2',6'-dimethylation), azobenzene presents higher stacking effect in *trans*-form because of the introduction of hydrophobic substitutes, methyl groups. The increase of hydrophobicity further stabilizes DNA duplex and benefits the hybridization of double strands when azobenzene derivatives are in *trans*-form. On the other hand, introduction of bulky methyl groups also increases the steric hindrance of moieties when azobenzene derivatives are in a non-planer *cis*-form, which results in the destabilization of DNA duplex and inhibits the hybridization of double strands. These enhancement of stability of duplex when azobenzene derivatives are in *trans*-form and

alleviation of stability of duplex when azobenzene derivatives are in *cis*-form, are expected to improve backward and forward strand displacements respectively, and finally achieving an increment of efficiency of photo-driven strand displacement in total.

However, it should also be pointed out that *ortho*-methylation on 2'- and 6'- inhibits the isomerization of azobenzene derivatives from *trans*-form to *cis*-form. This is the emulative inhibition of efficient forward strand displacement so that balanced result should be obtained.

Monomers of three azobenzene derivatives, unmodified azobenzene (**umAzo**), 2'-methyl azobenzene (**mmAzo**) and 2',6'-dimethyl azobenzene (**dmAzo**), were synthesized and incorporated into **Mod** as **Mod-6um**, **Mod-6mm** and **Mod-6dm**, as shown in Table 2.4.

With three **Mod**s tethering different azobenzene derivatives, melting temperatures of **Tem**/**Mod** are firstly measured to compare their thermodynamic property. The result is shown in Table 2.5.

Table 2.4. Sequences of **Mod** tethering **umAzo**, **mmAzo** and **dmAzo**

	Sequence
Tem	5'-GTT ACG CAT CGG TGC TAG ATC G-3'
Mod-6um	3'-CAA**X**TGC**X**GTA**X**GCCA**X**CGA**X**TCT**X**AGC-5'
Mod-6mm	3'-CAA**Y**TGC**Y**GTA**Y**GCCA**Y**CGA**Y**TCT**Y**AGC-5'
Mod-6dm	3'-CAA**Z**TGC**Z**GTA**Z**GCCA**Z**CGA**Z**TCT**Z**AGC-5'

X=unmodified azobenzene moiety (**umAzo**)

Y=2'-methyl azobenzene moiety (**mmAzo**)

Z=2',6'-dimethyl azobenzene moiety (**dmAzo**)

Table 2.5. Melting temperature (T_m) of **Tem**/**Mod** duplex tethering three azobenzene derivatives

	T_m/°C[a]	
	trans-	*cis*-
Tem/Prod	74.3	
Tem/Mod-6um	77.0	N.A.
Tem/Mod-6mm	82.0	N.A.
Tem/Mod-6dm	84.5	N.A.

[a] Conditions: 1 μM each duplex, 100 mM NaCl, 10 mM phosphate buffer (pH 7.0), PLL-*g*-Dex (N/P=2). When *trans*-T_m of **Tem**/**Mod** is measured, solution containing DNA duplex is firstly incubated at 90°C for 10 min to convert as much azobenzene into *trans*-form. When *cis*-T_m of **Tem**/**Mod** is measured, solution containing DNA duplex is irradiated with UV light (365 nm) for 10 min at 60 °C to isomerize as much azobenzene into *cis*-form. Temperature change in annealing process is 1°C / min.

Similar to previous T_m data in section 2.3.1, T_ms of all three **Tem**/**Mod**^{trans} duplexes are higher than it of **Tem**/**Prod** duplex, while T_ms of **Tem**/**Mod**^{cis} duplexes are not observed. Furthermore, with the further methylation on 2'- and 6'- of azobenzene molecule from **umAzo** to **dmAzo**, melting temperatures increased.

This result is coincident with previous research, suggesting an increasing stability of **Tem**/**Mod**^{trans} due to the increasing stacking effect of azobenzene derivatives moieties brought by the methyl group modified on *ortho*-position of benzene ring. This increased stability should enhance the backward strand displacement as expected thermodynamically.

Though the enhanced steric hindrance cannot be verified since melting temperatures of all **Tem**/**Mod**^{cis} duplexes were not observed. It is still obvious that **Tem**/**Mod**^{cis} duplexes could not form due to the strong destabilizing effect caused by steric hindrance.

Next, kinetic properties of photo-driven DNA strand displacement employing three **Mod** were studied by the same experiments in section 2.3.2: adding pre-irradiated **Mod** to the sample containing pre-hybridized **Tem**/**Prod** duplex. The reaction speed is evaluated by monitoring the change of fluorescent emission intensity of FAM group at wavelength of 520 nm. The results are shown in Fig. 2.7.

a.

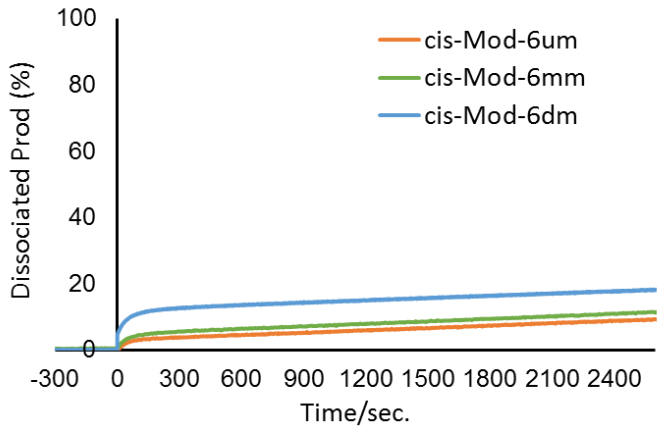

b.

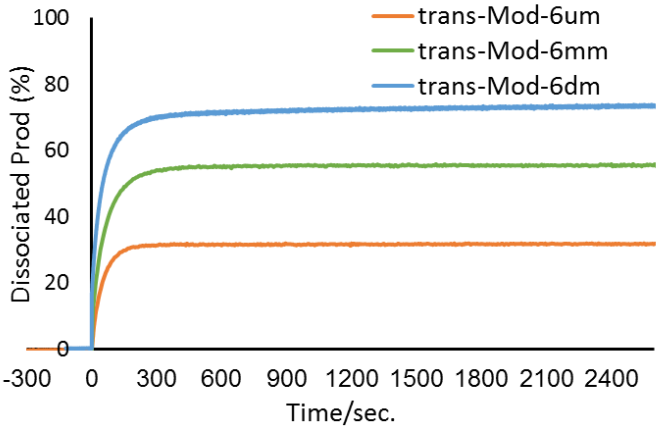

Figure 2.7. Time course of invasion of (a) **Mod**^{cis} and (b) **Mod**^{trans} into the **Tem**/**Prod** duplex. Orange, green and blue curves indicate the reaction with **Mod-6um**, **Mod-6mm** and **Mod-6dm** respectively. Conditions: 1 μM **Tem**, 1 μM **Prod**, 1 μM **Mod**, 100 mM NaCl, 10 mM phosphate buffer (pH 7.0), PLL-*g*-Dex (N/P=2), 50 °C.

The amount of displaced **Prod** depended on the azobenzene derivative presenting in the **Mods**. From Fig. 2.7a, all three **Mod**^{trans} triggered the backward strand displacement in rapid initiating speed and in all three cases strand displacements reached equilibrium within 3 minutes. Moreover, the *DP*s at equilibruim in all three strand displacements achieved by adding **Mod**^{trans} showed dependency on methylation, in coincident tendency with melting temperature measurements: the strand diaplacement driven by **dmAzo**-tethered **Mod-6dm** reached the best equilibrium (highest DP_{vis}). Meanwhile, there is almost no strand displacement triggered by the addition of **Mod**^{cis}, agreeing with the melting temperature measurement as well.

After confirming the thermodynamic and kinetic properties are as expected: *ortho*-methylation may improve the efficiency of photo-driven strand displacement, the alternating irradiaiotn experiment was conducted to compared the *DP* and *PE* of assays employing three different **Mod**. The result is shown in Fig. 2.8.

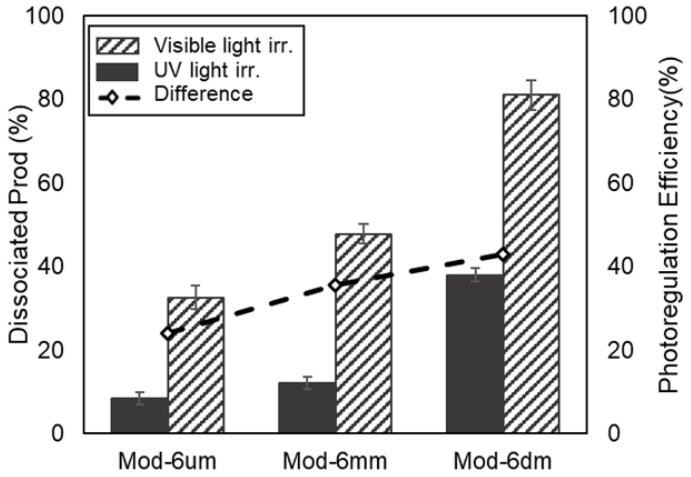

Figure 2.8. Photo-driven strand displacement mediated by modulator strands **Mod-6um**, **Mod-6mm**, and **Mod-6dm** tethering different azobenzene derivatives. Solid bars show DP_{UV}s after UV light irradiation and striped bars show DP_{vis}s after visible light irradiation. Open diamonds represent the photoregulation efficiency (*PE*) of strand displacement, which is the difference between values of solid bars and striped bars. Conditions: 1 μM **Tem**, 1 μM **Prod**, 1 μM **Mod**, 100 mM NaCl, phosphate buffer (pH 7.0), PLL-*g*-Dex (N/P=2), 50 °C.

In Fig. 2.8, left vertical axis referring to bar chart labeled the *DP* of each experiments, and right vertical axis referring to dashed curve labeled the *PE* of each experiments. Stripped bars show DP_{vis} values that indicate efficiency of backward strand displacement while solid bars show DP_{UV} values indicating efficiency of forward strand displacement. Open diamonds represents the *PE* of each trials.

First, DP_{UV} was measured after UV light irradiation of a solution of **Tem**/**Mod**^{trans} duplex and **Prod**. In the experiments that employed **Mod-6um** and **Mod-6mm**, DP_{UV} is around 10%, which correlates with the percentage expectation based on the performance of the forward strand displacement (Fig. 2.7b). In contrast, DP_{UV} obtained in the **Mod-6dm**-participated experiment is 38%, the lowest strand displacement efficiency induced by UV irradiation among the azobenzene derivatives tested in this study. I next irradiated samples with visible light, which induced reversion of azobenzene derivatives moieties to the *trans*-form. Since almost complete cis-to-trans isomerization was obtained upon visible light irradiation, the DP_{vis} value obtained in each experiment employing different azobenzene derivatives coincided well with that at equiliburium (Fig. 2.7a).

As for the total efficiency of photo-driven DNA strand displacement, among the tested azobenzene derivatives, trial with **Mod-6dm** tethering **dmAzo** moieties shows the highest *PE* value at 43% (trials with **Mod-6um** and **Mod-6mm** are 24% and 36%, respectively) because high displacement efficiency of backward starnd displacement compensates for low efficiency of forward strand displacement. As expectation, an increasing *PE* tendency is obtained from **Mod-6um**-participated photo-driven strand displacement to **Mod-6dm**-participated one, which is in agreement with thermodynamic and kinetic studies. Importantly, a significant increased DP_{vis} was observed, suggesting **dmAzo**-tethered **Mod-6dm** effectively improved the efficiency of backward strand displacement.

However, against expectation, DP_{UV} of alternating irraidiation experiment employing **Mod-6dm** also increased greatly thus distubed the further enlargement of *PE*. This might be caused by the inefficient isomerizaion of **dmAzo** from *trans*-form to *cis*-form in duplex. Generally, UV-induced *trans*-to-*cis* isomerizaiton occurred much more efficiently when

azobenzene moieties are in single strand comparing with those in hybridized double strands. This is due to the more limited space in duplex to restrict the convertion of benzene rings. **dmAzo** that are modified by two bulky methyl group especially is inluenced by such inhibition of convertion in DNA duplex. What's more, the addition of PLL-*g*-Dex further stablizes the duplex so that increased the energy barrier for azobenzene moieties to isomerize from *trans*-form to *cis*-form. The increase of DP_{UV} is considered a comprehensive consequence by above effects. This inference can also explane the lower DP_{UV} obtained in kinetic study in Fig. 2.7b: the isomerization of azobenzene derivatives moieties was induced by being pre-irradiated in a single-stranded **Mod** before adding to the sample to trigger the reaction, which should achieve a higher isomerizing rate compared with it in alternating irradiation experiment.

To conclude, 2',6'-dimethyl azobenzene (**dmAzo**) improved the *PE* by stabilizing **Tem**/**Mod**^{trans} duplex to boost the backward strand displacement. However, undesirable increase of DP_{UV} was observed probably due to the combined effect of inhibited isomerization and too strong stabilization caused by the addition of PLL-*g*-Dex.

2.4.2. Incorporating quantity of azobenzene derivatives

One of the other important factor that may influence the efficiency of photo-driven DNA strand displacement is the number of azobenzene derivatives moieties that are incorporated into **Mod**.[18]

As shown in Scheme 2.6, it is easy to reason that incorporating more moieties may affect the strand displacement reactions in the same way as *ortho*-methylation of azobenzene does, since more azobenzene derivatives moieties generate higher stacking effect in *trans*-form due to the existence of more hydrophobic benzene rings; they meanwhile engender higher steric hindrance in *cis*-form to destabilize the duplex.

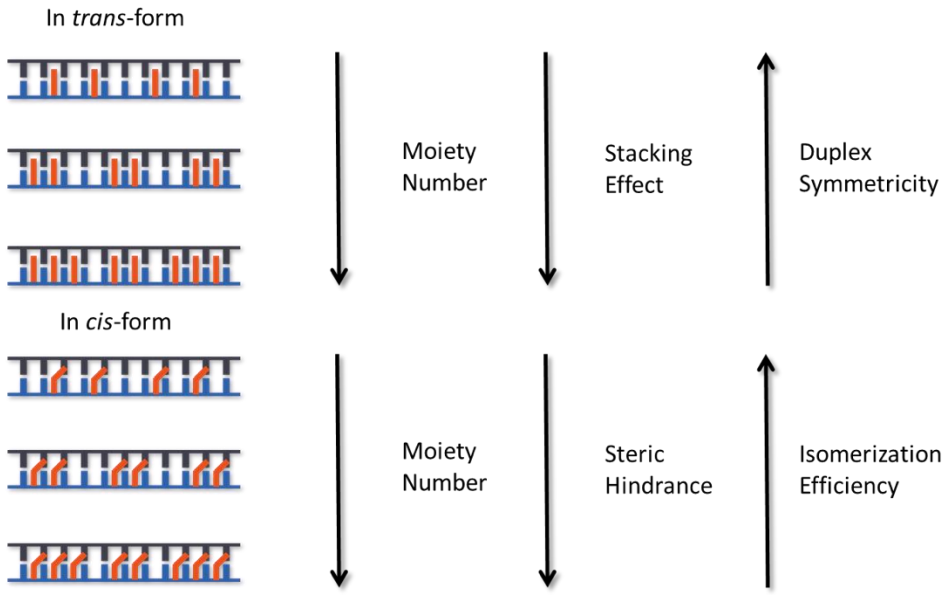

Scheme 2.6. Incorporation of more **dmAzo** moieties shows an enhanced stacking effect in *trans*-form and steric hindrance in *cis*-form, whereas the isomerization efficiency is lowered due to the restricted steric environment. This change of modulator property influences the photo-regulation of azobenzene-tethered DNA duplex.

However, previous research suggests that duplex loses its symmetricity with more azobenzene moieties introduced into one of the strands. Too many intercalators between native Watson-Crick base pairs seriously twists the double helical structure, which decreases the stability of duplex.

These two antagonistic effects in photo-regulated binding behavior of DNA strands should achieve a balanced status with appropriate incorporating numbers of azobenzene derivatives moieties, therefore achieving the highest efficiency of photo-driven DNA strand displacement.

To figure out the appropriate incorporating number of azobenzene derivatives moieties into **Mod**, I designed three **Mod**: **Mod-4dm** tethering four **dmAzo** moieties, **Mod-6dm** tethering six **dmAzo** moieties and **Mod-8dm** tethering eight **dmAzo** moieties, as shown in Table 2.6.

Table 2.6. Sequences of **Mod** tethering four, six and eight **dmAzo** moieties

	Sequence
Tem	5'-GTT ACG CAT CGG TGC TAG ATC G-3'
Mod-4dm	3'-CAAT**Z**GCGTA**Z**GCCA**Z**CGATC**Z**TAGC-5'
Mod-6dm	3'-CAA**Z**TGC**Z**GTA**Z**GCCA**Z**CGA**Z**TCT**Z**AGC-5'
Mod-8dm	3'-CA**Z**ATG**Z**CG**Z**TAG**Z**CC**Z**ACG**Z**AT**Z**CTA**Z**GC-5'

Z=2',6'-dimethyl azobenzene moiety (**dmAzo**)

With three **Mod**s tethering four, six and eight **dmAzo** moieties, the melting temperatures of **Tem**/**Mod** duplexes were measured to compare the stability of each duplex. The result is shown in Table 2.7.

Table 2.7. Melting temperature (T_m) of **Tem**/**Mod** duplex four, six and eight **dmAzo** moieties

	T_m/°C[a]	
	trans-	*cis*-
Tem/Prod	74.3	
Tem/Mod-4dm	79.5	N.A.
Tem/Mod-6dm	84.5	N.A.
Tem/Mod-8dm	77.0	N.A.

[a] Conditions: 1 μM each duplex, 100 mM NaCl, 10 mM phosphate buffer (pH 7.0), PLL-*g*-Dex (N/P=2). When *trans*-T_m of **Tem**/**Mod** is measured, solution containing DNA duplex is firstly incubated at 90°C for 10 min to convert as much azobenzene into *trans*-form. When *cis*-T_m of **Tem**/**Mod** is measured, solution containing DNA duplex is irradiated with UV light (365 nm) for 10 min at 60 °C to isomerize as much azobenzene into *cis*-form. Temperature change in annealing process is 1°C / min.

Similar to previous T_m data in section 2.3.1 and 2.4.2, T_ms of all three **Tem**/**Mod**^{trans} duplexes are higher than it of **Tem**/**Prod** duplex, while T_ms of **Tem**/**Mod**^{cis} duplexes are not observed. Importantly, T_m of **Tem**/**Mod-6dm**^{trans} duplex remains the highest, suggesting the highest duplex stability with six **dmAzo** incorporated.

To indicate, when less than six **dmAzo** moieties are introduced into 22-mer **Mod**, stabilization by stacking effect has advantage over destabilization due to the loss of symmetricity so that continuous incorporation of **dmAzo** moieties stabilizes the duplex; however, when more than six **dmAzo** moieties are introduced into **Mod**, the increase of stacking effect cannot compensate for the too much twisted double helical structure and too much lost symmetricity, inducing the destabilization of the **Tem**/**Mod**^{trans} duplex.

Consistent result was revealed by alternating irradiation experiment on photo-driven DNA strand displacement reaction hiring **Mod-4dm**, **Mod-6dm** and **Mod-8dm**, as shown in Fig. 2.9.

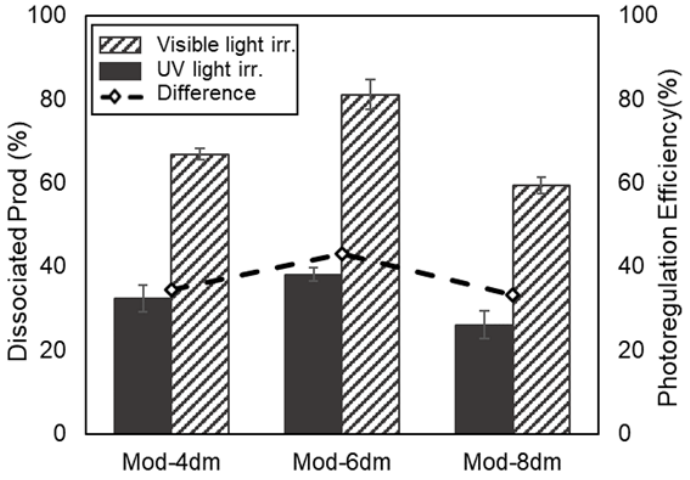

Figure 2.9. Photo-driven strand displacement mediated by modulator strands tethering different numbers of **dmAzo**. Solid bars show DP_{UV}s after UV light irradiation and striped bars show DP_{vis}s after visible light irradiation. Open diamonds represent the Photoregulation Efficiency (*PE*) of strand displacement. Conditions: 1 μM **Tem**, 1 μM **Prod**, 1 μM **Mod**, 100 mM NaCl, phosphate buffer (pH 7.0), PLL-*g*-Dex (N/P=2), 50 °C.

The highest *PE* reached when six **dmAzo** moieties are incorporated into **Mod-6dm** demonstrated the balanced relationship of antagonistic two effects mentioned above. Moreover, the change of DP_{UV} and DP_{vis} shows the same trend with *PE*, suggesting a collaborative relationship between stacking effect and steric hindrance with changing the incorporating number of **dmAzo** moieties.

2.5. Influence of chaperon polymer PLL-*g*-Dex

The above results indicate that the stabilization of **Tem/Mod**^{trans} duplex is not the sole contributor to the efficient strand displacement because strongly stacked **dmAzo** in the duplex retards *trans*-to-*cis* isomerization and suppresses forward strand displacement process.

To investigate how the addition of PLL-*g*-Dex affects the strand displacement processes, I conducted the polymer control experiment to compare the efficiency of photo-regulation in the presence or absence of PLL-*g*-Dex.

The result is as shown in Fig. 2.10.

Compared with the photo-driven strand displacement that almost did not occur in the absence of PLL-*g*-Dex, the backward strand displacement presented an over 70% increase in DP_{vis}. This enhancement indicates the predominant accelerating effect of participation of PLL-*g*-Dex into the reaction. However, I also found an increase of DP_{UV} in the absence of PLL-*g*-Dex, which suggested an undesirable inhibition of forward strand displacement. This is probably due to the inefficient isomerization of **dmAzo** moieties from *trans*-form to *cis*-form.

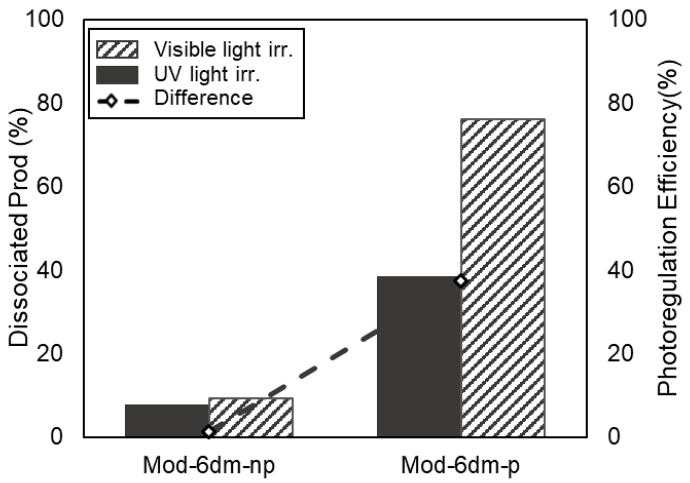

Figure 2.10. Photo-driven DNA strand displacement occurred in the absence or presence of PLL-*g*-Dex. Solid bars show DP_{UV}s after UV light irradiation and striped bars show DP_{vis}s after visible light irradiation. Open diamonds represent the Photoregulation Efficiency (*PE*) of strand displacement. Conditions: 1 μM **Tem**, 1 μM **Prod**, 1 μM **Mod**, 100 mM NaCl, phosphate buffer (pH 7.0), PLL-*g*-Dex (N/P=2 (p) or none (np)), 50 °C.

However, looking back to Fig. 2.7b, when **Mod-6dm**^{cis} was added to a sample containing pre-hybridized **Tem**/**Prod** duplex, the *DP* was only 15% or so, compared to a 38% DP_{UV} in alternating irradiation experiment. The reason of this inconsistency is reasoned to be the different steric environments for **dmAzo** moieties in two experiments. In the kinetic test, **Mod-6dm** was irradiated beforehand in a single-stranded form and then added to sample; nevertheless, in alternating irradiation experiment, UV light was irradiated on the sample containing all components and most **Mod-6dm** strands were in a hybridized form with **Tem**. Therefore, **dmAzo** moieties isomerized to *cis*-form tethering free single strands in the kinetic experiment, which provides enough steric environment for the configurational change. While **dm**Azo moieties isomerized in the duplex of **Tem**/**Mod**, more restricted environment thereby inhibited the efficiency of photo-induced isomerization.

According to the result in Fig. 2.10, this effect of steric environment to inhibit isomerization of azobenzene derivatives moieties might be strengthened by the addition of PLL-*g*-Dex polymer, which usually strongly binds to DNA duplex and stabilizes the duplex

by alleviation of the counterion condensation. In the complex consists of PLL-*g*-Dex and DNA double strands, steric environment is narrowed thus further inhibits the *trans*-to-*cis* isomerization of azobenzene derivatives moieties.

When percentage of isomerized **dmAzo** moieties decreases, more **Mod**s tethering **dmAzo** moieties in *trans*-form still strongly hybridized **Tem** so that strand displacement of **Prod** to release **Mod** does not occur, resulting in a high DP_{UV}. In this way, PLL-*g*-Dex strongly affects the photo-driven DNA strand displacement especially forward strand displacement process.

As for backward strand displacement, the azobenzene derivatives moieties isomerize in single-stranded **Mod** so that isomerization from *cis*-form back to *trans*-form should not be significantly influenced by addition of PLL-*g*-Dex.

To validate above assumption, alternating experiments with PLL-*g*-Dex in a gradient concentration were conducted.

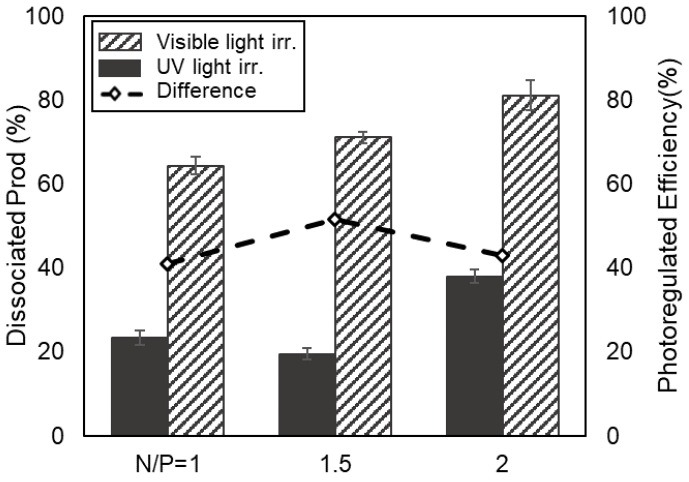

Figure 2.11. Photo-driven strand displacement mediated by **Mod-6dm** in the presence of PLL-*g*-Dex at various N/P ratios of 1, 1.5, and 2. Solid bars show DP_{UV}s after UV light irradiation and striped bars show DP_{vis}s after visible light irradiation. Open diamonds represent the Photoregulation Efficiency (*PE*) of strand displacement. Conditions: 1 μM **Tem**, 1 μM **Prod**, 1 μM **Mod**, 100 mM NaCl, phosphate buffer (pH 7.0), PLL-*g*-Dex (N/P=1, 1.5 or 2), 50 °C.

The result is shown in Fig. 2.11

Alternating irradiation experiments with a decreasing dosage of PLL-*g*-Dex (quantified by N/P ratio) from N/P ratio of 2.0 to N/P ratio of 1.0 were conducted. The condition, N/P ratio of 2.0 of PLL-*g*-Dex has been so far followed in the investigations of chemical modification and incorporating number of azobenzene moiety.

It is observed that DP_{UV} remarkably decreased from 38% to 20% when concentration of PLL-*g*-Dex decreased from N/P ratio of 2.0 to 1.5, whereas the decrease in DP_{vis} was marginal. Further decline of PLL-*g*-Dex concentration to N/P ratio of 1.0 did not obviously suppressed DP_{UV}, however, DP_{vis} decreased to 62% instead. Overall, maximum of *PE* of 53% was obtained when PLL-*g*-Dex was added in N/P ratio of 1.5 to DNA.

This result supports the assumption given above. The decrease in dosage of PLL-*g*-Dex in a rational range recovers the isomerizing efficiency of **dmAzo** moieties in the **Tem**/**Mod** duplex so that the forward strand displacement is enhanced resulting in an increase of *PE*. This is probably due to the moderate stabilization of **Tem**/**Mod**^{trans} duplex compared with the case of N/P ratio of 2.0, which provides a more appropriate steric space for *trans*-to-*cis* isomerization of **dmAzo** moieties. The DP_{UV} of 20% obtained here is consistent with the result shown in Fig. 2.7b in kinetic studies, indicating that reduction of the N/P ratio from 1.5 to 1.0 did not lower DP_{UV}. However, the further decrease of PLL-*g*-Dex concentration to N/P ratio of 1.0 might result in a much weaker stabilizing effect that suppressed backward strand displacement process.

To conclude from this result, there is an optimized dosage of PLL-*g*-Dex to achieve the most efficient photo-driven DNA strand displacement at N/P ratio of 1.5.

The stability changes of each duplex in the presence of PLL-*g*-Dex in different concentration is also demonstrated by melting temperature measurement, as shown in Table 2.8.

Table 2.8. Melting temperature (T_m) of **Tem**/**Mod** duplex in the presence of PLL-*g*-Dex at various N/P ratio

N/P ratio	T_m/°C[a]		
	Tem/**Prod**	**Tem**/**Mod-6dm*^{transs}***	**Tem**/**Mod-6dm*^{cis}***
1.0	74.0	80.0	N. A.
1.5	74.0	82.0	N. A.
2.0	74.5	84.5	N. A.

[a] Conditions: 1 μM each duplex, 100 mM NaCl, 10 mM phosphate buffer (pH 7.0), PLL-*g*-Dex (N/P=2). When *trans*-T_m of **Tem**/**Mod** is measured, solution containing DNA duplex is firstly incubated at 90°C for 10 min to convert as much azobenzene into *trans*-form. When *cis*-T_m of **Tem**/**Mod** is measured, solution containing DNA duplex is irradiated with UV light (365 nm) for 10 min at 60 °C to isomerize as much azobenzene into *cis*-form. Temperature change in annealing process is 1°C / min.

Though strong steric hindrance brought by six **dmAzo** in *cis*-form effectively inhibits the duplex formation of **Tem**/**Mod-6dm*^{cis}***, revealing from the failed observation of respective melting temperatures in all three cases, there are an obvious decrease of melting temperatures of **Tem**/**Mod*^{trans}*** with respect to the decrease of N/P ratio. This is agreed with the decreasing DP_{vis} measured in polymer control experiment of Fig. 2.11 when reducing the dosage of PLL-*g*-Dex. Surprisingly, melting temperatures of **Tem**/**Prod** almost did not decrease as **Tem**/**Mod-6dm*^{trans}*** did, indicating there might be a different type of interaction between PLL-*g*-Dex and azobenzene derivatives moieties, compared binding interaction between polymer and natural base pairs.

To conclude, moderate dosage of PLL-*g*-Dex achieve the highest *PE* by properly stabilizing the duplex of **Tem**/**Mod*^{trans}***, enabling the most efficient *trans*-to-*cis* isomerization of azobenzene derivatives moieties. Over high and weak stabilization of **Tem**/**Mod*^{trnas}*** duplex inhibit forward strand displacement process and backward strand displacement

process respectively, leading to a decrement of efficiency of the whole photo-driven DNA strand displacement reaction.

2.6. Equilibrium of photo-driven DNA strand displacement

Both isomerization of azobenzene derivatives and DNA strand displacement are equilibrated processes, which will not be discussed in this thesis in detail,

In this section, one of the factors that are considered very crucial to photo-driven DNA strand displacement by affecting equilibrium is discussed, which is the equivalent of **Mod**. To note, the expression of "the equivalent of **Mod**" in this thesis refers to **Mod**'s equivalent with respect to **Tem**.

Staring backward strand displacement, as shown in Scheme 2.7, the equilibrium that **Mod**^{trans} hybridizes **Tem** to release **Prod** should be considerably boosted by higher concentration of **Mod** and lower concentration of **Prod**. To shift the equilibrium in favour of **Tem**/**Mod**^{trans} duplex formation, the stoichiometry of **Mod** with respect to **Tem**, i.e., equivalent of **Mod** was increased. It is expected that excess single-stranded **Mod** would not disturb *trans*-to-*cis* isomerization of azobenzene derivatives in the forward strand displacement since **dmAzo** should easily isomerize to *cis*-form in a single strand.

Alternating irradiation experiments employing **Mod-6dm** at a gradient equivalent were conducted to investigated its effect on the backward strand displacement process.

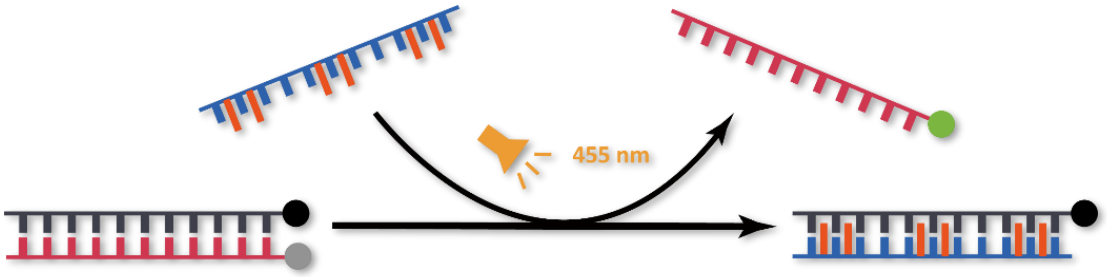

Scheme 2.7. Equilibrium of backward strand displacement process. **Mod** in excess equivalents boost the equilibrium from left side to right side.

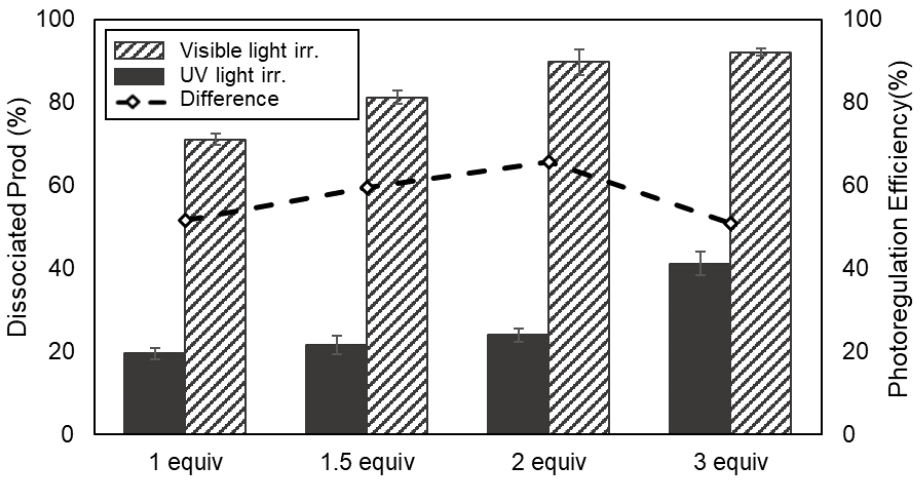

Figure 2.12. Effect of equivalence of **Mod-6dm** on the photoregulation efficiencies. Solid bars show DP_{UV}s after UV light irradiation and striped bars show DP_{vis}s after visible light irradiation. Open diamonds represent the Photoregulation Efficiency (*PE*) of strand displacement. Conditions: 1 μM **Tem** and **Prod**, 1, 1.5 ,2 or 3 μM **Mod**, 100 mM NaCl, phosphate buffer (pH 7.0), PLL-*g*-Dex (N/P=1.5), 50 °C.

The result is shown in Fig. 2.12.

An increasing DP_{vis} was observed with the growing equivalents of **Mod**, from 71.1% at 1.0 equivalent **Mod** to 92.3% at 3.0 equivalents **Mod**. Simultaneously, DP_{UV} marginally increased from 19.5% at 1.0 equivalent **Mod** to 23.9% at 2.0 equivalents **Mod**, while it blinked to over 40% when **Mod** of 3.0 equivalents participated the photo-driven strand displacement reaction. As a combined result, *PE* arrived about 66% with the addition of 2.0 equivalents of **Mod**.

Coincident with foregoing assumption, increased DP_{vis} obtained regarding increase of **Mod** equivalent suggests an effective improvement of backward strand displacement, probably toward promoting the equilibrium of **Tem**/**Mod**^{trans} hybridization and **Product** discharge. This enlargement of **Mod** stoichiometry has not noticeably inhibited the forward strand displacement in the first (up to 2.0 equivalents of **Mod**), yet finally caused an almost doubled DP_{UV} when equivalents of **Mod** rises to 2.0.

The sudden surge in DP_{UV} when 3.0 equivalents of **Mod** joined reaction might be a qualitative change when large excess **Mod**s that contained partially isomerized **dmAzo** in *trans*-form also started to hybridize **Tem**, thereby inhibited the forward strand displacement. However, there remains little evidence to support this speculation.

To conclude, excess equivalents of **Mod** enhanced the photo-driven DNA strand displacement reaction by affecting the backward strand displacement process while disregarded the forward strand displacement process, contributing to solely increase of DP_{vis} which finally achieved the maximum *PE* of 66%.

2.7. Photo-reversibility of photo-driven DNA strand displacement

Orchestrating all factors together, alternating irradiation with UV and visible light was conducted for several rounds, in order to examine the reversibility of photo-driven DNA strand displacement reactions.

The result is shown in Fig. 2.13.

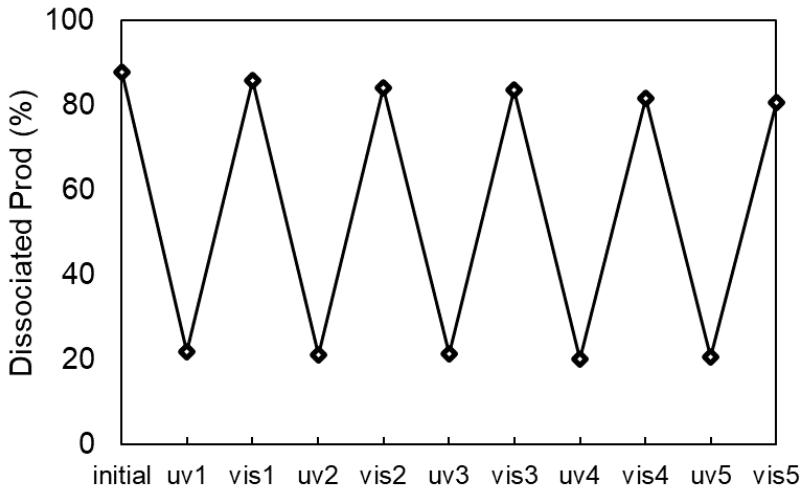

Figure 2.13. Repetitive DNA strand displacement cycle induced by alternating irradiation with UV (365 nm) and irradiation with visible (455 nm) light. Conditions: 1 μM **Tem**, 1 μM **Prod**, 2 μM **Mod**, 100 mM NaCl, phosphate buffer (pH 7.0), PLL-*g*-Dex (N/P=1.5), 50 °C.

The reversible strand displacement was achieved upon alternating irradiation with UV and visible light in an average *PE* of 63%. The slight decrease of DP_{vis} is due to the photo-cleavage of FAM group.

This result suggested a constant efficiency of strand displacement regulated by light irradiation facilitated by chaperon polymer PLL-*g*-Dex. Unlike toehold strand displacement, the efficiency of this photo-driven DNA strand displacement did not decline because there is no waste duplex produced and accumulated in the system to contaminate the nano-environment.

Moreover, this method is performed in simple phosphate saline buffer solution. Since it does not require any additional chemicals except PLL-*g*-Dex to achieve the efficient strand displacement, I suppose this method can be applied to various environment containing biomacromoleculars that are usually sensitive to *p*H, additional chemicals or temperature change.

2.8. Conclusion

In this chapter, a method that utilizes light irradiation to regulate DNA strand displacement has been developed.[19] Unlike the temperature, chemicals or other external stimulus, this method is isothermal and involves only light irradiation as stimulus to avoid any change of the physical or chemical environment. Especially, this method provides the alternative solution for nano-dynamics employing toehold strand displacement reaction, which usually involves a decreased efficiency due to the production of waste duplex.

Forward and backward strand displacement processes are investigated to find out the major influencing factors that affect the efficiency of this photo-driven system. In section 2.3, thermodynamic and kinetic properties are studied by melting temperature measurements and **Mod**-addition fluorescence analysis, given the conclusion that both strand displacement processes are thermodynamically and kinetically feasible. Then how azobenzene moieties intercalated in **Mod** influences efficiency of photo-regulation are thoroughly researched by

stating two topics: *ortho*-methylation of azobenzene molecule and incorporating quantity of azobenzene derivatives moieties. Alternating irradiation experiments demonstrated that 2',6'-dimethylation of azobenzene to give **dmAzo** moieties improved the efficiency of photo-regulation by enhancing the backward strand displacement through stabilizing **Tem**/**Mod**^{trans} duplex. In the experiment to figure out the appropriate incorporating number of azobenzene derivatives moieties, too many incorporations caused the loss of duplex symmetricity while too less resulted in the insufficient stabilization of **Tem**/**Mod**^{trans} duplex. A proper incorporating density is suggested to be Azo : Native of 1 : 3 in quantity. In the following section 2.5, the effect of chaperon polymer is studied by controlling the dosage of PLL-*g*-Dex. The result expectedly reveals the moderate concentration, N/P ratio of 1.5, effectively promoted the photo-driven DNA strands displacement reaction. Over use of PLL-*g*-Dex surprisingly inhibited the *trans*-to-*cis* isomerization of azobenzene derivatives moieties in duplex, thus suppress the forward strand displacement process. Concentration of one of the participants **Mod** is discussed in section 2.6, rationalized by the assumption that excess equivalents of **Mod** should boosts the equilibrium in the backward strand displacement. Experiments with **Mod** in a gradient equivalent supported the assumption and indicated a proper **Mod** equivalents of 2.0 to most efficiently facilitate the equilibrium. Finally, taken all above opinions into consideration, the reversible photo-driven DNA strand displacement reactions was achieved. Upon alternating irradiation with UV and visible light, the efficiency kept constant during five cycles.

Utilizing this method, constant and reversible control of nanomachines or other DNA nano-dynamics can be conveniently realized.

2.9. Experiment Section

2.9.1. Materials.

All conventional phosphoramidite monomers, CPG columns, and reagents for DNA synthesis were purchased from Glen Research. Other reagents for the synthesis of phosphoramidite monomers were purchased from Tokyo Chemical Industry, Wako, and Aldrich. Oligonucleotides **Tem** and **Prod** containing natural bases, FAM, and Dabcyl were purchased from Integrated DNA Technologies. Oligodeoxyribonucleotides **Mod-6um**, **Mod-6dm**, **Mod-4dm**, and **Mod-8dm** modified with **umAzo** and **dmAzo** were outsourced to Nihon Techno Service Co., Ltd.

Poly(L-lysine hydrobromide) (PLL-HBr, Mw = 7.5 × 103) and dextran (Dex, Mw = 8.0 × 103) were obtained from Sigma-Aldrich and Funakoshi Co., respectively. Poly(L-lysine)-graft-Dextran (PLL-g-Dex) cationic comb-type copolymer was synthesized by a reductive amination reaction of dextran with PLL according to previously published protocol. The resulting copolymer was purified by ion exchange and dialysis, then obtained by freeze drying. The composition (10 wt% PLL and 90 wt% dextran) of the copolymer was confirmed by 1H-NMR analysis.

2.9.2. Synthesis of oligonucleotides

Modified oligonucleotides tethering mmAzo (Mod-6mm) were synthesized on an automated DNA synthesizer (H-8-SE, Gene World) by using phosphoramidite monomer containing 2'-methyl azobenzene, which was synthesized as previously reported. After workup, oligonucleotides were purified by reversed-phase HPLC and characterized by using a MALDI-TOF mass spectrometer (Autoflex II, Bruker Daltonics). MALDI-TOF MS for Mod-6mm: 9038 m/z (calculated 9036).

2.9.3. Photoisomerization of azobenzene

For *trans*-to-*cis* isomerization, UV light at 365 nm was applied using an OminiCure LX405s Spot Curing System with a UV LED head V2 019-00181R (Lumen Dynamics, 9500

mW/cm2). For *cis*-to-*trans* isomerization, visible light at 455 nm was applied using a SLA-1000-2 two-channel Universal LED Driver with a BioLED Optical Head LCS-0455-03 (Mightex, 280 mW).

2.9.4. Melting temperature measurements

The melting curves were obtained with a JASCO model V-560 spectrometer and a JASCO model FP-6500 spectrometer equipped with programmable temperature controllers; 10 mm x 3 mm quartz cells were used. The T_m was determined from the maximum in the first derivative of the melting curve, which was obtained by measuring the absorbance at 260 nm as a function of temperature. The temperature ramp was 1.0 °C/min. Before **Mod**^{trans}/**Tem** measurement, **Mod** was incubated at 90 °C for 10 min to isomerize azobenzene into *trans*-form. Before **Mod**^{cis}/**Tem** measurement, **Mod** was irradiated by UV light for 10 min at 60 °C. Conditions: 1 μM DNA, 100 mM NaCl, 10 mM phosphate buffer (pH 7.0).

2.9.5. Fluorescence measurement

Fluorescence spectra were measured with JASCO FP-6500 spectrofluorometer. Excitation wavelength was 495 nm with bandwidth of 3 nm (both emission and excitation). Dissociated Prod (%) was calculated from the fluorescence emission intensities at 520 nm:

$$\text{Dissociated Prod } (DT) = (F_x\text{-}F_q) / (F_i\text{-}F_q)$$

where F_x is the fluorescence intensity of sample, F_i is the fluorescence emission intensity of FAM-labeled **Prod**, and F_q is the fluorescence emission intensity of hybridized **Tem** and **Prod**.

2.9.6. Kinetic study

For kinetic studies of **Mod**^{trans} invading into **Tem**/**Prod**, **Tem** and **Prod** were dissolved in phosphate buffer and PLL-*g*-Dex was added for a total volume of 1995 μL. The solution was moved into a quartz cell (10 mm x 10 mm) equipped with a stirrer, and the cell was incubated at 50 °C in fluorescence spectrometer. To isomerize most azobenzene moieties in

Mod into the *trans*-form, the **Mod** sample was dissolved in 10 μL phosphate buffer, heated to 90 °C, and maintained for 10 min in the dark. After starting the fluorescence time course monitoring, the **Mod** strand was immediately added into the cell to initiate strand displacement. For kinetic studies of **Mod**^{cis} invading into **Tem**/**Prod**, the same procedure was followed, except that a 10-min UV irradiation to isomerize azobenzene into the *cis*-form replaced the heating step. *DP* (%) was calculated from fluorescent emission intensity.

2.9.7. Photo-driven DNA strand displacement

For strand displacement reactions, all DNA strands were firstly dissolved in phosphate buffer followed by the addition of PLL-*g*-Dex to the designed concentration in a total volume of 600 μL. Then the solution was moved into a quartz cell (10 mm x 2 mm) and incubated at 50 °C for 10 min. In forward strand displacement process, the sample was irradiated with UV light for 2 min and incubated for 3 min in the dark for completing strand displacement, after which fluorescence measurements were conducted. In backward strand displacement, the sample was irradiated with visible light for 1 min and incubated for 4 min in the dark, after which fluorescence was measured. All the experiments were performed at 50 °C unless mentioned in captions.

2.9.8. Alternative irradiation experiment

All DNA strands were dissolved in phosphate buffer followed by the addition of PLL-*g*-Dex to the indicated concentration in a total volume of 600 μL. The solution was moved into a quartz cell (10 mm x 2 mm) and incubated at 90 °C for 10 min and 50 °C for 10 min. After incubation, the fluorescence emission intensity measured was taken to be the initial point. The sample was next irradiated by UV light for 2 min and incubated for 3 min to measure the **uv1** point, and then irradiated by visible light for 1 min and incubated for 4 min to measure the **vis1**. The UV and the visible light irradiations were conducted alternatingly. All irradiation steps were performed at 50 °C in the dark.

2.10. Appendixes

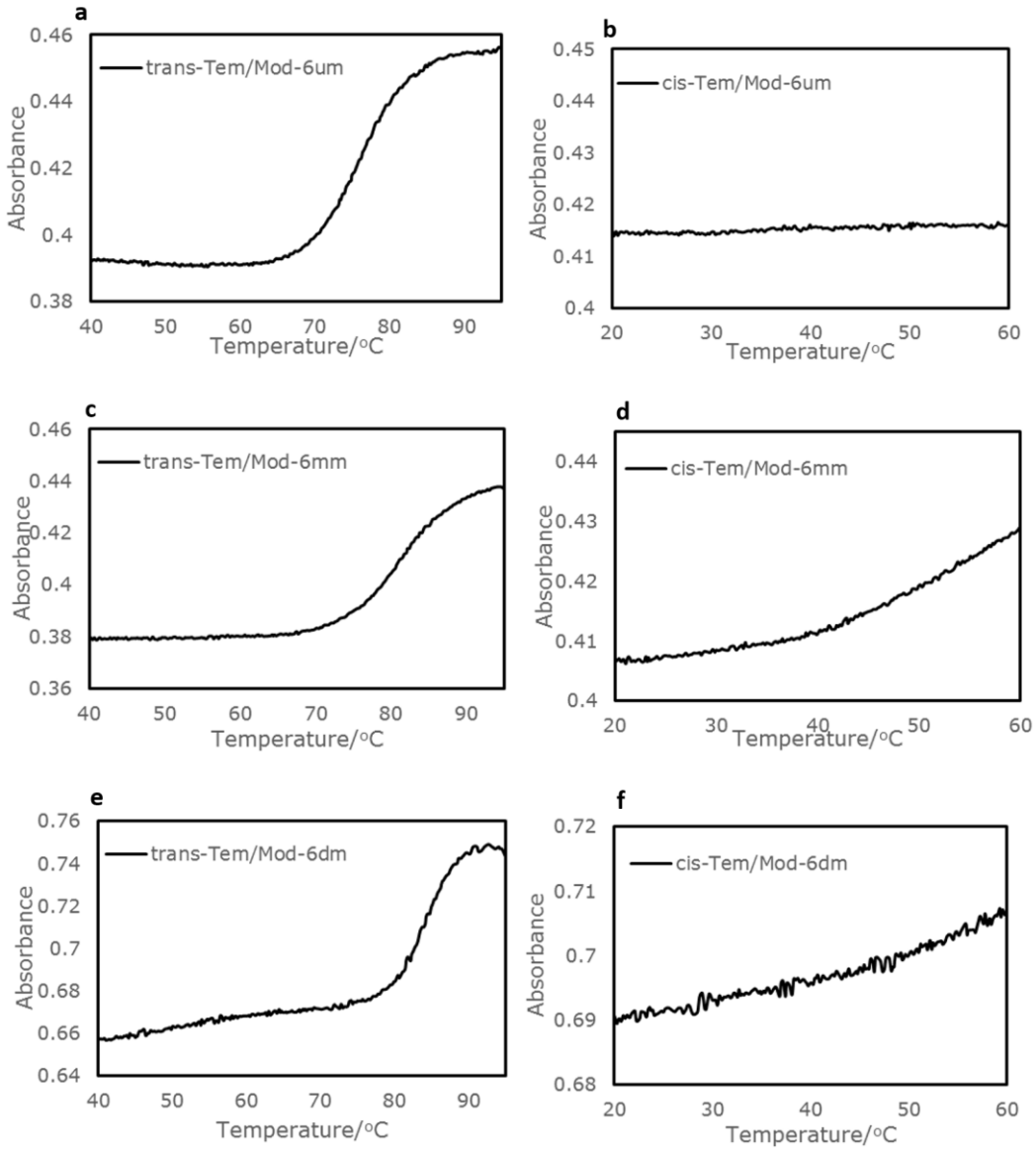

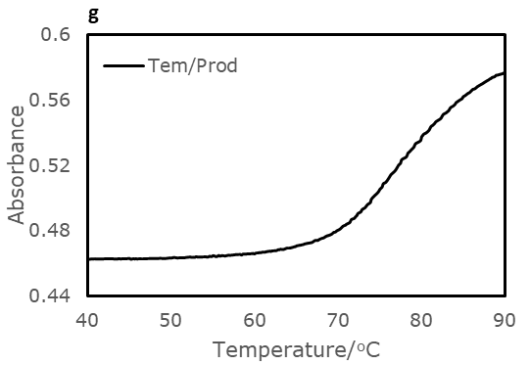

Figure S2.1. Melting curves of (a) **Tem**/**Mod-6um**^{trans}, (b) **Tem**/**Mod-6um**^{cis}, (c) **Tem**/**Mod-6mm**^{trans}, (d) **Tem**/**Mod-6mm**^{cis}, (e) **Tem**/**Mod-6um**^{trans}, (f) **Tem**/**Mod-6um**^{cis}, and (g) **Tem**/**Prod**. Conditions: 1.0 µM **Tem**, 1.0 µM **Mod** strand, PLL-*g*-Dex (N/P=2). Buffer: 10 mM phosphate (pH 7.0), 100 mM NaCl. Volume: 600 µL. Wavelength: 260 nm.

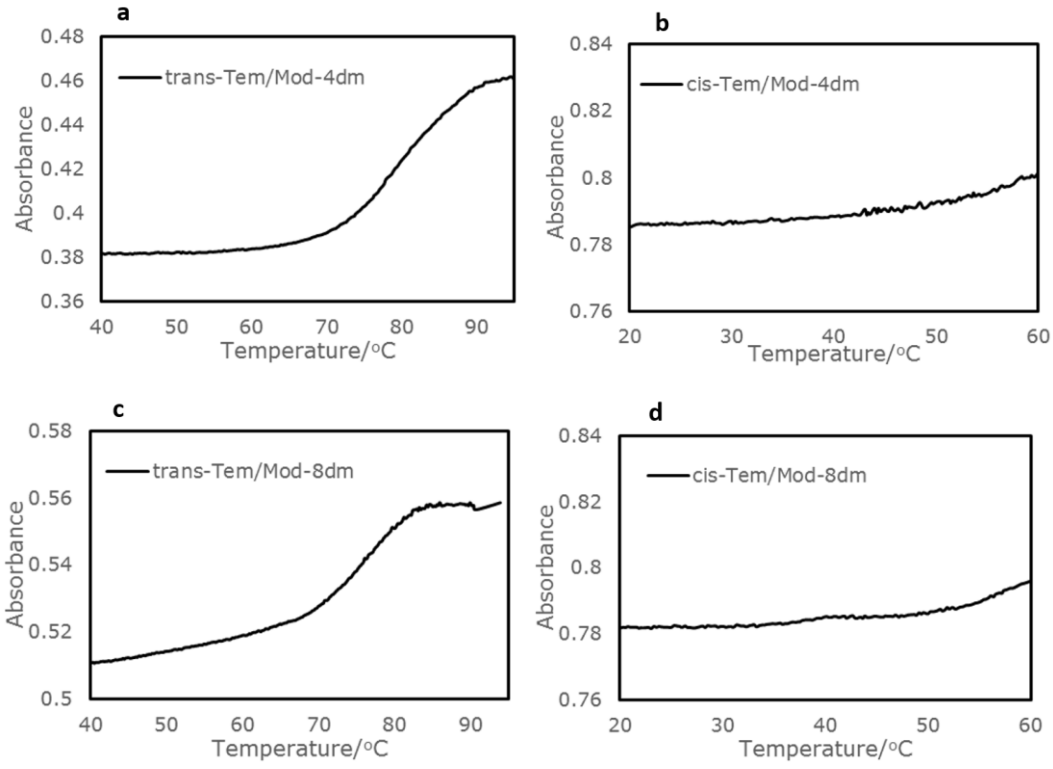

Figure S2.2. Melting curves of (a) **Tem**/**Mod-4dm**^{trans}, (b) **Tem**/**Mod-4dm**^{cis}, (c) **Tem**/**Mod-8dm**^{trans}, and (d) **Tem**/**Mod-8dm**^{cis}. Conditions: 1.0 µM **Tem**, 1.0 µM **Mod** strand, PLL-*g*-Dex (N/P=2), 10 mM phosphate (pH 7.0), 100 mM NaCl. Volume: 600 µL. Wavelength: 260 nm.

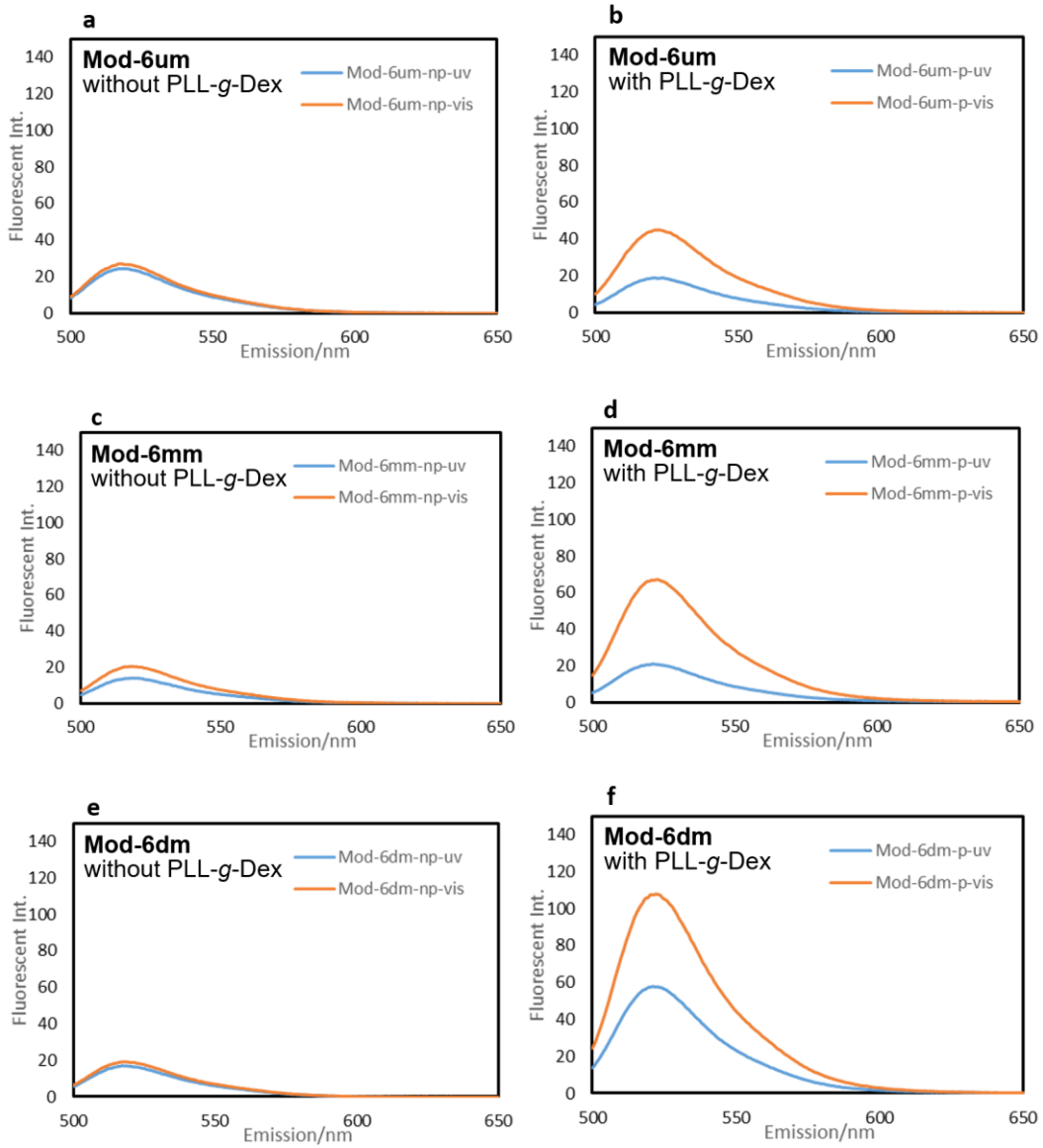

Figure S2.3. Fluorescence spectra of photo-driven DNA strand displacement mediated by **Mod** strands tethering different azobenzene derivatives in the presence and absence of PLL-*g*-Dex: (a) **Mod-6um** in the absence of PLL-*g*-Dex, (b) **Mod-6um** in the presence of PLL-*g*-Dex, (c) **Mod-6mm** in the absence of PLL-*g*-Dex, (d) **Mod-6mm** in the presence of PLL-*g*-Dex, (e) **Mod-6dm** in the absence of PLL-*g*-Dex, and (f) **Mod-6dm** in the presence of PLL-*g*-Dex. Conditions: 1 μM each DNA, 100 mM NaCl, 10 mM phosphate buffer (pH 7.0), PLL-*g*-Dex (N/P=2), 50 °C. Excitation wavelength: 495 nm.

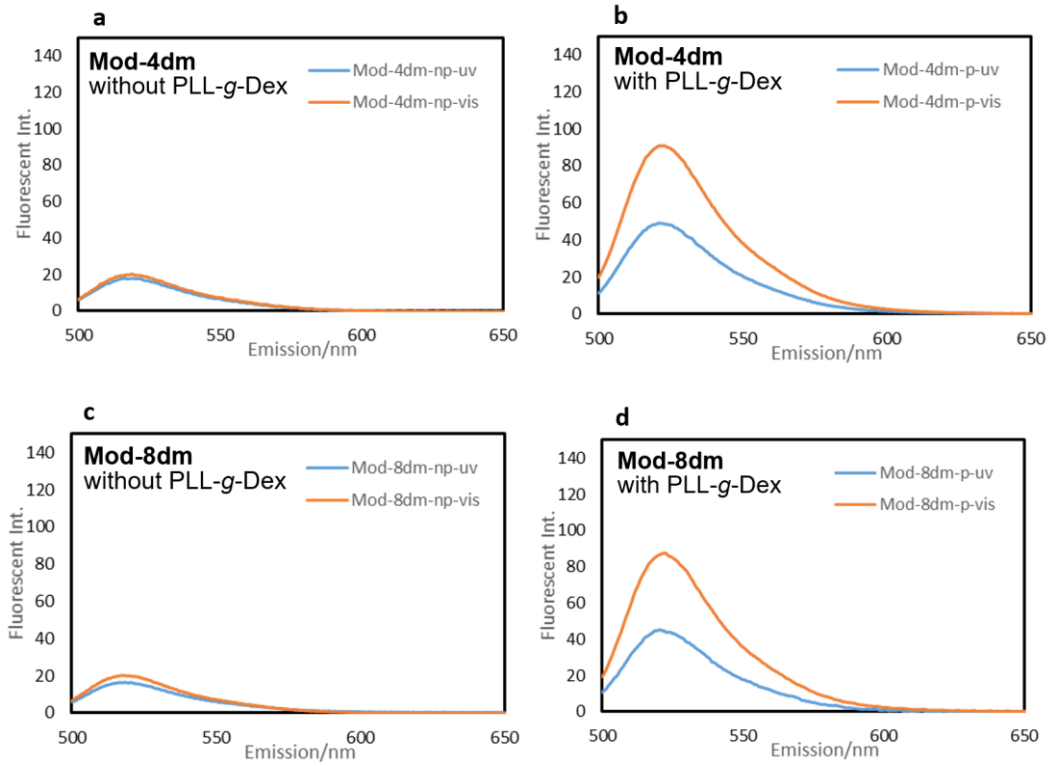

Figure S2.4. Fluorescence spectra of photo-driven DNA strand displacement mediated by modulator tethering different numbers of **dmAzo**: (a) **Mod-4dm** in the absence of PLL-*g*-Dex, (b) **Mod-4dm** in the prsence of PLL-*g*-Dex, (d) **Mod-8dm** in the absence of PLL-*g*-Dex, (d) **Mod-8dm** in the prsence of PLL-*g*-Dex. Conditions: 1 μM each DNA strand, 100 mM NaCl, 10 mM phosphate buffer (pH 7.0), PLL-*g*-Dex (N/P=2), 50 °C. Excitation wavelength: 495 nm.

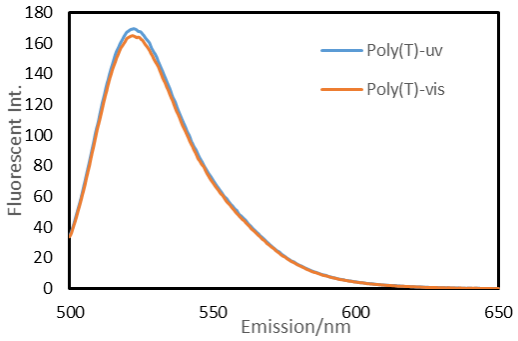

Figure S2.5. Fluorescence spectra of photo-driven DNA strand displacement using Poly(T) (sequence shown below) as **Tar** control, mediated by **Mod-6dm** in the prsence of PLL-*g*-Dex. Conditions: 1 µM each DNA strand, 100 mM NaCl, 10 mM phosphate buffer (pH 7.0), PLL-*g*-Dex (N/P=2), 50 °C. Excitation wavelength: 495 nm.

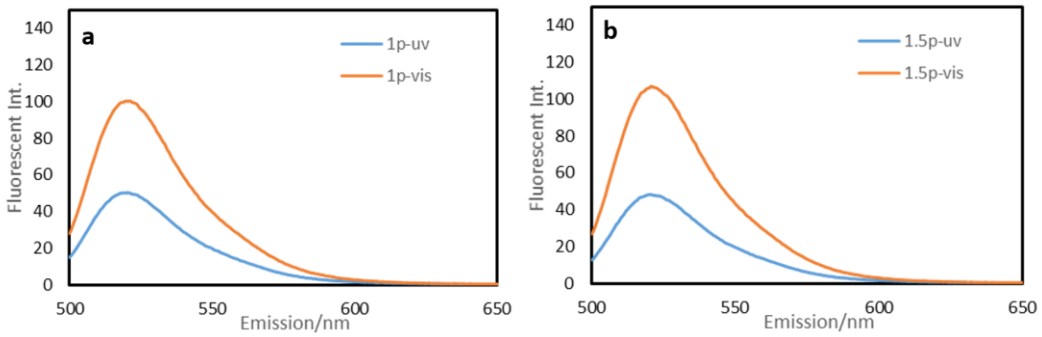

Figure S2.6. Fluorescence spectra of photo-driven DNA strand displacement mediated by **Mod-6dm** in the presence of PLL-*g*-Dex at (a) N/P of 1 and (b) N/P of 1.5. Conditions: 1.0 µM **Tem**, 1.0 µM **Prod**, 1.0 µM, **Mod**, PLL-*g*-Dex (N/P=1 or 1.5), 10 mM phosphate (pH 7.0), 100 mM NaCl. Volume: 600 µL. Excitation wavelength: 495 nm. Temperature: 50 °C

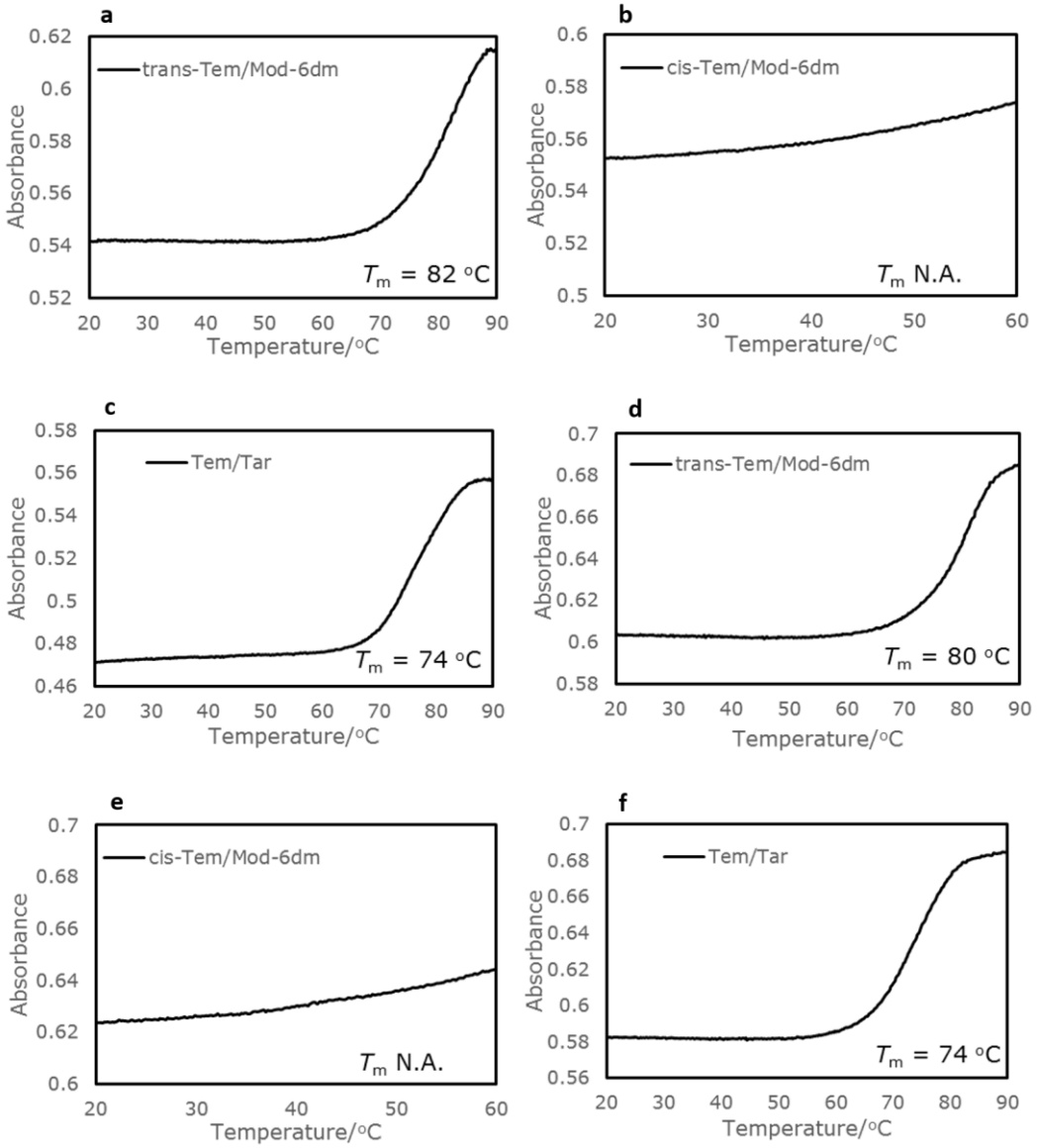

Figure S2.7. Melting curves of **Tem**/**Mod-6dm**^{trans}, **Tem**/**Mod-6dm**^{cis}, and **Tem**/**Prod** at N/P of 1.5 (a, b, c) and N/P of 1.0 (d, e, f). Conditions: 1.0 μM **Tem**, 1.0 μM **Mod**, 1.0 μM **Prod**, 10 mM phosphate (pH 7.0), 100 mM NaCl.

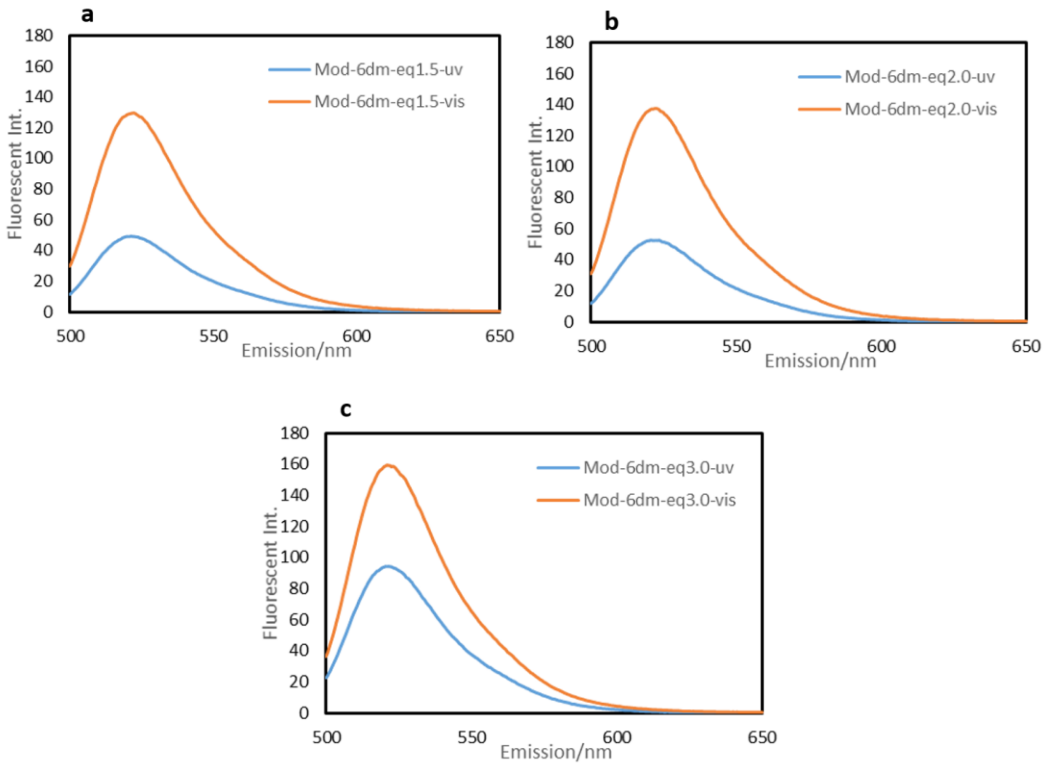

Figure S2.8. Fluorescence spectra of photo-driven DNA strand displacement mediated by **Mod-6dm** at (a) 1.5 equivalents **Mod-6dm**, (b) 2.0 equivalents **Mod-6dm**, (c) 3.0 equivalents **Mod-6dm**. Conditions: 1.0 μM **Tem**, 1.0 μM **Prod**, PLL-*g*-Dex (N/P=1.5), 10 mM phosphate (pH 7.0), 100 mM NaCl. Volume 600 μL. Excitation wavelength: 495 nm. Temperature: 50 ^{o}C

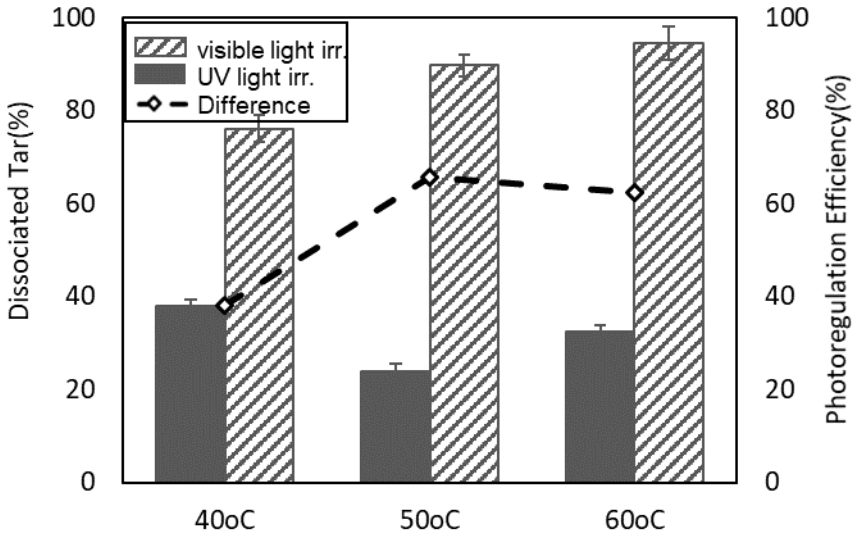

Figure S2.9. Photo-driven strand displacement mediated by **Mod-6dm** at different temperature. Solid bars show DP_{UV}s after UV light irradiation and striped bars show DP_{vis}s after visible light irradiation. Open diamonds represent the photoregulation efficiency (*PE*) of strand displacement, which is the difference between values of solid bars and striped bars. Conditions: 1 μM **Tem**, 1 μM **Prod**, 1 μM **Mod**, 100 mM NaCl, phosphate buffer (pH 7.0), PLL-*g*-Dex (N/P=2).

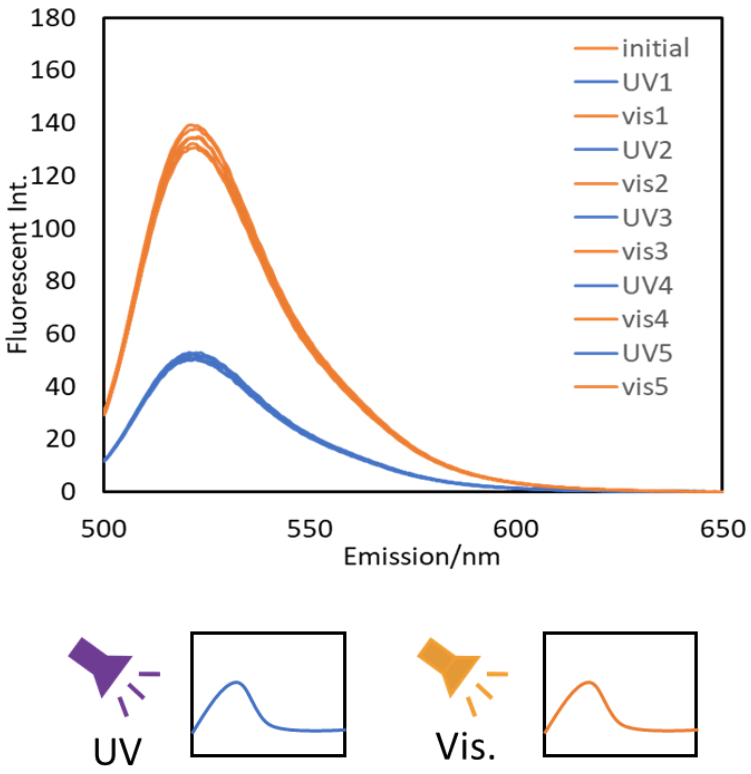

Figure S2.10. Repetitive DNA strand displacement cycle induced by alternating irradiation with UV and visible light. Conditions: 1.0 μM **Tem**, 1.0 μM **Prod**, 2.0 μM **Mod**, PLL-*g*-Dex (N/P=1.5). Buffer: 10 mM phosphate (pH 7.0), 100 mM NaCl. Volume: 600 μL. Excitation wavelength: 495 nm. Temperature: 50 ^{o}C

Table S1. *DP* and *PE* of photo-driven strand displacement mediated by modulator strands **Mod-6um**, **Mod-6mm**, and **Mod-6dm** tethering different azobenzene derivatives.

Sample		Mod-6um	Mod-6mm	Mod-6dm
DP (%)	UV	8.5	12.11	38.1
	Vis	32.6	47.8	81.1
PE (%)		24.1	35.7	43.0

Table S2. *DP* and *PE* of photo-driven strand displacement mediated by modulator strands tethering different numbers of **dmAzo.**

Sample		Mod-4dm	Mod-6dm	Mod-8dm
DP (%)	UV	32.4	38.1	26.0
	Vis	66.8	81.1	59.3
PE (%)		34.4	43.0	33.3

Table S3. *DP* and *PE* of photo-driven strand displacement mediated by **Mod-6dm** in the presence of PLL-*g*-Dex at various N/P ratios.

PLL-*g*-Dex (N/P)		1	1.5	2
DP (%)	UV	23.3	19.5	38.1
	Vis	64.4	71.1	81.1
PE (%)		41.1	51.6	43.0

Table S4. *DP* and *PE* of photo-driven strand displacement mediated by different equivalents of **Mod-6dm**.

Equiv. of Mod-6dm		1	1.5	2	3
DP (%)	UV	19.5	21.6	23.9	41.2
	Vis	71.1	81.2	89.7	92.1
PE (%)		51.6	59.6	65.7	50.9

2.11. Reference

[1] N. Srinivas, T. E. Ouldridge, P. Sulc, J. M. Schaeffer, B. Yurke, A. A. Louis, J. P. K. Doye, E. Winfree, *Nucleic Acids Res.,* **2013**, *41*, 10641-10658.

[2] B. Yurke, A. J. Turberfield, A. P. Mills, F. C. Simmel, J. L. Neumann, *Nature,* **2000**, *406*, 605-608.

[3] L. P. Feng, S. H. Park, J. H. Reif, H. Yan, *Angew. Chem. Int. Ed.,* **2003**, *42*, 4342-4346.

[4] C. A. Mirkin, R. L. Letsinger, R. C. Mucic, J. J. Storhoff, *Nature,* **1996**, *382*, 607-609.

[5] J. W. J. Li, W. H. Tan, *Nano Lett.,* **2002**, *2*, 315-318.

[6] G. Seelig, B. Yurke, E. Winfree, *Lect Notes Comput Sc,* **2005**, *3384*, 329-343.

[7] H. Kashida, X. G. Liang, H. Asanuma, *Curr. Org. Chem.,* **2009**, *13*, 1065-1084.

[8] H. Asanuma, T. Ito, T. Yoshida, X. G. Liang, M. Komiyama, *Angew. Chem. Int. Ed.,* **1999**, *38*, 2393-2395.

[9] H. Asanuma, X. G. Liang, T. Yoshida, M. Komiyama, *Chembiochem,* **2001**, *2*, 39-44.

[10] H. Asanuma, T. Takarada, T. Yoshida, D. Tamaru, X. G. Liang, M. Komiyama, *Angew. Chem. Int. Ed.,* **2001**, *40*, 2671-2673.

[11] H. Asanuma, X. Liang, H. Nishioka, D. Matsunaga, M. Liu, M. Komiyama, *Nat. Protoc.,* **2007**, *2*, 203-212.

[12] A. Maruyama, H. Watanabe, A. Ferdous, M. Katoh, T. Ishihara, T. Akaike, *Bioconjugate Chem.,* **1998**, *9*, 292-299.

[13] W. J. Kim, Y. Sato, T. Akaike, A. Maruyama, *Nat. Mater.,* **2003**, *2*, 815-820.

[14] W. J. Kim, T. Akaike, A. Maruyama, *J. Am. Chem. Soc.,* **2002**, *124*, 12676-12677.

[15] W. J. Kim, T. Ishihara, T. Akaike, A. Maruyama, *Chem-Eur J,* **2001**, *7*, 176-180.

[16] H. Nishioka, X. G. Liang, H. Kashida, H. Asanuma, *Chem. Commun.,* **2007**, 4354-4356.

[17] H. Nishioka, X. G. Liang, H. Asanuma, *Chem-Eur J,* **2010**, *16*, 2054-2062.

[18] H. Asanuma, D. Matsunaga, M. Komiyama, *Nucleic Acids Symp Ser (Oxf),* **2005**, 35-36.

[19] B. H. Cheng, H. Kashida, N. Shimada, A. Maruyama, H. Asanuma, *Chembiochem,* **2017**, *18*, 1568-1572.

2.12. Content of Schemes, Figures and Tables

3. Study on photo-regulatable DNA amplification reaction

3.1. Introduction

Since the first report of polymerase chain reaction (PCR)[1] in 1980s, PCR has become one of the indispensable techniques in biology, medicine and biotechnology fields. It enables the efficient, convenient and designable amplification of long DNA strand, which is irreplaceable in modern research.

Principle of PCR (Scheme 3.1) is very neat: target duplex of DNA is heated up to over 90 ^{o}C to be dissociated in single strands, then following cooling down process (generally called annealing process) ensures the hybridization of two primer strands onto the initial region of target duplex, immediately initializing the polymerase-induced elongation to produce two duplexes in the same sequence with initial duplex. This process is repeated by heating and cooling the sample, in which copies of target DNA duplex increase in an exponential manner.

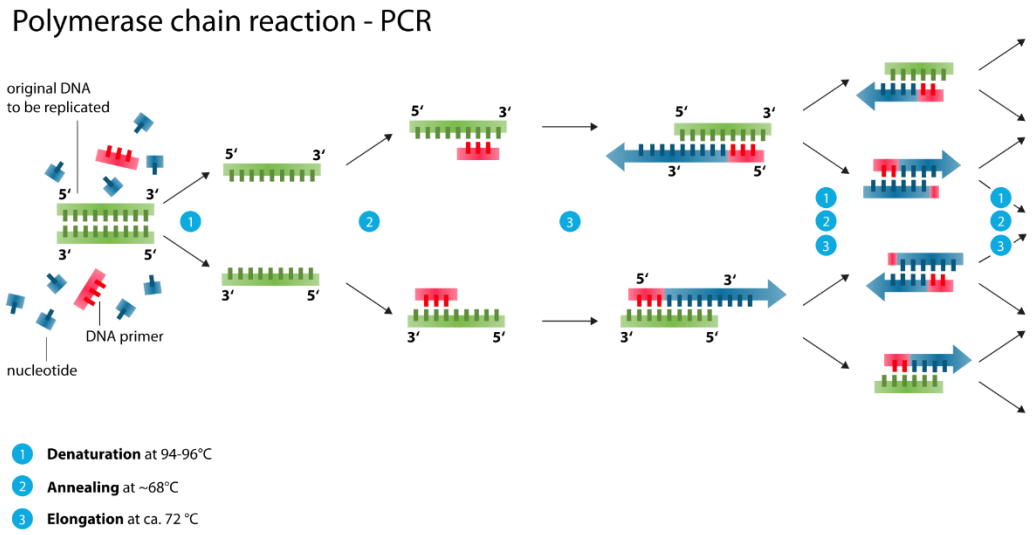

Scheme 3.1. Principle of PCR assay. (By Enzoklop-Own work, Wikipedia)

Although PCR has been being utilized as the most popular DNA amplification technic, it possesses some drawbacks, such as necessary thermal cycles that is not friendly to system including component that is not thermostable.

Therefore, various isothermal amplification assays have been developed as alternatives for efficient amplification of DNA that are applicable for system containing molecules such as enzymes that are not resistant to heating,[2] such as strand displacement amplification,[3] nucleic acid sequence-based amplification,[4] rolling circle amplification,[5-6] loop-mediated isothermal amplification,[7] helicase-dependent amplification[8] and recombinase polymerase amplification.[9] Some methods even allow performing amplification process in an extra- or intracellular environment.[10-12]

These isothermal methods are designed for two main purposes: efficient and precise production of target nucleic acids, and amplification of signal for sensitive detection of target.

Most famous isothermal DNA amplification methods include rolling circle amplification (RCA)[5-6] and hybridization chain reaction (HCR).[13]

As shown in Scheme 3.2, RCA employs a circular padlock template onto which a primer was bound. The exo-polymerase enlongates primer to a long single-stranded product by

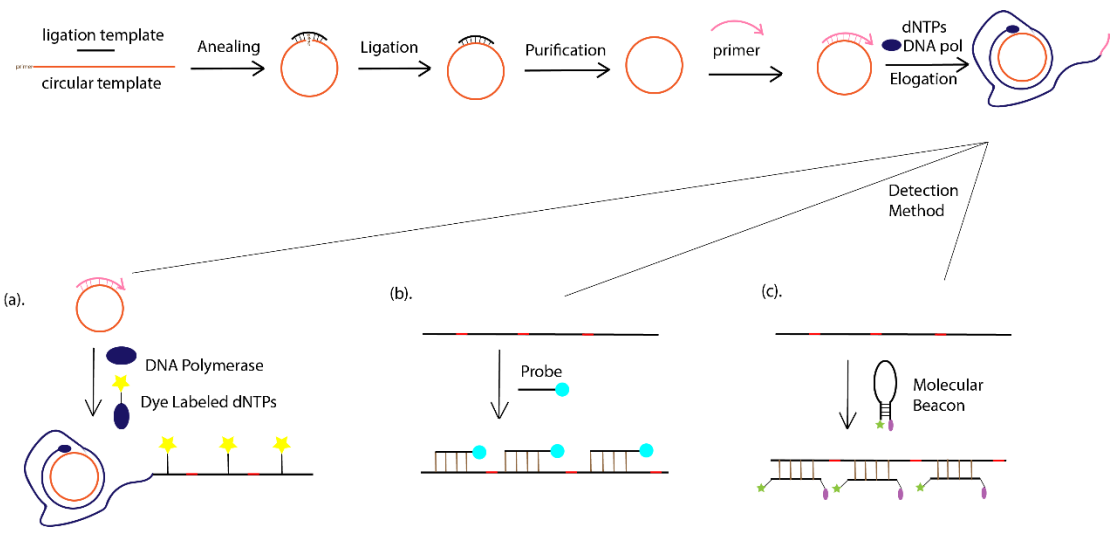

Scheme 3.2. Schematic illustration of rolling circle amplification (By Tanxt-Own work, Wikipidia)

repeatedly synthesize closed-circle copies rounding the padlock template. The long single-stranded product acts as the second template that binds to many second primers sequentially. With the elongation of theses second primers, strand displacement occurs to release tandem sequences of the original circular template, which are used as the templates in next cycle.

As shown in Scheme 3.3, HCR is an enzyme-free signal amplification method that is based on a chain toehold strand displacement reaction triggered by input of target. It is not aiming at the production of nucleic acids but the enlargement of signal for detection purpose. Two partially self-complementary DNAs both form hairpin structure and leave toehold portions. When triggered by the input of the target strand through target's binding onto the toehold portion followed by strand displacement to dissociate the hairpin structure, a chain reaction of hybridization and toehold stand displacement occurs between two DNA substrates to form a long wire-like structure. With the incorporation of fluorophores, signal of input strand can be amplified rapidly in a spontaneous behavior.

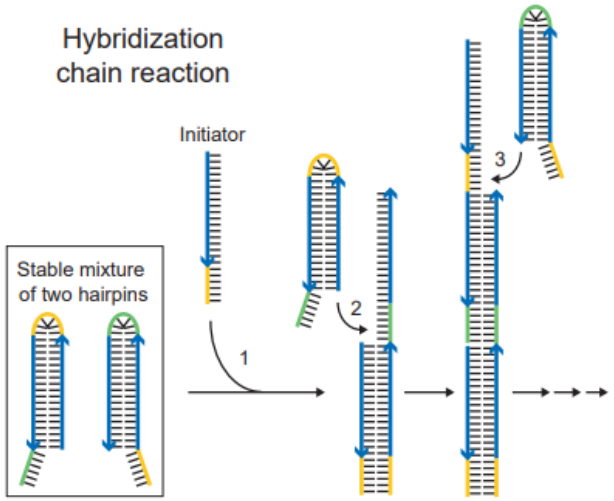

Scheme 3.3. Schematic illustration of hybridization chain reaction (by Daniel Evanko, *Nature Method*, **1**, 186-187 (2004))

There are another group of methods that employ two nucleic acid substrates tagged by two reactive chemical groups respective, and the reaction between two groups occurred when the template strand exists to hybridized two partially complementary substrate strands. Based

on this concept, Kool and co-workers have developed various designs for detection and imaging of target nucleic acid sequence.[14-18] The amplification of signal in the presence of target sequence always accounts for growing fluorescence generated by a templated transformational reactions or chemical ligations, which is continuously enabled by strand displacement reactions.

3.2. Method

In this study, the development of isothermal DNA amplification strategy based on the photo-driven DNA strand displacement[19] is aimed. This is the first design of a DNA amplification method that is proposed to be manipulated by light irradiation with facility and controllability.

Unlike the heterothermal PCR regulated by the changing temperature, spontaneous HCR driven by toehold-included hairpin components or other signal amplification induced by transformational reactions, this method is designed to perform in both isothermal and controllable manner. This is also the first proposal that allows photo-regulatable manipulation and simultaneously yields the amplification product with templated ligation. It is supposed that this method is compatible for both chemical ligation and ligase-induced ligation, which leaves many choices to harvest the appropriate materials for further application.

In the strategy of photo-regulatable DNA amplification, a ligation step is introduced into the original photo-driven DNA strand displacement: after the UV-irradiation-induced dissociation of **Tem**/**Mod** duplex, two substrate strands (substrates, **SL**s) in a much higher concentration than **Tem** and **Mod** hybridize the **Tem**. Then the templated ligating reaction occurred with the **Tem** as scaffolds to give the **Prod** as outputs.

The complete process is illustrated in Scheme 3.4.

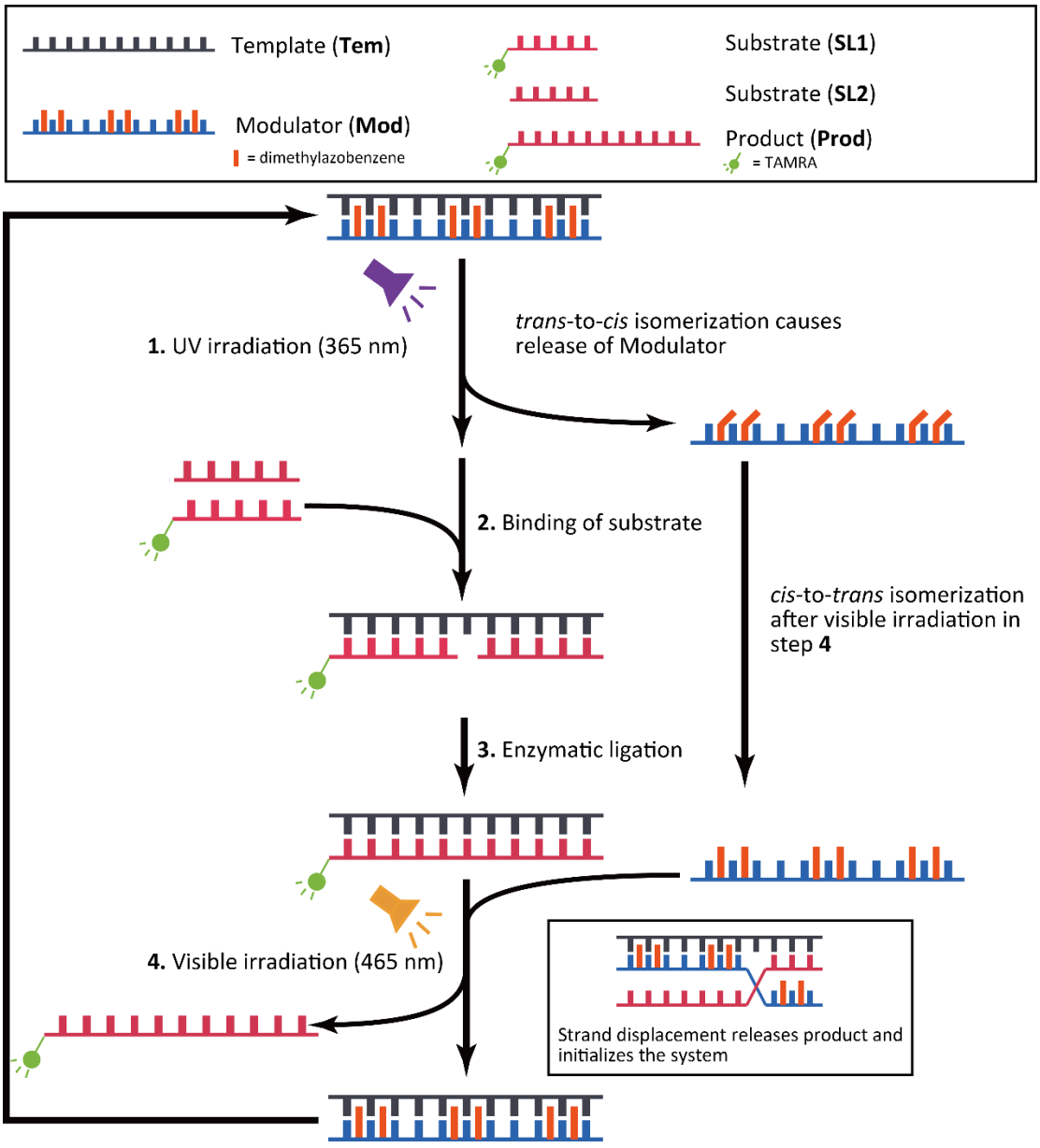

Scheme 3.4. Strategy of photo-regulatable DNA amplification reaction

The system consists of a template strand (**Tem**), an azobenzene-tethered modulator (**Tem**) that is complementary to template strand, and two substrate strands (SLs) each of which is complementary to half of the template. One of the substrate strands is labelled with a TAMRA-group at the 3' end for the quantification of amplification result. Both substrate

strands may be functionalized at 3'- or 5'-end with chemical modifications depending on the type of ligating reaction.

Initially, the azobenzene moieties in **Mod** are in *trans*-form, and this allows its hybridization with **Tem**. Once irradiated with ultraviolet light (UV, 365 nm), azobenzene moieties isomerize to the *cis*-form, inducing dissociation of the duplex of **Tem**/**Mod** thereby permitting **Tem** to hybridize two **SL**s. Ligating reaction then occurs to produce a product strand (**Prod**). The system is then irradiated with visible light (465 nm), by which azobenzene moieties revert to the *trans*-form. This induces the strand displacement so that $\mathbf{Mod}^{cis}$ binds to **Tem** releasing the ligation product **Prod** and initializing the system. In this way, toward alternating irradiation with UV and visible light, amplification of the product can be precisely, quantitatively, and repetitively controlled.

In this strategy, similar to other amplification methods, concentration of **SL**s is set as much higher than it of **Tem**. With the system turning over, the amplified product **Prod** accumulates in the solution thus competitively binds to **Tem** against **SL**s since **Prod** is in doubled length than each **SL** that possesses advantage to form more stable duplex with **Tem**. To keep the system efficient, increase of the concentration of **SL**s can prevent the loss of binding advantage of **SL**s onto **Tem** against **Prod**.

It should be noted that this "amplification" method is not a conventional assay for amplifying target DNA as PCR does, nevertheless, it can amplify the fluorescent signals raised during recognition of target DNA that may contribute to the future development of tools for genetic disease diagnosis.

3.3. Templated ligating reaction of DNA

Templated ligating reaction (Scheme 3.5), the core step of this method, is very crucial for this photo-regulatable system since it directly determines the yield of the amplification.

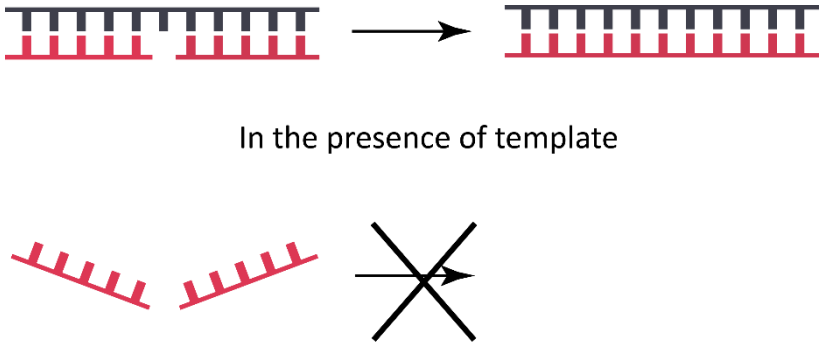

Scheme 3.5. Templated ligation that only reacts in the presence of template

The performance of DNA templated ligating reaction that works in this method can be affected in many ways: the choice of ligating reaction, resistance against light irradiation, template-dependency and so on. Additionally, a cationic copolymer PLL-*g*-Dex is employed in this photo-regulatable amplification assay so that a proper ligating reaction should be compatible with PLL-*g*-Dex, which means neither reactivity of ligation nor activity of PLL-*g*-Dex is obstructed during the whole process.

Basically, two types of templated ligating reactions are usually considered to achieve such a nick sealing process, in which two strands bind to template strand adjacently to leave a non-bonding "nick".

One of them is ligase-induced ligation, which occurs in DNA replication, double strand break repair mechanisms or DNA mismatch repair mechanisms. Ligase-induced ligation usually requires mild conditions and proceed in a moderate reaction speed. Significantly, conjugation of two oligonucleotides by many DNA ligases includes a necessary template recognition process, which averts the detrimental non-templated ligation. Moreover, ligase-induced ligation always offers a natural linkage, phosphodiester bond, thus the ligated product can be freshly used in following biological assays without any loss of the affinity. However, ligating reaction catalyzed by DNA ligase generally proceeds in a low reaction speed compared with chemical ligation. It is also very sensitive and fragile to reacting

conditions so that addition of PLL-*g*-Dex and light irradiation might influence its reactivity in an unpredictable way.

As for chemical ligating reactions, there has been many successful attempts to employ them in various applications, including detections of small molecules or signal amplification of target in extremely low concentration. They are always robust and resistant to the change of environment while presenting high reaction speed as well as yield. Many chemical ligating reactions have been reported in recent tens of years, achieving sensitive method for detection of nucleic acids. However, most of them incorporate unnatural linker into the product, restricting their further utility in physiological environment. Besides, it is also unable to predict if addition of PLL-*g*-Dex disturbs the reaction or not.

To figure out the template-dependent ligating reaction to develop photo-regulatable DNA strand displacement system, I conducted experiments to investigate the performance of two types of ligating reaction mentioned above respectively.

3.3.1. Chemical ligating reaction ---- "click" ligation

3.3.1.1. Copper(I)-catalyzed alkyne-azide cycloaddition (CuAAC)

CuAAC as one of the most conventional orthogonal labelling reaction was studied (Scheme 3.6).[20]

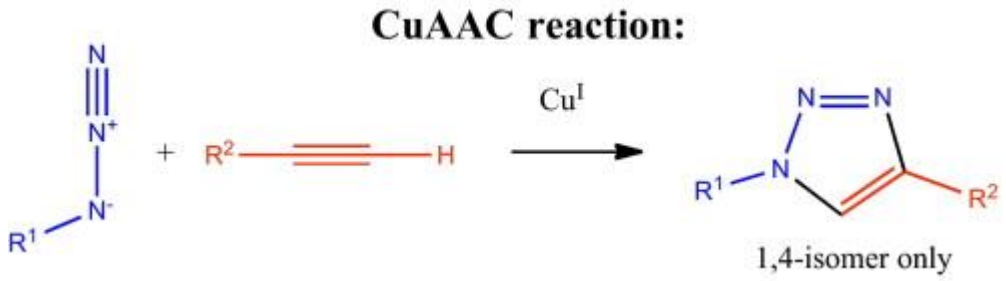

Scheme 3.6. Copper (I) catalysed cycloaddition reaction of an alkyne goup and an azide group.[20]

Sequence used in this study is shown in Table 3.1. A 11-mer **SL-alk** strand is labelled with an alkynyl group at its 5'-end and a FAM group at its 3'-end as one of the **SL**; and a 11-mer **SL-azi** strand is labelled with a azido group as another **SL**. Both of **SL-alk** and **SL-azi** are half complementary to **Tem** to form a "nick" structure ready for ligation. The label with FAM group is to visualize and quantify yield of ligation by electrophoresis assay (polyacrylamide gel electrophoresis analysis, PAGE).

Table 3.1. Sequences used in CuAAC reaction

	Sequence
Tem	5'-GTT ACG CAT CGG TGC TAG ATC G-3'
SL-Azi	3'-/**3AzideN**/CAC GAT CTA GC-5'
SL-Alk	3'-/**FAM**/CAA TGC GTA GC/**5Hexynyl**/-5'
Mod	3'-CAA**Z**TGC**Z**GTA**Z**GCCA**Z**CGA**Z**TCT**Z**AGC-5'

Z=2',6'-dimethyl azobenzene moiety (**dmAzo**)

Firstly, the key property that a desired ligation to be used in photo-regulatable DNA amplification reaction was investigated, the template-dependency. It is fundamental and necessary in a target amplification system, since amplification should only occur in the presence of target, i.e. the target specificity. If amplification occurred even without target, it cannot be used in any diagnostic strategy.

The template-dependency is verified by monitoring the yield at various concentrations of **Tem** and **SL**s. The reaction mixture was firstly made and incubated to ensure the hybridization of **Tem**/**SL** duplex containing a "nick" without Cu^{+} that triggers the ligation. Once the ligand-bound Cu^{+} was added to initialize the ligation, aliquots were taken at the prescribed times and immediately terminated with EDTA solution. All samples were subjected to a denatured PAGE then, by which I could confirm the generation of ligated product and quantified the exact yield at each prescribed times. Concentrations of both **Tem** and **SL**s were set at 2 μM.

The result is shown in Fig. 3.1.

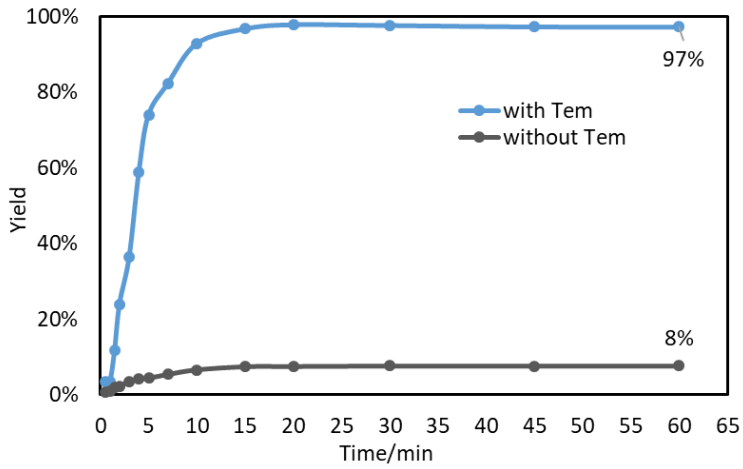

Figure 3.1. Time course of CuAAC in the presence (blue) and absence (gray) of **Tem**. Conditions: 2.2 μM **Tem** or none, 2 μM **SL-Alk**, 2 μM **SL-Azi**, 2 mM ascorbate sodium, 1 mM THPTA, 0.2 mM $CuSO_4$, 100 mM NaCl, phosphate buffer (pH 7.0) 25 ^oC.

Quantification shows a rapid ligating reaction that ligation yield of over 90% is obtained with in 15 min in the presence of **Tem,** while ligation almost does not proceed in the absence of template. The ligation in the presence of **Tem** finally reached a yield of 97%, compared with a yield of 8% in the absence of **Tem**.

This result demonstrates that "click" ligation CuAAC does achieve high ligation rate and performs only in the assistance of template. This is agreed with conclusion in literatures that employed CuAAC to templatedly ligate oligonucleotides for detection or amplification purpose.

Next, to simulate the actual conditions in amplification reaction where a much higher equivalents of **SL**s will be used with respect to **Tem**, the same experiment was conducted with samples including inequitable concentration of **Tem** and **SL**s. In this experiment, concentration of **SL**s was set at 500 nM while concentration of **Tem** was controlled.

The result is shown in Fig. 3.2.

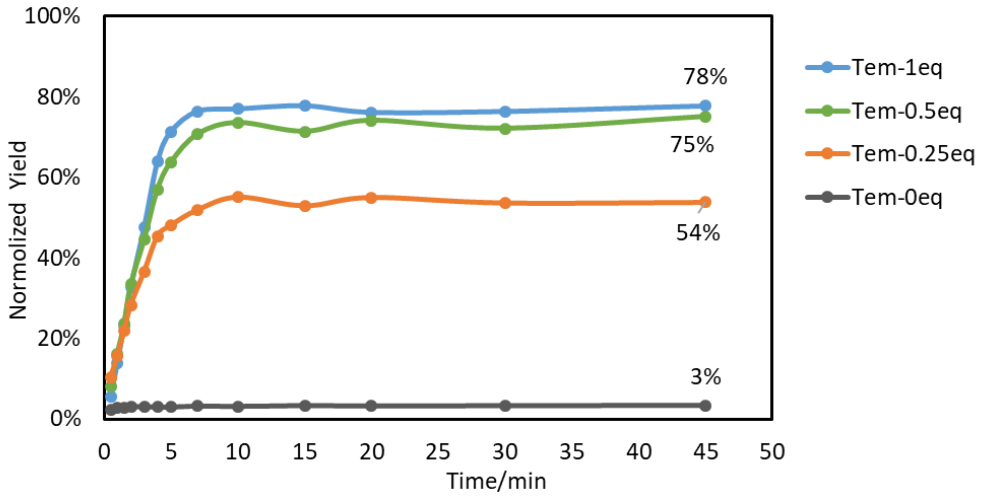

Figure 3.2. Time course of CuAAC in the presence of **Tem** at various concentration. Conditions: 500 (blue), 250 (green), 125 (orange) nM **Tem** or none (gray), 500 nM **SL-Alk**, 500 nM **SL-Azi**, 0.5 mM ascorbate sodium, 0.5 mM THPTA, 50 µM $CuSO_4$, 100 mM NaCl, phosphate buffer (pH 7.0) 25 °C.

The normalized yield instead of original yield was calculated to compare ligations in the presence of **Tem** in a gradient equivalent, as shown in the legend in Fig. 3.2. This is because templated ligation occurred only when substrate strands bind to template so that theoretically only equal equivalent of product can be obtained with respect to template. Therefore, the 100 % yield should be determined by concentration of **Tem**. For this reason, yields obtained from gel electrophoresis is normalized by concentration of **Tem** in each ligation assays for comparison.

As shown, all three ligations in the presence of **Tem** in 1.0, 0.5 and 0.25 equivalents to **SL**s arrived in the maximum yield within 10 minutes, giving final yields of 78%, 75% and 54% respectively. The reaction in the absence of **Tem** eventually resulted in almost no ligation.

It is reasonable that reaction proceeded in higher speed when concentration of substrates was lower since equivalents of catalysts were maintained as the same as used in higher concentration of substrates in previous experiment, which means the concentration of catalysts were lower. When **Tem** is in the equal equivalent with **SL**s, the yield of 78% was

lower than the yield of 97% in previous experiment (Fig. 3.1), probably due to the decreased concentration of **SL**s. The decrease of concentration lowered the melting temperature of **Tem**/**SL** so that result in an inhibited yield. This effect might also be account for the reducing yields of ligations in lower equivalents of **Tem**, which was against the expectation that higher equivalents of **SL**s could benefit the equilibrium of **Tem**/**SL** duplex hybridization. Anyhow, the CuAAC reaction showed outstanding template-dependency in a rapid reaction speed.

Next, CuAAC reaction's compatibility with cationic chaperon polymer PLL-*g*-Dex was studied.

CuAAC reaction was performed with the addition of PLL-*g*-Dex in the presence or absence of **Tem** with an equal concentration of **SL**s. After mixing all contents except ligand-bound Cu^{+}, the reaction was triggered by adding catalysts. Aliquots were taken at 0 min (after adding catalyst), 5 min and 10min, and subjected to denatured PAGE.

The result is shown in Fig. 3.3.

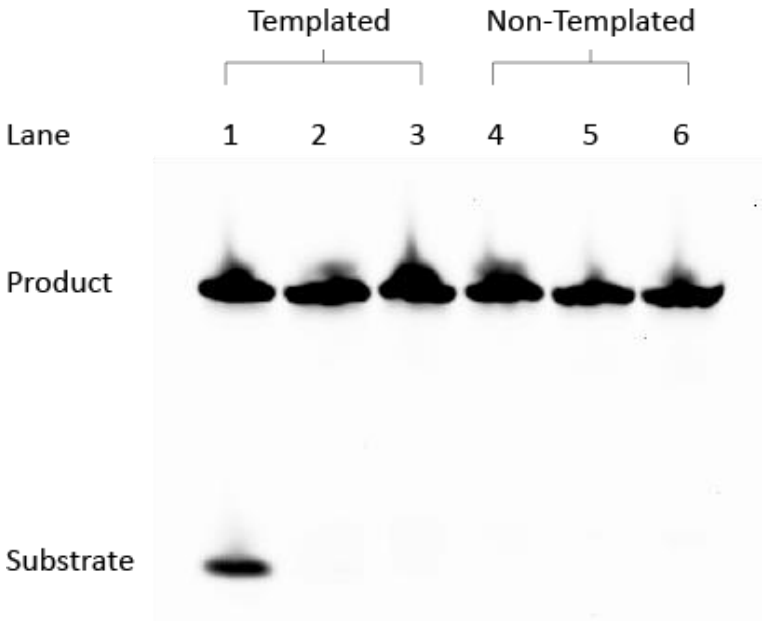

Figure 3.3. PAGE of CuAAC reaction in the presence of PLL-*g*-Dex. Lane 1-3, reaction time 0 min, 3 min, 5 min, in the presence of **Tem**; lane 4-6, reaction time 0 min, 3 min, 5 min, in the absence of **Tem**. Conditions: 200 nM **Tem** or none, 10 μM **SL-Alk**, 10 μM **SL-Azi**, 10 mM ascorbate sodium, 10 mM THPTA, 1 mM $CuSO_4$, PLL-*g*-Dex (N/P=1.5), 100 mM NaCl, phosphate buffer (pH 7.0) 25 °C.

Ligating reactions proceeded excessively quickly either with **Tem** or without **Tem** in the presence of PLL-*g*-Dex. The reaction with **Tem** even finished in the first several seconds after triggered by Cu^{+} before sampled (since the mixing and sampling operation takes several seconds anyways, 0 min does not impeccably indicate the initial timing of the reaction).

It is surprising that PLL-*g*-Dex incredibly accelerated the ligating reaction in a template-independent manner. Even in the case that no **Tem** participated the reaction, all substrates were ligated after merely five minutes. This result denies the possibility to apply CuAAC reaction for photo-regulatable DNA strand displacement system since it would cause non-targeted amplification.

3.3.1.2. Strain-promoted alkyne-azide cycloaddition (SPAAC)

Another common "click" ligation, Strain-Promoted Alkyne-Azide Cycloaddtion (SPAAC) reaction was also examined as one of the candidates for a templated amplification reaction (Scheme 3.7).

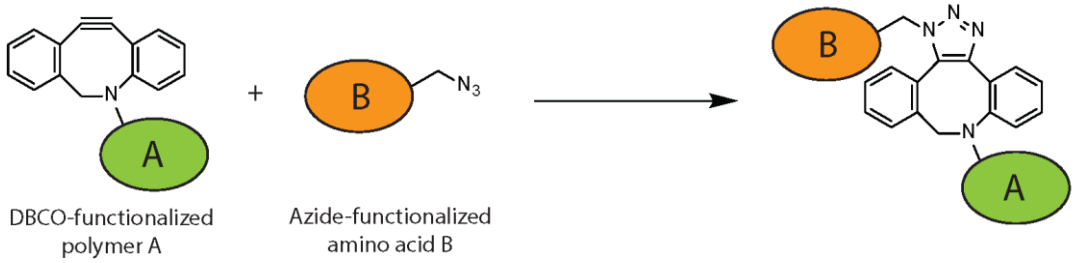

Scheme 3.7. Strain-promoted alkyne-azide cycloaddition reaction (by iGEM Team TU Eindhoven 2014)

Compared with CuAAC, it is a copper-free coupling reaction, which is promisingly suitable for those applications in cellular environment. It is also reported to process in higher speed and show better template-dependency rather than CuAAC reaction.[21] SPAAC implicates reaction between a strained alkyne group and an azide group through [3+2] cycloaddition reaction to give a 1,2,3-triazol structure.

Though there has been plenty of cyclooctynes derivatives that efficiently participate SPAAC reaction, dibenzocyclootane (DBCO) is still one of the most used strained group as it is commercially available.

To test if SPAAC reaction fulfill the requirement of template-dependency in photo-regulatable DNA strand displacement facilitated by the cationic chaperon polymer PLL-*g*-Dex, a DBCO group is attached at the 5'-end of a 11-mer **SL-DBCO**, on the 3'-end of which a FAM group is labeled as one of the **SL**s; and a 11-mer **SL-azi** strand is labelled with a azido group as another **SL**. Both of **SL-DBCO** and **SL-azi** are half complementary to **Tem** to form a "nick" structure ready for ligation. The label with FAM group is to visualize and quantify yield of ligation by electrophoresis assay (polyacrylamide gel electrophoresis analysis, PAGE).

The sequence of strands used in this section is shown in Table 3.2.

Table 3.2. Sequences used in SPAAC reaction

	Sequence
Tem	5'-GTT ACG CAT CGG TGC TAG ATC G-3'
SL-Azi	3'-/3AzideN/CAC GAT CTA GC-5'
SL-DBCO	3'-/FAM/CAA TGC GTA GC/DBCO/-5'
Mod	3'-CAAZTGCZGTAZGCCAZCGAZTCTZAGC-5'

Z=2',6'-dimethyl azobenzene moiety (**dmAzo**)

Firstly, template-dependency was examined in phosphate saline buffer solution. **Tem**, **SL-DBCO** and PLL-*g*-Dex were premixed in the buffer solution and incubated. Once the **SL-Azi** was added, the reaction was triggered. Reaction was sampled and terminated at 0min, 3min and 5min. The result is as shown in Fig .3.4.

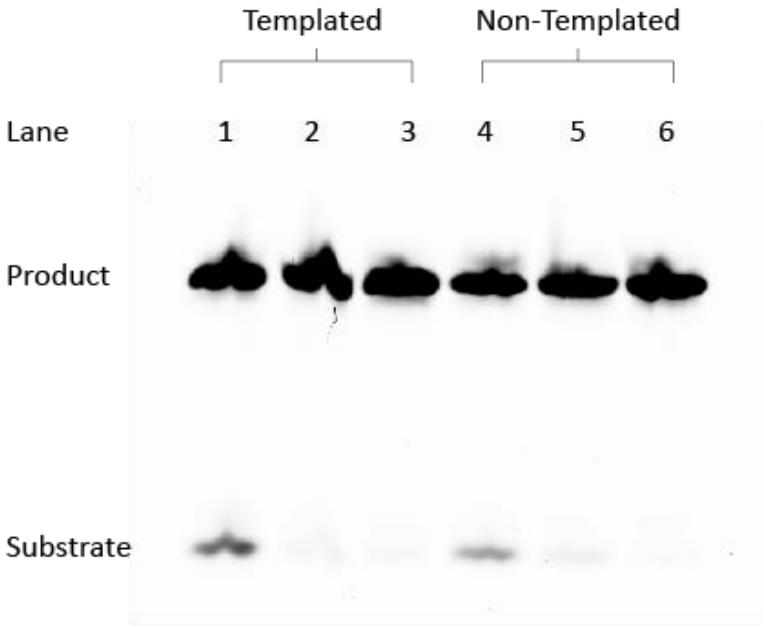

Figure 3.4. PAGE of SPAAC reaction in the presence of PLL-*g*-dex. Lane 1-3, reaction time 0 min, 3 min, 5 min, in the presence of **Tem**; lane 4-6, reaction time 0 min, 3 min, 5 min, in the absence of **Tem**. Conditions: 200 nM **Tem** or none, 10 μM **SL-DBCO**, 10 μM **SL-Azi**, PLL-*g*-Dex (N/P=1.5), 100 mM NaCl, phosphate buffer (pH 7.0), 25 ºC.

The SPAAC reaction occurred rapidly either with **Tem** or without **Tem** in the presence of PLL-*g*-Dex. The reaction with **Tem** even finished in the first several seconds after triggered by Cu^{+} before sampled (since the mixing and sampling operation takes several seconds anyways, 0 min does not impeccably indicate the initial timing of the reaction). The same as CuAAC reaction, the SPAAC reaction showed no template-dependency, either, probably due to the addition of PLL-*g*-Dex.

To figure out if the non-templated ligation occurred because of the overhigh concentration of substrates, I next conducted the PLL-*g*-Dex-assisted SPAAC reaction with or without template in a series of concentrations of substrates. Concentration of **SL**s was set in gradient: 2μM, 1μM, 0.5μM and 0.1μM while concentration of **Tem** was 1/10 of substrates in all cases.

The results are shown in Fig. 3.5.

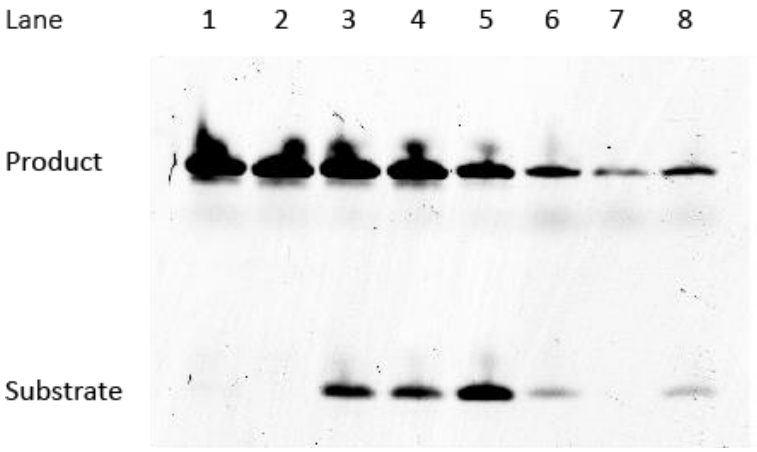

Figure 3.5. PAGE of SPAAC reaction at various concentration. Lanes 1, 3, 5, 7 indicate reaction in the presence of **Tem** and lanes 2, 4, 6, 8 indicate reaction in the absence of **Tem**. Lane 1 and 2, 200 nM **Tem** or none, 2 µM **SL**s; lane 3 and 4, 100 nM **Tem** or none, 1 µM **SL**s; lane 5 and 6, 50 nM **Tem** or none, 0.5 µM **SL**s; lane 7 and 8, 10 nM **Tem** or none, 0.1 µM **SL**s. Conditions: PLL-*g*-Dex (N/P=1.5), 100 mM NaCl, phosphate buffer (pH 7.0), 25 ^{o}C, 5 min reaction time.

In all four cases, reactions processed very rapidly even without template. This result supported the previous result (Fig. 3.4) that SPAAC reaction in the presence of PLL-*g*-Dex did not perform in a template-dependent manner.

However, it is obvious that the decrease of substrates concentration inhibited non-templated reaction, resulting in a decreasing yield of ligation, though it remained too high to be utilized in photo-regulatable DNA strand displacement system (except for lane 5, which might be the result of an contaminated sample).

3.3.1.3. PLL-*g*-Dex in templated chemical ligating reaction

Facing the failure in achieving templated "click" ligation, the reason why addition of PLL-*g*-Dex led to the non-templated reaction is very intriguing. An assumption was raised attempting to explain the annoying result.

It is assumed that PLL-*g*-Dex strongly binds to substrate strands via static interaction, which mimics the process of DNA templation thereby increase the chance for two substrate

strands to get closer enough and react. It is reasonable since combination of PLL-*g*-Dex and DNA duplex or single strand is not specific to sequence. If PLL-*g*-Dex acted as template to allow the ligation, theoretically all the chemical ligating reaction might lose their template-dependency in the existence of PLL-*g*-Dex.

To validate the assumption, a PLL-*g*-Dex concentration control experiment was implemented.

With samples containing only two **SL**s (each for 10 μM), dosage of PLL-*g*-Dex ranged from N/P ratio of 0 to N/P ratio of 2.0. In this experiment, SPAAC reaction was used since it was reported to possess great template-dependency and better biocompatibility according to literatures. The sample was prepared by simply dissolving **SL-DBCO** and PLL-*g*-Dex at pre-determined N/P ratio and SPAAC reaction was initialized by adding **SL-Azi**.

According to the result in section 3.3.1.2, non-templated SPAAC occurred. It this non-templated behavior is due to the polymer-templation as my assumption indicates, processivity of ligation should present a polymer-concentration-dependent manner since PLL-*g*-Dex provides scaffolds for substrates to get adjacent.

The gel electrophoresis result is shown in Fig. 3.6, and the calculation is shown in Fig. 3.7.

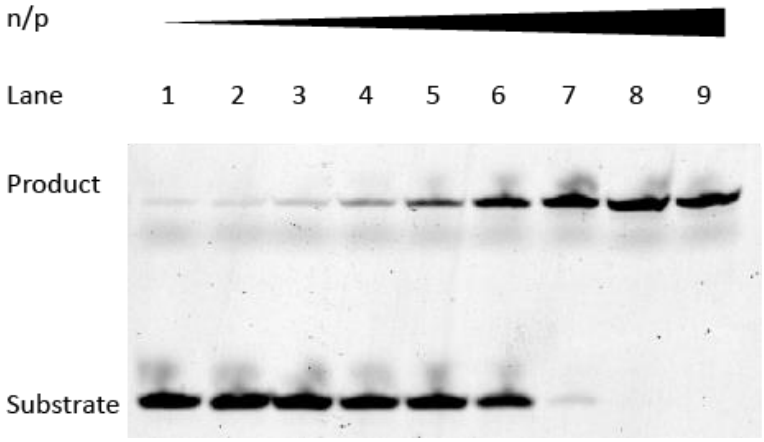

Figure 3.6. PAGE of non-templated SPAAC reaction in the presence of PLL-*g*-dex at various concentration. From lane 1 to 9, N/P ratios are 0, 0.01, 0.05, 0.1, 0.2, 0.5, 1, 1.5 and 2. Conditions: 10 μM **SL-DBCO**, 10 μM **SL-Azi**, 100 mM NaCl, phosphate buffer (pH 7.0), 25 °C, 5 min reaction time.

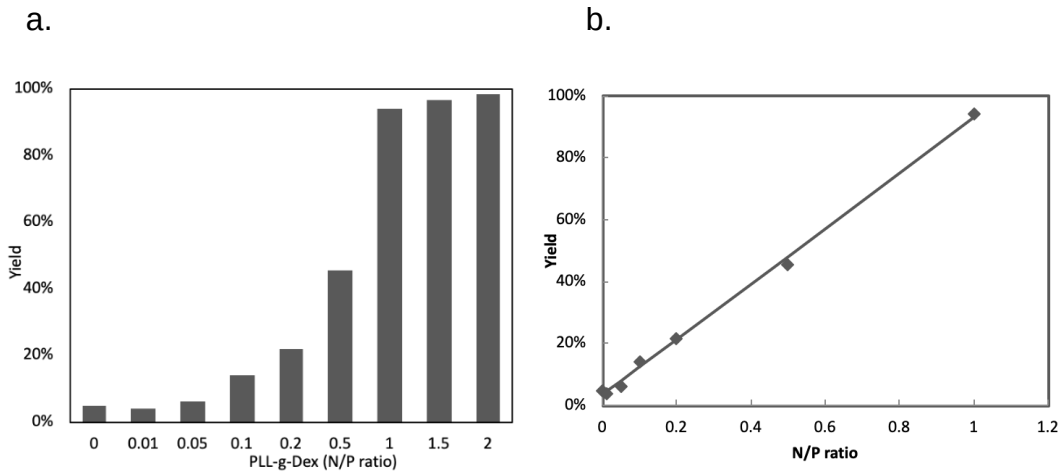

Figure 3.7. Yields of every SPAAC reaction in Fig. 3.6 (a) and the regression of the yield with respect of N/P ratio (b).

From Fig. 3.6, surprisingly, non-templated SPAAC reaction revealed a strong dependency on the dosage of PLL-*g*-Dex: with the increase of PLL-*g*-Dex dosage, yield of non-templated ligation.

The band intensity was calculated thus transformed into yield bar chart (Fig. 3.7a), which was further regressed on N/P ratio to give the Fig. 3.7b.

The result suggested yield of non-templated ligation strongly dependent on the dosage of PLL-*g*-Dex. Yield kept growing with the increase of N/P ratio of PLL-*g*-Dex to reach 95% at N/P ratio of 1.0, which represents an equal concentration of amino groups in PLL-*g*-Dex and phosphate groups in DNA. Yield stopped growing after N/P ratio increased over 1.0. It is very important that yield just arrived about 100% when N/P ratio was 1.0, with which dosage all **SL**s was bound to PLL-*g*-Dex. This fact that ligation occurs when substrates combines with PLL-*g*-Dex supports the assumption that PLL-*g*-Dex acts as template instead of **Tem** in non-templated "click" ligation.

The regression result further funds the assumption by giving an almost perfect linear relation of yield with respect to N/P ratio of PLL-*g*-Dex. This linear relation suggests the processivity of non-templated ligation is quantitatively dependent on the dosage of PLL-*g*-Dex, which is similar to the yield of templated ligation's dependency on template.

Though the result of polymer dosage control experiment strongly supported the assumption that PLL-*g*-Dex templated the SPAAC reaction without a DNA template, the mechanism how the templation took place remains unknown. Therefore, it is difficult to claim that the non-templated reaction is enabled by templation of PLL-*g*-Dex. However, if the assumption is valid, all chemical ligating reaction may undergo the same process and caused the non-templated ligation.

By all means, it is clearly stated that the addition of PLL-*g*-Dex disapproves template-dependency of "click" ligating reaction. Other templated ligating reaction that specifically occurs in the presence of template should be explored.

3.3.2. Ligase-induced ligating reaction

To solve the problem that non-templatd reaction occurred in the "click" ligating reaction, I considered ligase-induced ligation as a solution.

Unlike chemical ligating reaction, ligase binds to the "nick" position and repairs the break through forming a phosphodiester bond between 5'-phosphorylated and 3'-OH termini. There are some ligases such as ATP-dependent T7 DNA ligase specifically recognize and repair the double-strand breaks especially sticky ends and nicks. Therefore, the ligase-induced ligating reaction is promising to achieve the template-dependent ligation.

3.3.2.1. Ligation calculated by thermostable ligase

Firstly, two thermostable DNA ligases, a NAD^+-based *Taq* ligase and a ATP-based 9^o N^{TM} ligase, were researched in the presence or absence of PLL-*g*-Dex.

The result is shown in the gel electrophoresis analysis in Fig. 3.8.

The sequences of strands used in this chapter are shown in Table. 3.3.

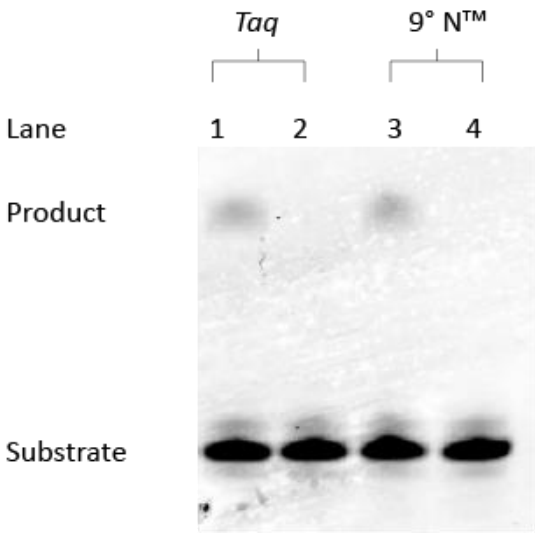

Figure 3.8. Ligation catalyzed by thermostable ligases in the presence (lanes 2 and 4) and absence (lanes 1 and 3) of PLL-*g*-Dex. Lanes 1 and 2, *Taq* ligase; lanes 3 and 4, 9° N™ ligase. Conditions: 1 µM **Tem** or none, 10 µM **SL-1**, 10 µM **SL-2**, PLL-*g*-Dex (N/P=1.5) or none, 16 U/µL ligase, 1 x ligase reaction buffer solution, 50 °C.

Table 3.3. Sequences used in ligase-induced ligation

	Sequence
Tem	5'-GTT ACG CAT CGC TGC TAG ATC G-3'
SL-1	3'-/TAMRA/CAA TGC GTA GC/**p**/-5'
SL-2	3'-GAC GAT CTA GC-5'
Mod	3'-CAAZTGCZGTAZGCCAZCGAZTCTZAGC-5'

Z=2',6'-dimethyl azobenzene moiety (**dmAzo**)

The result in Fig. 3.8 suggested unsuccessful ligation in the samples containing PLL-*g*-Dex. In both cases employing *Taq* ligase or 9° N™ ligase, templated ligation were inhibited with the addition of PLL-*g*-Dex. These two thermostable ligases have similar structures, thus PLL-*g*-Dex might inhibit their reactivity by directly interacting structurally or forming complex with DNA duplex, which could not be recognized by ligase active site.

3.3.2.2. Other common ligases

Then, I turned to two more commonly used DNA ligases: salt-tolerated T3 ligase and a double-strand dependent T7 ligase, both of which have been reported to ligate templated substrates efficiently. The reason why the most widely used T4 was not considered here is due to its reactivity to ligate blunt ends double strands, which might result in unwanted side reaction of duplex/duplex ligation.

The ligation catalyzed by T3 ligase was performed to study if it normally functioned in the presence of PLL-*g*-Dex, as shown in Fig. 3.9.

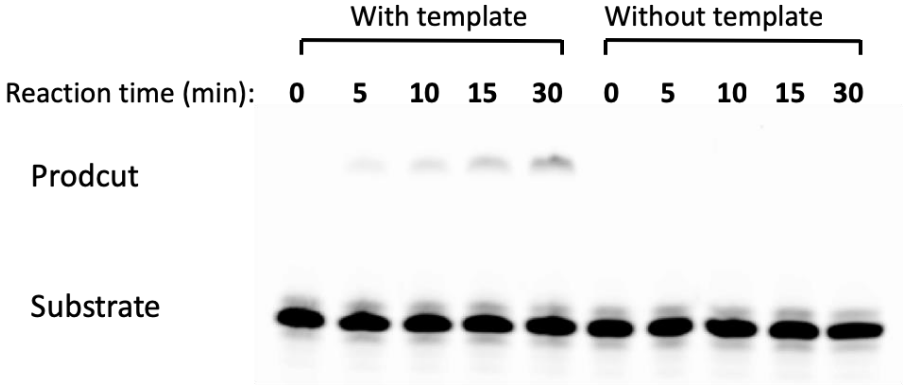

Figure 3.9. Template-dependency of ligation catalyzed by T3 DNA ligase. Conditions: 200 nM **Tem** or none, 10 μM each **SL-1** and **SL-2**, PLL-*g*-Dex at N/P = 1.5, 16 U/μL T3 ligase, performed in 1 x T3 reaction buffer at 37 °C.

The result suggests an expected templated ligation of substrates, which did not occur in the absence of **Tem**. Therefore, T3 DNA ligase is a good ligation-catalyst to be used in photo-regulatable DNA amplification reaction. Since T3 ligase and T7 ligase share the similarity in structure, T7 ligase should catalyze the ligation in the same template-dependent fashion.

To figure out the efficiency of T3 and T7 ligases when they work with PLL-*g*-Dex, five-cycle photo-regulatable amplification reactions were carried out.

The result is shown in Fig. 3.10.

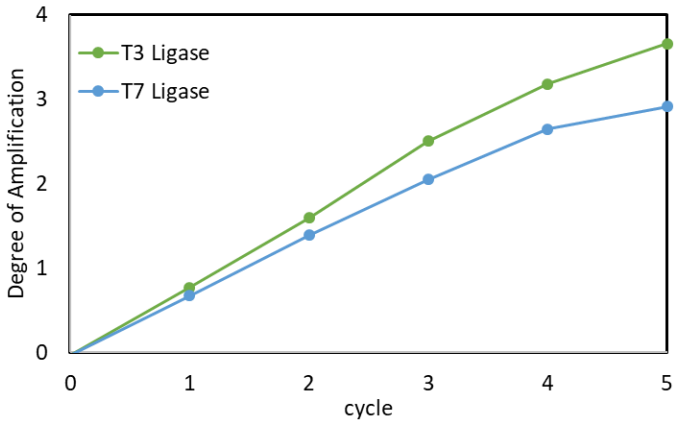

Figure 3.10. Photo-regulatable DNA amplification reaction catalyzed by T3 and T7DNA ligase. Conditions: 200 nM **Tem**, 10 μM each **SL-1** and **SL-2**, PLL-*g*-Dex at N/P = 1.5, 16 U/μL T3 or T7 ligase, performed in 1 x T3 or T7 reaction buffer at 37 °C.

T3 DNA ligase presented a higher reactivity than T7 in this method, which might due to its better salt-tolerate property. According to this result, T3 DNA ligase was employed for the further study of photo-regulatable DNA amplification reaction.

3.4. Photo-regulation of DNA amplification

After figuring out that the T3 ligase shows the best reactivity working in the presence of PLL-*g*-Dex, amplification reaction was conducted according to the design in section3.2.

All DNA strands (**Tem**, **SL**s and **Mod**) and PLL-*g*-Dex were dissolved in T3 ligase reaction buffer and incubated at 37°C for several minutes. As the T3 ligase was added to initialized the reaction, sample was irradiated by UV light (365 nm) for five minutes, followed by thirty minutes ligation step in dark and finally visible light (455 nm) was irradiated for five minutes to initialize the system again to finish an amplification cycle. Aliquots were taken and terminated in EDTA-contained loading buffer solution immediately after adding T3 ligase and visible light irradiation step in every amplification cycle, as shown in Scheme 3.8.

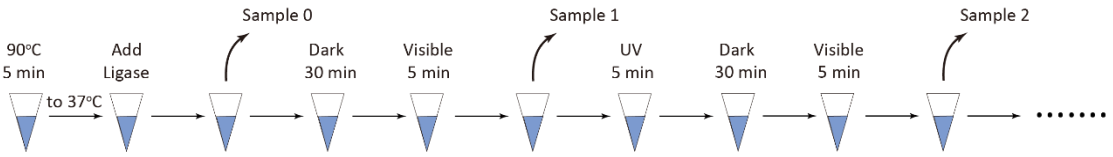

Scheme 3.8. Protocol of photo-regulatable DNA amplification assay. DNAs and PLL-*g*-Dex are first dissolved in 1 x reaction buffer solution and incubated at 37 °C. after adding ligase, the ligation is triggered. A complete irradiation cycle includes 5 min UV light irradiation at 365 nm, 30 min reaction in dark and 5 min visible light irradiation at 455 nm. Aliquots are collected after adding ligase and at the last of every cycle.

To achieve a multiple amplification, the concentration ratio of template and substrate is 1:50, therefore there should be theoretically 2% of substrate to be ligated in a single cycle. Here I define the Degree of Amplification (*DA*) value to evaluate the extent of amplification reaction (for the detailed definition see Experimental Section). For instance, 2.0 DA indicates that the amount of ligated substrate, i.e. product, is 2 times higher than that of template, which is 400 nM.

The result of fourteen cycles of amplification are shown in Fig. 3.11.

When the number of light irradiation cycles increased, the intensity of the ligated product band increased (Fig. 3.11a). This is the direct evidence that product was successfully amplified during the alternating irradiation by UV and visible light.

As shown in Fig. 3.11b, the calculated *DA* curve with respect to amplification cycles revealed that total amplification yield increased almost linearly in 14 cycles. The slowed increase in last several cycles is probably caused by emulative inhibition derived from the decrease in substrate concentrations and the increase of product concentration. This result demonstrated the successful photo-regulatable DNA amplification reaction assisted by PLL-*g*-Dex. After fourteen cycles, a total amplification yield of approximately 800% was obtained, equaling an average yield of 57% for every cycle. This average yield for every cycle is reasonable if the photo-regulation efficiency of 65% that was obtained in photo-driven strand displacement reaction and yield T3-ligase-induced ligation are both taken into consideration.

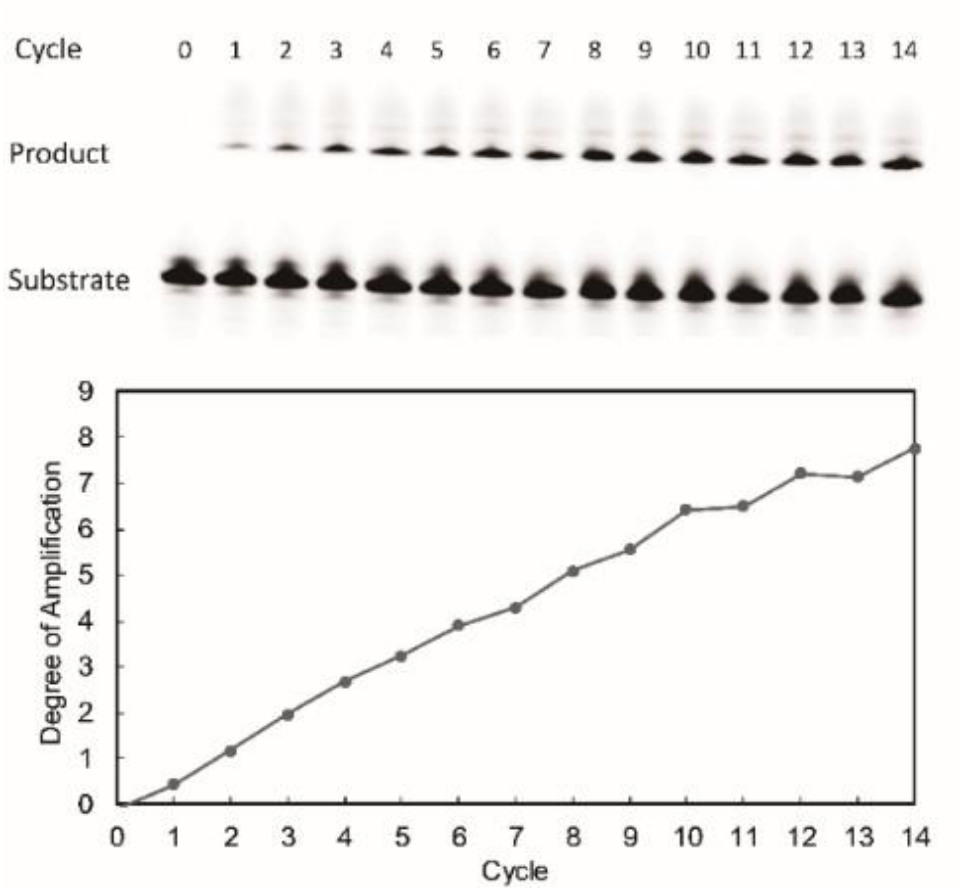

Figure 3.11. Amplification is almost linear over 14 irradiation cycles. PAGE image shows 14-cycle photo-regulatable DNA amplification. Lane 0, before adding of T3 ligase; lanes 1-14, products of first to fourteenth cycles. *DA* after each cycle calculated from fluorescence intensity of bands in PAGE image. Conditions: 200 nM **Tem**, 10 µM each **SL-1** and **SL-2**, 2 µM **Mod**, PLL-*g*-Dex at N/P = 1.5, 16 U/µL T3 ligase, performed in 1 x T3 reaction buffer at 37 ^{o}C.

Though the amplification was slowed after twelve cycles due to the emulative inhibition so that the amplification after fourteen cycles are not shown here, a higher number of amplification cycles is predictable with a larger initial equivalent ratio of **SL**s and **Tem**.

3.5. Azobenzene, Modulator and light dependency of the photo-regulatable DNA strand displacement

So far, successful an isothermal DNA amplification composed of a photo-driven strand displacement mechanism and a ligase-induced ligating reaction was achieved to amplify the signal of target linearly. To note, this is the first nucleic acids amplification method that is controllable by light irradiation in different wavelength.

The precise manipulation with light irradiation is designed to undergo the following pathway:

1). Light irradiation (UV or visible light) induces the isomerization of azobenzene derivatives

2). Configurational change brought by azobenzene stabilizes/destabilizes **Tem**/**Mod** duplex

3). Strand displacement

Though the efficiency of photo-regulation has been thoroughly investigated in chapter 2, there remains doubt that if every step in the photo-regulation pathway is necessary for a photo-regulatable DNA amplification reaction.

To verify the above issue, a series control experiments were carried out to individually enquiry if a complete photo-regulation occurs tracking the designed pathway. In each experiment, incorporation of azobenzene derivatives, chemical modification of azobenzene moieties, participation of **Mod** as well as implementation of light irradiation were arranged to be absent respectively. For each experiment, five-cycle alternating irradiation was conducted and reaction was terminated to be visualized and quantified by gel electrophoresis assay.

The *DA* of control experiments are shown in Fig. 3.12.

The sequence of **Mod**s used in this study is shown in Table 3.4.

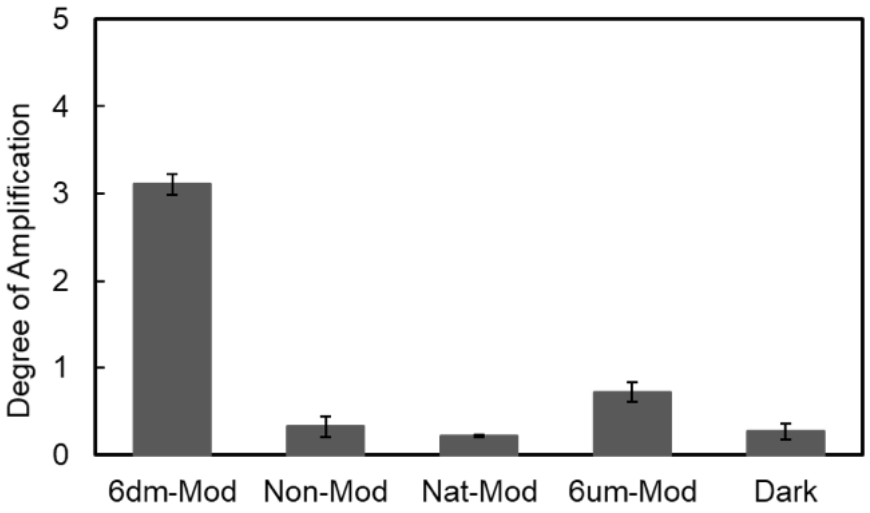

Figure 3.12. Five-cycle photo-regulatable DNA amplification with different **Mod**. Conditions: 200 nM **Tem**, 10 μM each **SL-1** and **SL-2**, 2 μM **Mod** or none, PLL-*g*-Dex at N/P = 1.5, 16 U/μL T3 ligase, performed in 1 x T3 reaction buffer at 37 °C.

Table 3.4. Sequences used in photo-controllability experiment

	Sequence
Tem	5'-GTT ACG CAT CGC TGC TAG ATC G-3'
SL-1	3'-/TAMRA/CAA TGC GTA GC/**p**/-5'
SL-2	3'-GAC GAT CTA GC-5'
Mod-Nat	3'-CAATGCGTAGCCACGATCTAGC-5'
Mod-6um	3'-CAAXTGCXGTAXGCCAXCGAXTCTXAGC-5'
Mod-6dm	3'-CAAZTGCZGTAZGCCAZCGAZTCTZAGC-5'

X=unmodified azobenzene moiety (**umAzo**)

Z=2',6'-dimethyl azobenzene moiety (**dmAzo**)

Compared with amplification facilitated by **Mod-6dm**, all other amplification reactions showed a decreased *DA* to various extents. The amplification without the participation of **Mod** could not process at all, revealed by a very low *DA*. Apparently the strand displacement

could not occur without the existence of **Mod**. A similar low *DA* was obtained in the trial with native **Mod**, meaning the **Mod** where no azobenzene derivatives were incorporated into. This result demonstrates the necessity that only without stabilization and destabilization of duplex caused by incorporation of azobenzene derivatives in *trans*- or *cis*-form, the strand displacement could hardly occur to direct a strand-displacement-based amplification. The comparably low *DA* of amplification with **Mod-6um** tethering unmodified azobenzene moieties showed the consistence with conclusion in chapter 2: chemical modification strongly improved the efficiency of photo-regulation by enhancing hydrophobic stacking effect of azobenzene derivatives in *trans*-form and steric hindrance of them in *cis*-form simultaneously. Finally, absence of light irradiation disabled the amplification, either, demonstrating a light-specific promotion of this method.

Based on above results, it can be concluded that photo-regulation of this DNA amplification reaction undergoes the pathway as designed, alternatively validating the photo-responsivity of method in this study.

3.6. Discrimination of mismatch in target sequence

As a signal amplification method that may be applied to target sequence detection tool in clinical diagnosis, one of the most important property is to recognize nucleotide mismatch in the target sequence.

To test if this photo-regulatable DNA amplification method can discriminatively amplify target signal, a series template strands containing mismatches were employed in a five-cycle amplification assay. Besides, amplification trials with a polyT template and without template were also performed as controls.

The sequence used in this experiment are shown in Table 3.5.

The result of experiment is shown in Fig. 3.13.

Table 3.5. Sequences used in mismatch-discrimination experiment

	Sequence
Tem	5'-GTT ACG CAT CGC TGC TAG ATC G-3'
Mis11	5'-GTT ACG CAT C**C**C TGC TAG ATC G-3'
Mis7/16	5'-GTT ACG **G**AT CGC TGC **A**AG ATC G-3'
Mis11/16	5'-GTT ACG CAT C**C**C TGC **A**AG ATC G-3'
PolyT	5'-TTT TTT TTT TTT TTT TTT TTT T-3'
SL-1	3'-/TAMRA/CAA TGC GTA GC/**p**/-5'
SL-2	3'-GAC GAT CTA GC-5'
Mod-6dm	3'-CAAZTGCZGTAZGCCAZCGAZTCTZAGC-5'

Bases in **Red** indicate the mismtaches

Z=2',6'-dimethyl azobenzene moiety (**dmAzo**)

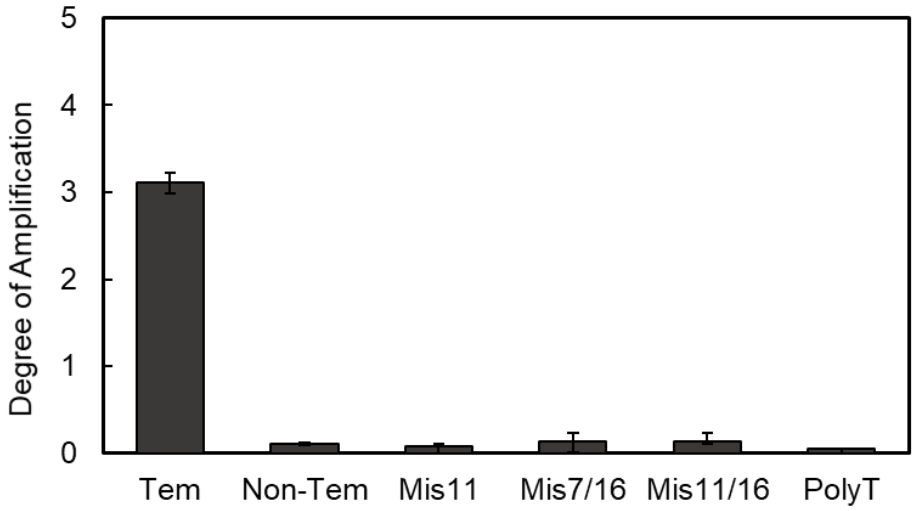

Figure 3.13. Photo-regulatable DNA amplification is sequence-specific. Degree of Amplification value was calculated from fluorescence intensity of bands in PAGE. Conditions: 200 nM **Tem**, 10 µM **SL-1** and **SL-2**, 2 µM **Mod**, PLL-*g*-Dex at N/P ratio of 1.5, 16 U/µL T3 ligase, performed in 1 x T3 reaction buffer at 37 oC. For all samples, 5 cycles of amplification were conducted.

The introduction of mismatch into template sequence significantly reduce the complementarity of duplex thereby suppresses the duplex forming process.

I conducted photo-regulatable amplification reactions with **Mis11**, **Mis7/16** and **Mis11/16** as template strand respectively. According to the result in Fig. 3.11, amplification was not observed with all three mismatched templates, revealed by the excessively low *DA*. The introduction of mismatch into template sequence significantly reduce the complementarity of **Tem**/**SL** duplex thereby suppresses the duplex forming process. In the control experiments with **polyT** template or without any template, there was no amplification product observed. Apparently, the decreasing stability of duplex generated from mismatches prevented the ligation thus the photo-driven strand amplification was not triggered. This result indicates that the strategy achieves accurate amplification of a specific target sequence.

3.7. Conclusion

In this chapter, I have developed a photo-regulatable and isothermal DNA amplification method that relies on light-induced isomerization of an azobenzene in modulator oligonucleotide and chaperone polymer PLL-**g**-Dex.

I first investigated the templated ligating reaction to find out the appropriate ligating solution for this strategy. Two types of "click" ligation, CuAAC and SPAAC, showed the loss of template-dependency in the presence of cationic polymer PLL-*g*-Dex. It is reasoned by a polymer dosage control experiment that revealed a linear relation of non-templated ligation yield with respect to concentration of PLL-*g*-Dex, demonstrating that PLL-*g*-Dex may act as a template instead of DNA template strand to provide scaffolds for occurrence of ligation. This result suggests that other chemical ligating reaction may lead to the same result. Therefore, the ligation catalyzed by DNA ligase was investigated and presented template-dependency in the presence of PLL-*g*-Dex. Finally, T3 DNA ligase showed the highest sympathy to catalyze the most efficient amplification among three DNA ligases.

When alternating irradiation was conducted to examine the strategy with ligase-induced ligation, the amplification was observed over 14 cycles in a linear increased yield. The photo-responsivity was researched by looking into every step in the photo-regulation pathway by a series experiment. Outstanding photo-controllability revealed by this method offers possibilities of precise control of an amplification process, which so far has been consecutive and uninterruptable in other isothermal amplification methods such as rolling circle amplification. The discriminability of mismatched template was studied by incorporating several template strands containing one or two mismatches. In all cases, amplification successfully recognized the mismatched sequence resulting in a negative behavior. In this way, I claim that this method provides an alternative solution for designing new diagnostic tool of genetic diseases.

3.9. Experiment section

3.9.1. Materials

All conventional phosphoramidite monomers, CPG columns, and reagents for DNA synthesis were purchased from Glen Research. Other reagents for the synthesis of phosphoramidite monomers were purchased from Tokyo Chemical Industry, Wako, and Aldrich. All oligonucleotides except Mod, were purchased from Integrated DNA Technologies. T3, T4, and T7 ligase as well as reaction buffers were purchased from New England Lab (NEB).

Poly(L-lysine hydrobromide) (PLL-HBr, Mw = 7.5 × 103) and dextran (Dex, Mw = 8.0 × 103) were obtained from Sigma-Aldrich and Funakoshi Co., respectively. Poly(L-lysine)-graft-dextran (PLL-*g*-Dex) cationic comb-type copolymer was synthesized by a reductive amination reaction of dextran with PLL according to a previously published protocol. The resulting copolymer was purified by ion exchange and dialysis, then obtained by freeze drying. The composition (10 wt% PLL and 90 wt% dextran) of the copolymer was confirmed by ^{1}H-NMR analysis.

3.9.2. Photo-irradiation

For *trans*-to-*cis* isomerization, UV light at 365 nm was applied using an OminiCure LX405s Spot Curing System with a UV LED head V2 019-00181R (Lumen Dynamics, 9500 mW/cm2). For cis-to-trans isomerization, visible light at 455 nm was applied using an SLA-1000-2 two-channel Universal LED Driver with a BioLED Optical Head LCS-0455-03 (Mightex, 280 mW).

3.9.3. Synthesis of oligonucleotides

The modified oligonucleotide **Mod** tethering 2',6'-dimethyl azobenzenes was synthesized on an automated DNA synthesizer (H-8-SE, Gene World) using phosphoramidite monomers containing 2',6'-dimethyl azobenzene, which were synthesized as previously reported. After workup, the oligonucleotide was purified by reversed-phase HPLC and characterized using

a MALDI-TOF mass spectrometer (Autoflex II, Bruker Daltonics). MALDI-TOF MS for **Mod**: 9160 m/z (calculated for [Mod^+H^+]: 9162).

3.9.4. General procedures for photo-regulatable amplification

All DNA strands (**Tem**, **SL**s, and **Mod**) were dissolved in 1 x ligase reaction buffer in microtubes to a final concentration as mentioned in captions, followed by the addition of PLL-*g*-Dex to a total volume of 50 μL. Throughout the experiments, the ratio of amino groups of the PLL-*g*-Des to phosphate groups of DNA (the N/P ratio) was kept at 1.5 if not mentioned. Then mixture was incubated at 37 ºC for 10 min, before 10 min visible irradiation (465 nm light) was conducted. The ligase was added, and the reaction was initialized by irradiation with 365 nm light for 5 min. After UV irradiation, reactions were incubated in dark for 30 min and then irradiated with visible light for 5 min to finish a single amplification cycle. Aliquots were taken after every cycle and terminated in loading buffer (80% formamide, 50 mM EDTA, 0.025% bromophenol blue, and 20% glycerol). All the experiments were performed at 37 ºC if not mentioned.

3.9.5. Photo-regulatable amplification in the absence of template, PLL-*g*-Dex, modulator or without light irradiation

DNA strands were dissolved in 1 x T3 ligase reaction buffer and treated for the indicated number of cycles as described in the general method. For the experiment without PLL-*g*-Dex, no polymer was added to the sample. For the experiment without light irradiation, the reaction was kept in dark after the addition of ligase and incubated for equivalent times as the other samples. For all samples, amplification was performed 5 cycles.

3.9.6. Template-dependency analysis

In these experiments, the template strand (**Tem**, **Mis11**, **Mis7/16**, **Mis11/16**, or **PolyT**) was dissolved in 1 x T3 ligase reaction buffer, and reactions were performed as described in the general method. For all four samples, amplification was performed five cycles.

3.9.7. Photo-stability of ligase

Before ligation, T3 ligase equivalent (16 U/μL) together with PLL-*g*-Dex (N/P=1.5) was pre-irradiated with UV and visible light (each 30 min) or incubated in dark (60 min). Then the DNA mixture (**Tem**, **SL1**, and **SL2**) was added (volume up to 50 μL) to start the ligation, after 30 min reaction in dark, the reaction was terminated with loading buffer.

3.9.8. Gel electrophoresis quantification of yield

Samples mixed with loading buffer were subjected to electrophoresis on a 20% polyacrylamide gel containing 8 M urea at 750 V for 2.5 h. Images were taken with an FLA-9500 scanner (GE Healthcare) by monitoring the fluorescence of TAMRA attached to the substrate **SL1**. Quantitative analyses were conducted using Image Quant TL (GE Healthcare). Color intensity of the areas including substrate bands (I_s), product bands (I_p), and background (I_b) were quantified. Degree of Amplification value was calculated by the following formula:

$$\text{Degree of Amplification (\%)} = (I_p - I_p)/(I_s + I_p - 2 \times I_p) / 0.02$$

Solution containing 5 μM **SL1** and 5 μM **Prod** was subjected to the lane 1 of gel as the marker.

3.9.9. Melting temperature measurements

The melting curves were obtained with a JASCO model V-560 spectrometer and a JASCO model FP-6500 spectrometer equipped with programmable temperature controllers; 10mm x 2mm quartz cells were used. Tm value was determined from the maximum in the first derivative of the melting curve, which was obtained by measuring the absorbance at 260 nm (in UV/Vis case) as a function of temperature. The temperature ramp was 1.0 ^{o}C/min. Before measuring melting temperature of **Tem**/**Mod**$^{\textit{transs}}$ duplex, **Mod** was incubated at 90^{o}C for 10 min to isomerize as much azobenzene derivatives into *trans*-form. Before measuring melting temperature of **Tem**/**Mod**$^{\textit{cis}}$ duplex, Modulator was irradiated by UV light for 10 min at 60^{o}C. Conditions: 1 μM DNA, 100mM NaCl, 10 mM phosphate buffer (pH=7.0).

3.10. Appendixes

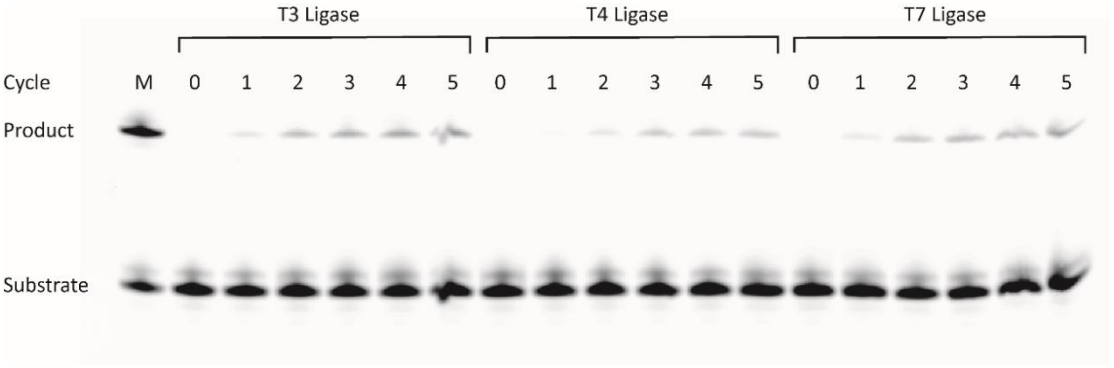

Figure S1. PAGE image (upper) and calculated yields of photo-regulatable amplifications with T3, T4, and T7 ligases. Lane M indicates the maker lane. Degree of amplification is calculated from PAGE. Conditions: 200 nM **Tem**, 10 µM each **SL**s, 2 µM **Mod**, PLL-*g*-Dex at N/P = 1.5, 16 U/µL ligase, performed in 1 x T3, T4 or T7 reaction buffer at 37 ^{o}C.

Figure S1. PAGE image of enzymatic ligation catalyzed with or without irradiation of T3 ligase: lane M, marker; lane 1, with irradiated T3 ligase and lane 2, with non-irradiated T3 ligase. Conditions: 5 µM Template, 5 µM each Substrate, PLL-*g*-Dex at N/P = 1.5, 16 U/µL T3 ligase in T3 reaction buffer at 37 ^{o}C. Reaction time is 2 hrs.

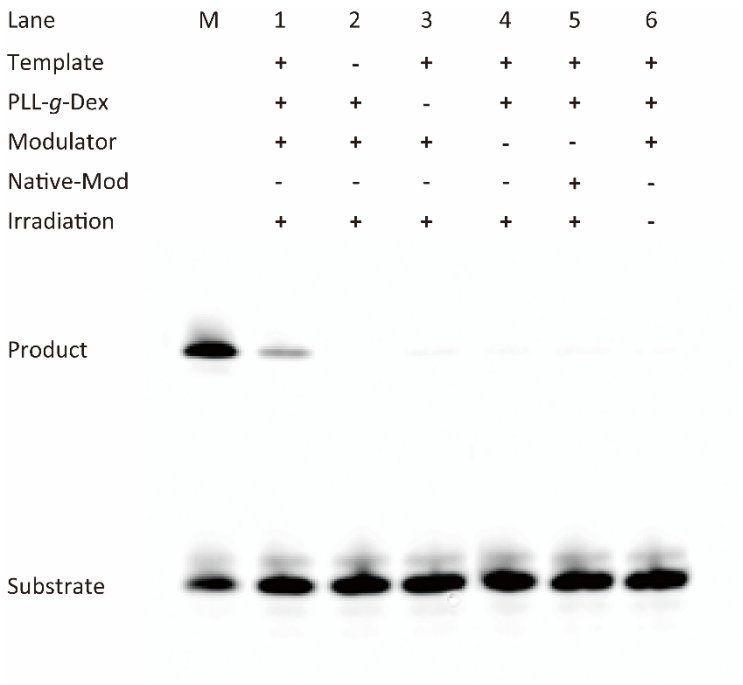

Figure S2. PAGE analyses of reactions with and without template, PLL-g-Dex, modulator, azobenzene-incorporation and light irradiation: lane M, marker; lane 1, amplification with all factors; lanes 2-6, amplifications in the lack of respective factor as shown in table. Conditions: 200 nM Template, 10 µM each Substrate, 2 µM Modulator/Native-Mod, PLL-*g*-Dex at N/P = 1.5, 16 U/µL T3 ligase in 1 x T3 reaction buffer at 37 °C. For all samples, 5 cycles of amplification were conducted.

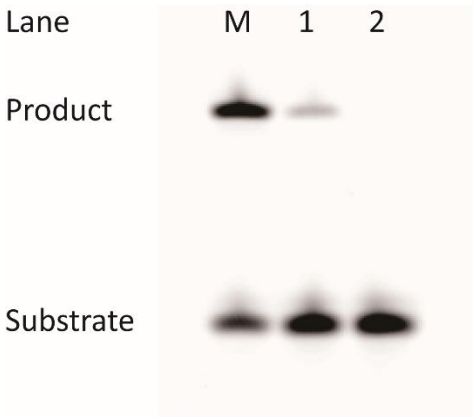

Figure S3. PAGE of reactions with PLL-*g*-Dex or PLL: lane M, marker; lane 1, with PLL-*g*-Dex and lane 2, with PLL. Conditions: 200 nM Template, 10 µM each Substrate, 2 µM Modulator, PLL-*g*-Dex at N/P = 1.5, 16 U/µL T3 ligase in 1 x T3 reaction buffer at 37 ^{o}C. For both samples, 5 cycles of amplification were conducted.

Figure S4. Photo-regulatable DNA amplification with azobenzene tethered modulator: lane M, marker; lane 1, with Azo-tethered modulator and lane 2, with DMAzo-tethered modulator. Conditions: 200 nM Template, 10 µM each Substrate, 2 µM Modulator, PLL-*g*-Dex at N/P = 1.5, 16 U/µL T3 ligase in 1 x T3 reaction buffer at 37 ^{o}C. For both samples, 5 cycles of amplification were conducted. The chemical structures of azobenzene (Azo) and 2',6'-dimethylazobenzene are shown.

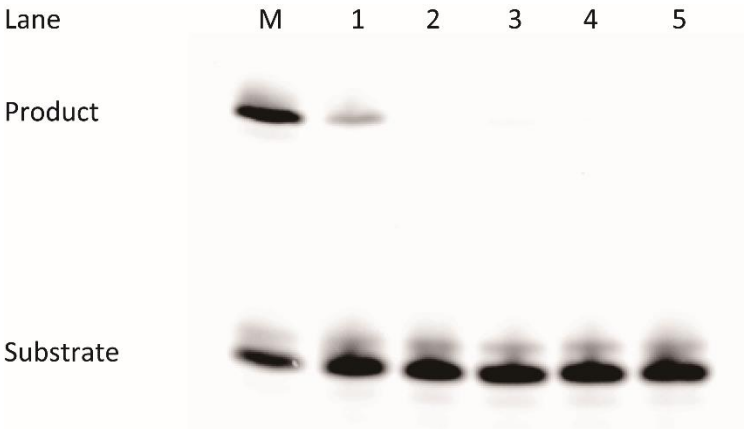

Figure S5. PAGE analyses of amplification reactions in the presence of indicated templates lane M, marker; lane 1, amplification with full-matched Template; lanes 2-5, amplifications with Mis11, Mis7/16, Mis11/16 or PolyT template. Conditions: 200 nM each template, 10 µM each Substrate, 2 µM Modulator, PLL-*g*-Dex at N/P = 1.5, 16 U/µL T3 ligase in 1 x T3 reaction buffer at 37 ^{o}C. For all samples, 5 cycles of amplification were conducted.

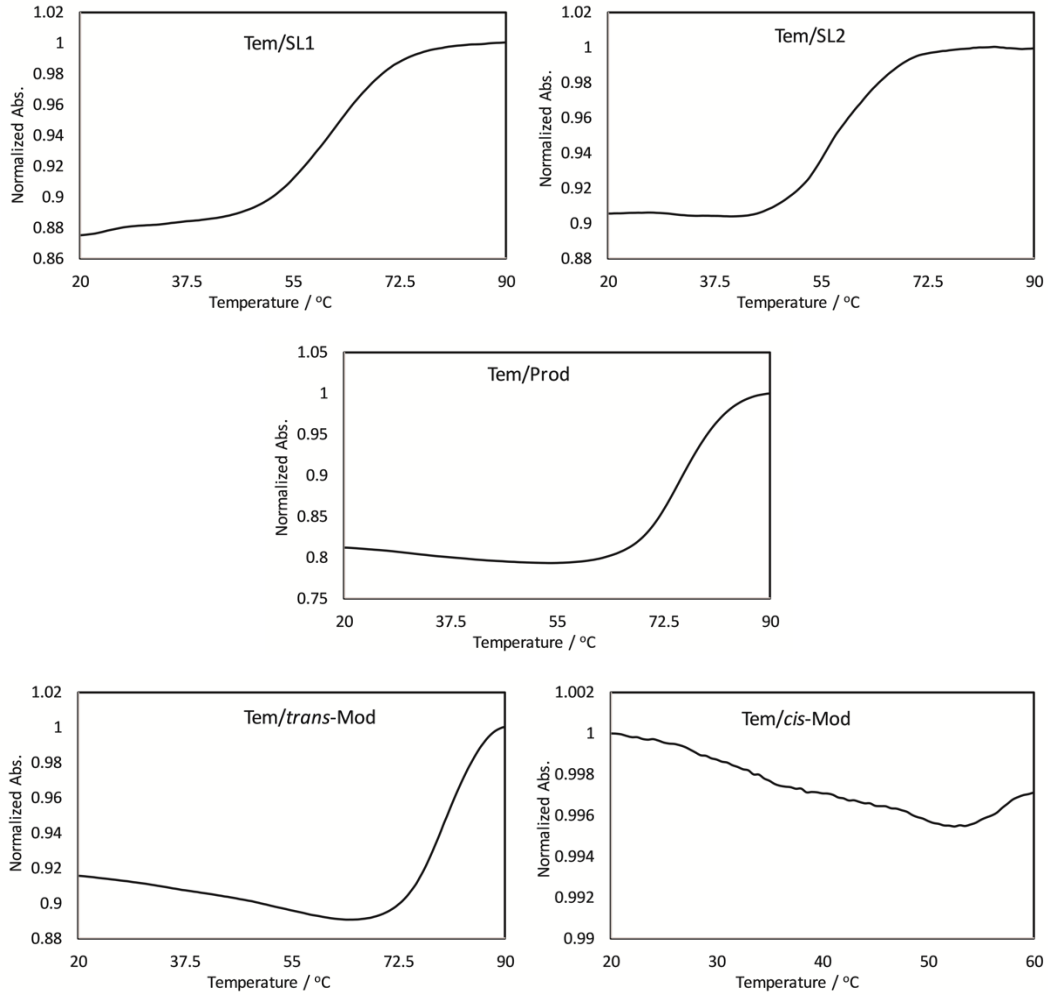

Figure S7. Normalized melting curves of all duplexes in photo-amplification system. Conditions: 1 μM Template with 1 μM SL1/SL2/Product/*trans*-Modulator/*cis*-Modulator, PLL-*g*-Dex at N/P = 1.5 in phosphate buffer (10 mM phosphate group, 100 mM NaCl, *p*H=7.00).

Table S1. Melting temperatures (T_ms) of duplexes.

Duplex	T_m/°C	
	trans-	*cis*-
Tem/SL1	58.5	
Tem/SL2	56.0	
Tem/Prod	75.0	
Tem/Mod	79.5	n.d.

3.11. Reference

[1] R. K. Saiki, D. H. Gelfand, S. Stoffel, S. J. Scharf, R. Higuchi, G. T. Horn, K. B. Mullis, H. A. Erlich, *Science,* **1988**, *239*, 487-491.

[2] Y. X. Zhao, F. Chen, Q. Li, L. H. Wang, C. H. Fan, *Chem. Rev.,* **2015**, *115*, 12491-12545.

[3] G. T. Walker, M. C. Little, J. G. Nadeau, D. D. Shank, *P. Natl. Acad. Sci. USA,* **1992**, *89*, 392-396.

[4] J. Compton, *Nature,* **1991**, *350*, 91-92.

[5] P. M. Lizardi, X. H. Huang, Z. R. Zhu, P. Bray-Ward, D. C. Thomas, D. C. Ward, *Nat. Genet.,* **1998**, *19*, 225-232.

[6] T. Murakami, J. Sumaoka, M. Komiyama, *Nucleic Acids Res.,* **2009**, *37*.

[7] T. Notomi, H. Okayama, H. Masubuchi, T. Yonekawa, K. Watanabe, N. Amino, T. Hase, *Nucleic Acids Res.,* **2000**, *28*.

[8] M. Vincent, Y. Xu, H. M. Kong, *Embo Rep,* **2004**, *5*, 795-800.

[9] O. Piepenburg, C. H. Williams, D. L. Stemple, N. A. Armes, *Plos Biol,* **2006**, *4*, 1115-1121.

[10] Z. Cheglakov, T. M. Cronin, C. He, Y. Weizmann, *J. Am. Chem. Soc.,* **2015**, *137*, 6116-6119.

[11] C. C. Wu, S. Cansiz, L. Q. Zhang, I. T. Teng, L. P. Qiu, J. Li, Y. Liu, C. S. Zhou, R. Hu, T. Zhang, C. Cui, L. Cui, W. H. Tan, *J. Am. Chem. Soc.,* **2015**, *137*, 4900-4903.

[12] Z. Wu, G. Q. Liu, X. L. Yang, J. H. Jiang, *J. Am. Chem. Soc.,* **2015**, *137*, 6829-6836.

[13] R. M. Dirks, N. A. Pierce, *P. Natl. Acad. Sci. USA,* **2004**, *101*, 15275-15278.

[14] R. M. Franzini, E. T. Kool, *J. Am. Chem. Soc.,* **2009**, *131*, 16021-+.

[15] R. M. Franzini, E. T. Kool, *Chem-Eur J,* **2011**, *17*, 2168-2175.

[16] H. Abe, E. T. Kool, *P. Natl. Acad. Sci. USA,* **2006**, *103*, 263-268.

[17] H. Abe, E. T. Kool, *J. Am. Chem. Soc.,* **2004**, *126*, 13980-13986.

[18] W. A. Velema, E. T. Kool, *J. Am. Chem. Soc.,* **2017**, *139*, 5405-5411.

[19] B. H. Cheng, H. Kashida, N. Shimada, A. Maruyama, H. Asanuma, *Chembiochem,* **2017**, *18*, 1568-1572.

[20] L. Y. Liang, D. Astruc, *Coord. Chem. Rev.,* **2011**, *255*, 2933-2945.

[21] M. Shelbourne, X. Chen, T. Brown, A. H. El-Sagheer, *Chem. Commun.,* **2011**, *47*, 6257-6259.

3.12. Contents of schemes, figures and tables

List of Related Publications

1. "Chaperone polymer-assisted, photo-driven DNA strand displacement"
   Cheng, B.; Kashida, H.; Shimada, N.; Maruyama, A.; Asanuma, H.
   ChemBioChem, 2017, 18, 1568-1572. DOI: 10.1002/cbic.201700394
   Selected as a "Front Cover"
2. "Photo-regulatable DNA isothermal amplification by template-mediated ligation"
   Cheng, B.; Kashida, H.; Shimada, N.; Maruyama, A.; Asanuma, H.
   Chem. Commun., 2018, in Press

List of Related Presentations

1. Cheng, B.; Kashida, H.; Shimada, N.; Maruyama, A.; Asanuma, H., " Photo-controllable DNA isothermal amplification by enzymatic ligation", The 45th International Symposium on Nucleic Acids Chemistry (ISNAC 2018), Nov. 2018

2. Cheng, B.; Kashida, H.; Shimada, N.; Maruyama, A.; Asanuma, H., " Photo-controllable DNA strand displacement facilitated by chaperon polymer", The Second International Symposium on Biofunctional Chemistry (ICBC 2017), Dec. 2017

3. Cheng, B.; Kashida, H.; Shimada, N.; Maruyama, A.; Asanuma, H., "Light-driven non-toehold DNA strand displacement assisted by chaperone polymer", The 44th International Symposium on Nucleic Acids Chemistry (ISNAC 2017), Nov. 2017 (Awarded as "ISNAC Outstanding Poster Award 2017")

4. Cheng, B.; Kashida, H.; Shimada, N.; Maruyama, A.; Asanuma, H., "Photo-driven DNA strands displacement mediated by azobenzene-tethered oligonucleotide", The 97th Chemical Society of Japan Annual Meeting (CSJ Spring 2017), Mar. 2017

Acknowledgement

More than five years ago when I decided to join Asanuma's lab, as an undergraduate student majored in polymer science, I had actually no idea about what a good researcher should be like and in which way nucleic acids research should be done. It was a quite difficult time in the first year when I came to Japan to find that hydrogel work did not go well. Fortunately, I got understanding and strong support from my supervisor, Hiroyuki Asanuma, to shift to a new topic, which is the start of this study. I thank him for his instruction on how to think logically, how to construct research from a single idea and how to express it to others. These benefit my research as well as my life.

I thank Hiromu Kashida, who have discussed most with me about my work during this five year. He provided many valuable advices that helped me improve this work. I cannot finish this study without his kind help.

I thank my co-workers, Atsushi Maruyama and Naohiko Shimada, who kindly provided polymer materials that are very crucial for this research. Their suggestions during submission of papers are indispensable for successful publication.

I thank Dr. Murayama who gave a lot of technical supports with my experiments, and Dr. Doi, who helped me very much with my research and life when I was struggled in the first year after I came to Japan. I also thank other lab members who have discussed with me in seminar and chatted with me in daily life.

My special thank is given to Leading Program Toryumon, without whose financial support I could not have finished my PhD.

My mother and father always stand behind me during my graduate life. Their encouragement and understanding are hugely supportive and soothing and I thank them very much.

Finally, I would like to give my appreciation to my wife, Qiuhan Yang. Her love and reinforcement have helped me to get through those hard times and reach this point.